

NORTHWESTERN UNIVERSITY

Writing and Reading Chemically Encoded Surfaces for Programming Cell Function and
Measuring Enzymatic Activity

A DISSERTATION

SUBMITTED TO THE GRADUATE SCHOOL IN PARTIAL FULFILLMENT OF THE
REQUIREMENTS

for the degree

DOCTOR OF PHILOSOPHY

Field of Chemistry

By

Maria de Lourdes Cabezas

EVANSTON, ILLINOIS

September 2018

© Copyright by Maria Cabezas 2018
All Rights Reserved

ABSTRACT

Writing and Reading Chemically Encoded Surfaces for Programming Cell Function and
Measuring Enzymatic Activity

Maria de Lourdes Cabezas

Understanding the chemical complexity of the extracellular matrix and how chemical, biological, and physical cues bring changes to the behavior of cells has remained a grand challenge. Addressing these questions requires not only achieving systematic control over the interaction between cells and the ECM but also utilizing suitable analytical techniques that can offer a quantitative readout of intracellular biochemical changes. Here, polymer pen lithography (PPL) and self-assembled monolayer laser desorption/ionization (SAMDI) mass spectrometry are uniquely positioned to offer researchers nanoscale surface fabrication and analytical tools that have significant advantages for designing chemical modifications and detecting chemical changes to molecularly encoded surfaces, respectively. Chapter 1 gives an overview of recapitulating the complexity of the ECM microenvironment and positions PPL and SAMDI-MS as surface fabrication and characterization techniques that can be used to answer fundamental questions about cell-substrate interactions and develop cell-based assays. Chapter 2 presents a methodology to generate nanopatterned substrates for combinatorial studies on cell behavior. Building upon this work, in Chapter 3 we utilize PPL to generate nanopatterns that can template the behavior of the cytoskeleton and program the fate of mesenchymal stem cells. These results show that PPL offers an unparalleled advantage over current printing approaches because it allows rapid prototyping of user-defined designs. More importantly, this work demonstrates that the cytoskeleton can be manipulated in a user-defined fashion to build organized sub-cellular structures and induce

programmed cell differentiation. Chapters 4 and 5 combine nanolithography with mass spectrometry to enable high-throughput cell-based assays with molecular readouts. Finally in chapter 6, we summarize these concepts and demonstrate how the work presented in this thesis provides fundamental insight to examine the role that ECM cues play in programming cell behavior as well as developing cell-based assays that can capture biochemical events within cells. Overall, this work provides a comprehensive view geared towards defining surface chemistry for biological applications.

Thesis Advisors: Professor Chad A. Mirkin and Professor Milan Mrksich

ACKNOWLEDGEMENTS

First and foremost, I would like to express my sincere gratitude towards my advisors Prof. Chad Mirkin and Prof. Milan Mrksich; this thesis would not have been possible without their mentorship, encouragement and support. Words cannot express how thankful I am that they gave me the opportunity to pursue a joint appointment during graduate school. It has been a truly rewarding experience to be part of two different groups having a diverse group of outstanding scientists. I would also like to acknowledge my committee members: Prof. Tom Meade, Prof. Guillermo Ameer and Prof. Teri Odom. In all of our meetings, they provided me with valuable and insightful feedback on how to present my work and make it clear to an audience. My work was also possible thanks to the office staff who always facilitated the best environment for students to do their work: Dr. Sarah Hurst Petrosko, Dr. Sara Rupich, Dr. Jen McGinnis, Elizabeth Forest, Mara Martini, Jorge Belmonte, Pam Watson, Dr. Tanushri Sengupta, and Yael Mayer.

While the graduate student's journey often involves long hours in the lab, it is by no means a lonely journey. Throughout these years, I have been fortunate to encounter great colleagues and collaborators; out of these interactions we have not only produced great work together but also formed strong friendships. I would like to thank my collaborators: Dr. Brian Meckes, Prof. Keith Brown, Dr. Eric Berns, and Dr. William Morris. One of the very first people who influenced the direction of my research is Dr. Louise Giam; I thank her for the initial mentorship that set me on the right track to develop the work presented in this thesis. Along the way, I relied on the expert advice and help of my colleagues from both groups: Patrick O'Kane, Dr. Kristin Beaumont, Alexei Ten, Lindsey Szymcak, Andrea D'Aquino, Kacper Skakuj, Edward Kluender, Natalie Fahey, Dr. Justin Modica, Jeffrey Chen, Jennifer Grant, and Liban Jibril. Although soon I will be departing

the lab, I am happy that these wonderful friendships are with me wherever I go: James Hedrick, Dr. David Walker, Eun Bi Oh, Jared Magoline, Priscy Pais Seth Garwin, Dr. Kelvin Chang, Dr. Alyssa Chinen-Mendez, Dr. Jose Mendez-Arroyo, Dr. Kyle Bantz, and Dr. Adam Eisenberg. Although distance limited our interactions to short visits and many skype calls, I also want to thank my friends outside NU: Betty Beck, Tom Beck, Betty Kreider, Donita Powell, Roseanne Fry, Jessica Yeary, Dr. Jackie Powell, Dr. Adam Powell, and Dr. Natalie Ramirez, for their unconditional support and encouragement.

During my undergraduate years at UT Austin, I had the amazing opportunity to work under the guidance of Prof. Richard Crooks. His initial mentorship inspired me to pursue graduate work and I want to thank him for his guidance and friendship throughout the years. Prof. Robbyn Anand and Dr. Brian Zaccheo have been wonderful colleagues and friends, often providing valuable insights about balancing life and career goals.

During my years at NU, I was also involved in many activities outside graduate school. Thanks to my flamenco dance teacher, Chiara Mangiameli, and the students at Studio Mangiameli, who shared with me the passion for dancing and artistic expression. I also want to thank Fr. Kevin Feeney, Fr. John Kartje and Mary Deeley who work at the Sheil Catholic Center providing students with spiritual direction and pastoral care.

Nobody has been more important to me in the pursuit of my academic goals than the members of my family (mom, dad and sister) and my boyfriend Andrey Ivankin, whose love and unconditional support guided me through this journey. A special acknowledgement also goes to my grandparents; this work would not have been possible without their sacrifice and dedication. Their perseverance and hard work was always centered with the goal that their children and future

generations would have opportunities to achieve higher education because they believed in the inherent value of education.

I pray that God bestows many blessings in all the people that I have encountered along the way.

Maria Cabezas

May 2018

PREFACE

This dissertation is submitted for the degree of Doctor of Philosophy at Northwestern University. The research conducted herein was conducted under the supervision of Professors Chad A. Mirkin and Milan Mrksich in the Department of Chemistry, between November 2011 and May 2018. The following work is original.

Part of this work has been presented in:

Cabezas, M. D., Eichelsdoerfer, D. J., Brown, K. A., Mrksich, M., and Mirkin, C. A. Combinatorial Screening of Mesenchymal Stem Cell Adhesion and Differentiation Using Polymer Pen Lithography. *Methods in Cell Biology*, Book Chapter, (Ed. M. Thery, M. Piel) *Elsevier*, 119, 261-276 (2014).

Berns, E. J., Cabezas, M. D., and Mrksich, M. A Cell Based Assay Using Self-Assembled Monolayers and MALDI Mass Spectrometry as a Platform for High-Throughput Screening. *Small*, 12, 3811-3818 (2016).

Cabezas, M. D., Mrksich, M and Mirkin, C. A. Nanopatterning Matrices Enable Enzyme Activity Measurements Using SAMDI Mass Spectrometry. *Nano Letters*, 17, 1373-1377 (2017).

Part of this work will be presented in:

Cabezas, M. D., Meckes, B. R., Mirkin, C. A. and Mrkisch, M. Nanoscale Control of Actin Assembly and Stem Cell Differentiation. *Manuscript in preparation* (2018).

LIST OF ABBREVIATIONS AND NOMENCLATURE

PPL	Polymer pen lithography
CF-SPL	Cantilever-free scanning probe lithography
DPN	Dip-pen nanolithography
ECM	Extracellular matrix
hMSC	Human mesenchymal stem cell
SAM	Self-assembled monolayer
SAMDI	Self-assembled monolayers for matrix desorption ionization
MALDI	Matrix-assisted laser desorption/ionization
MS	Mass spectrometry
TCAL	Tandem cell culture and lysis
PDMS	Polydimethylmethoxy silane
MHA	Mercaptohexadecanoic acid
EG3	Tri(ethylene) glycol-terminated thiol
EG6	Hexa(ethylene) glycol-terminated thiol
ALP	Alkaline phosphatase
OM	Osteogenic media
AD	Adipogenic media
PTP	Phosphotyrosine phosphatase
PTPI-I	Phosphatase inhibitor I
BPL	Beam pen lithography

This thesis is dedicated to all the teachers and educators.

TABLE OF CONTENTS

ABSTRACT	3
ACKNOWLEDGEMENTS	5
PREFACE	9
ABBREVIATIONS	10
TABLE OF CONTENTS.....	11
LIST OF FIGURES	14
CHAPTER ONE	19
<i>Introduction</i>	
1.1 Understanding the Complexity of the Extracellular Matrix Environment	20
1.2 Generating Nanopatterned Arrays for Studying Biological Systems.....	21
1.2.1 Fabrication of Nanopatterned Arrays Using Cantilever-Free Scanning Probe Techniques.....	22
1.2.2 Addressing the Throughput Challenge with Polymer Pen Lithography.....	23
1.2.3 Nanopatterned Arrays Enable Systematic Studies on Cell Behavior.....	24
1.3 Surface Characterization and Analysis Using SAMDI-MS	25
1.3.1 Defining the Chemistry of Self-Assembled Monolayers.....	26
1.3.1 Developing High-Throughput Lysate-Based Assays	27
1.4 Thesis Overview.....	28
CHAPTER TWO	30
<i>Nanoscale Patterning for Cell-Based Assays Using Polymer Pen Lithography</i>	
2.1 Designing Systematic Biological Studies of Cell Behavior	31
2.2 Materials and Instrumentation	33
2.3 Methods	
2.3.1 Fabrication of Master Arrays as Molds for Polymer Pen Arrays.....	36
2.3.2 Fabrication of Polymer Pen Arrays	38
2.3.3 Patterning of Mercaptohexadecanoic Self-Assembled Monolayers.....	38
2.3.4 ECM Protein Immobilization on Mercaptohexadecanoic Patterns	40
2.3.5 Combinatorial Screening of Cell Attachment.....	42
2.3.6 Mesenchymal Stem Cell Differentiation and Analysis	43
2.4 Discussion.....	45
2.5 Conclusions.....	47
CHAPTER THREE	49

	12
<i>Nanoscale Patterning Directly Controls Actin Fiber Formation and Cell Behavior</i>	
3.1 Introduction.....	50
3.2 Methods	52
3.2.1 Substrate Preparation	52
3.2.2 Cell Culture	52
3.2.3 Immunofluorescence and Confocal Microscopy.....	53
3.2.4 Image Analysis.....	53
3.3 Results and Discussion	54
3.3.1 Library Pattern Generation.....	54
3.3.2 Patterning Cells in Square-Shaped Geometries	55
3.3.3 Patterning Cells in Circular Geometries	61
3.3.4 Focal Adhesion Distribution Changes on Patterned Substrates.....	64
3.3.5 Controlling Cell Cytoskeleton Enhances Cell Programmability.....	66
3.4 Conclusions.....	68
CHAPTER FOUR.....	69
<i>Cellular Assays with a Molecular Endpoint Measured by SAMDI Mass Spectrometry</i>	
4.1 Introduction.....	70
4.2 Methods	72
4.2.1 Reagents	72
4.2.2 Preparation of SAMs	72
4.2.3 Assay for PTP Activity.....	73
4.2.4 Assay for Chemical Screen.....	74
4.2.5 Evaluation of Dose-Dependent Inhibition	75
4.2.6 Evaluation of Dose-Dependent Inhibition in Cell Lysates	75
4.2.7 Cell Viability Assays	76
4.2.8 Z'-Factor Determination	77
4.3 Results	77
4.3.1 TCAL-SAMDI Assay for Phosphatase Activity.....	77
4.3.2 Duplexing Enzyme Activity Measurements with TCAL-SAMDI.....	82
4.3.3 Screening with TCAL-SAMDI	83
4.4 Discussion.....	85
4.5 Conclusions.....	88
CHAPTER FIVE	89
<i>Nanopatterned Matrices Enable Cell-Based Assays with Molecular Readouts</i>	
5.1 Introduction.....	90
5.2 Methods	92
5.2.1 Reagents.....	92
5.2.2 Preparation of SAMs	93
5.2.3 Cell-based Assay for Enzymatic Activity.....	94
5.2.4 Lysis Promotes Interaction of PTPs with Peptide Substrate.....	94
5.2.5 Evaluation of PTP Activity with SAMDI.....	94
5.3 Results	95
5.3.1 Synthesis of Mixed Monolayers.....	95

	13
5.3.2 Cell Seeding and Assay Development.....	98
5.3.3 Cell Lysis and Analysis by TCAL-SAMDI.....	99
5.4 Discussion.....	101
5.5 Conclusions.....	102
CHAPTER SIX	103
<i>Conclusions and Future Outlook</i>	
6.1 Summary.....	104
6.2 Towards Printing Orthogonal Chemistries and Modulating the Chemical and Physical Properties of Soft Materials.....	105
6.3 Developing Single-Cell Assays with Molecular Readouts.....	106
REFERENCES	107
APPENDICES.....	115
Appendix A: Supporting Data for Chapter 4.....	116
Appendix B: Supporting Data for Chapter 5.....	117
CURRICULUM VITAE	120

LIST OF FIGURES

CHAPTER ONE

Figure 1.1 Schematic depicting a cell embedded in the extracellular matrix. Main components of the ECM (collagen, fibronectin and glycosaminoglycans) interact with cell membrane receptors associated to intracellular structures to maintain shape and homeostasis.....21

Figure 1.2 (a) Polymer pen arrays composed of elastomeric tips. (b) Micrograph of MHA features patterned on an Au-coated substrate after etching show the Olympic logo having high-resolution nanoscale features. (c) Large area patterning using PPL. (d) Custom-built PPL instrument for nanofabrication..... 24

Figure 1.3 Scheme depicting analysis of a monolayer using SAMDI-MS. Laser induced energy desorbs alkanethiolates (and their corresponding disulfides) which can be detected by their unique m/z peaks.....26

Figure 1.4 A self-assembled monolayer formed with alkyl-disulfides terminated with tri-ethylene glycol or maleimide groups, before and after peptide immobilization.....27

CHAPTER TWO

Figure 2.1 Polymer pen lithography (PPL) process used to generate extracellular matrix (ECM) protein patterns. (A) Schematic shows the major steps of this cantilever-free scanning probe technique which include: deposition of a template SAM followed by addition of a passivation layer, protein attachment to the patterned areas, and seeding cells on the molecular patterns. (B) Scheme for generating combinatorial libraries by tilting the polymer pen array. A range of feature sizes (475 nm to 1.2 μm) were obtained by controlling the tilt angle across one substrate. The resulting patterns were arranged in a 60 μm \times 60 μm area, where each pen wrote a 15 \times 15 array with 4 μm pitch distance. The resulting patterns were imaged by scanning electron microscopy after etching.....33

Figure 2.2 (A) The resulting fibronectin patterns can be visualized by immunofluorescence staining with AlexaFluor568-conjugated antibody against fibronectin. The pitch of the master array used to generate these features corresponded to 80 μm . (B) Optical micrograph of mesenchymal stem cells (MSCs) seeded on fibronectin adhesion sites displays cells attached to the patterned square regions. A master array having a pitch distance of 180 μm was used to generate these patterns.....41

Figure 2.3 Stem cell adhesion study using combinatorial fibronectin patterns to evaluate cell attachment and spreading. (A) A tilted polymer pen array (180 μm pen spacing) was used to generate 15 \times 15 array of fibronectin features spaced by 4 μm . MSCs were cultured on these patterns for 1 week and subsequently stained for alkaline phosphatase (ALP) (green), actin (red),

and the nucleus (blue). The labels on the resulting patterns shown in (B) indicate the x-position of patterns of a certain feature size across a substrate. The total area presented to the cell can be obtained by squaring the average protein feature size and multiplying by 225 for a 15×15 array of dot features.....43

Figure 2.4 Immunofluorescence micrographs show the expression of osteogenic marker alkaline phosphatase (ALP) in MSCs cultured on homogeneous (300 nm diameter) fibronectin patterns. (A) The confocal microscopy images in the merged channel display samples stained for actin in red, ALP in green, and the nucleus in blue. (B) Quantitative RT-PCR results for ALP were normalized to GAPDH levels. The bar graph also displays results that were normalized to the negative control in the absence of osteogenic media (OM-).....45

CHAPTER THREE

Figure 3.1 (A) Scheme for generating patterns of fibronectin features using PPL. (B) An etched Au-coated substrate reveals printed MHA features printed according to a user-defined pattern. (C) Immunofluorescence micrograph of stained fibronectin that has selectively adsorbed to the MHA features.....55

Figure 3.2 Actin fiber orientation within cells on square substrates. (A) Micrograph of an etched gold substrate with an MHA square dot matrix pattern. (B) Representative image of the actin cytoskeleton of a cell on a square dot matrix pattern. (C) Heatmap of the actin fibers in cells on a square dot matrix substrate (n=50). (D) Micrograph of an etched gold substrate with an MHA anisotropic square pattern. (E) Representative image of the actin cytoskeleton of a cell on an anisotropic square pattern. (F) Heatmap of the actin fibers in cells on a anisotropic square substrate (n=50). (G) The actin fiber orientation within cells on anisotropic and square dot matrix patterns.....56

Figure 3.3 Set of patterns used to identify cytoskeletal controlling features in a square geometry. (A)-(G), Computer generated images of the programmed fibronectin features patterned on gold substrates (Panel 1). Representative images of the actin cytoskeleton (red) for cells on these patterns are shown along with the nucleus (blue) (Panel 2-4).....58

Figure 3.4 3T3 Cells grown on square patterns. (A)-(D) Computer generated images of the programmed fibronectin features patterned on gold substrates (Panel 1). Representative images of the actin cytoskeleton (red) for cells these patterns are shown along with the nucleus (blue) (Panel 2-4). (E) Actin fiber orientation in 3T3 cells on square dot matrix and anisotropic patterns. (F) Fiber orientation in 3T3 cells with the peripheral fibers excluded.....60

Figure 3.5 Set of patterns used to identify cytoskeletal controlling features in a circular geometry. (A)-(H), Computer generated images of the programmed fibronectin features patterned on gold substrates (Panel 1). Representative images of the actin cytoskeleton (red) for cells on these patterns are shown along with the nucleus (blue) (Panel 2-4).....62

Figure 3.6 Actin fiber orientation within cells on circular substrate. (A) Micrograph of an etched gold substrate with an MHA dot matrix circle pattern. (B) Representative images of the actin cytoskeleton of cells seeded on dot matrix circle patterns. (C) Heatmap of the actin fibers in cells on dot matrix circles (n=50). (D) Micrograph of an etched gold substrate with an MHA 20-point circle. (E) Representative images of the actin cytoskeleton of cells seeded on 20-point circles. (F) Heatmap of the actin fibers in cells on the 20-point circle (n=50). (G) The distribution of radial fibers within the cells as a function of angle going around the cell for dot matrix and 20-point circle pattern. (H) FFT of the angular distribution of the radially oriented actin fibers within cells on the substrate.....64

Figure 3.7 Micrographs of the focal adhesions and actin cytoskeleton within cells on patterns. a-d, Representative confocal images of single cells grown on different patterns: square dot matrix (A), Anisotropic (B), dot matrix circles (C), and 20-point circles (C). The nucleus (Panel 1), focal adhesions (vinculin, panel 2), and actin cytoskeleton (panel 3) are labeled within each cell. Panel 4 shows the overlay of the different structures.....65

Figure 3.8 qPCR of osteogenic and adipogenic markers by hMSCs on patterned substrates. (A) Relative expression of RUNX2, an osteogenic transcription factor, by hMSCs on square patterns compared to cells grown on unpatterned substrates. (B) Relative expression of PPAR γ , an adipogenic transcription factor, by hMSCs on circular patterns compared to cells grown on unpatterned substrates.....67

CHAPTER FOUR

Figure 4.1. SAMDI on monolayers with two peptides. (A) Two peptides with terminal cysteines (a cell adhesion ligand (cyclic RGD peptide – cycRGD) and a phosphatase substrate (AIPYENPFARKC) are immobilized on alkanethiolate monolayers with 10% of the molecules presenting maleimides and 90% terminated with tri(ethylene glycol). (B) SAMDI spectrum of a monolayer with immobilized RGD peptide and phosphatase peptide. M1: alkanethiolate with RGD, M2: alkyldisulfide with RGD, M3: alkanethiolate with phosphatase peptide, M4: alkyldisulfide with phosphatase peptide, M4: alkyldisulfide with phosphatase peptide. (C) The same spectrum, showing the portion of the spectrum used for PTP activity analysis.....78

Figure 4.2. Tandem Culture and Lysis SAMDI (TCAL-SAMDI). (A) Cells (MDA-MB-231) are cultured on monolayers presenting both cell adhesion ligands and a phosphatase substrate, on a 384-spot plate. Green: live cells, Red: dead cells and gold spot. (B) A SAMDI spectrum from a spot without cells. (C) A SAMDI spectrum after lysis of cells.....79

Figure 4.3. Enzyme activity measurement with TCAL-SAMDI. (A) SAMDI-MS spectra showing the conversion of substrate (s) to product (p) as the number of HeLa cells cultured and lysed on monolayer-coated gold spots increases. Quantification of the dephosphorylation peak fraction, defined as the area under the curve of the product peak relative to that of the substrate and the product peaks in the SAMDI spectra, resulting from culturing and lysing. (B) HeLa cells and (C) MDA-MB-231 cells on monolayers presenting adhesion and substrate peptides. Insets in (B) and (C) are magnified regions of the graphs. (*p<0.01).....81

Figure 4.4. Duplexing enzyme activity measurements with TCAL-SAMDI. (A) SAMDI spectra of a spot with no cells (top) and with 10,000 cells (bottom) shows the conversion of two substrates (PTP s: PTP substrate; cas s: caspase-3 substrate) to their products when cells are cultured, treated with STS, and lysed on the surface. (B) Caspase-3 activity measured by SAMDI (*p < 0.05).....83

Figure 4.5 Compound 1 identified by chemical screening via TCAL-SAMDI. (A) Chemical structure of 1. (B) SAMDI analysis of PTP activity measured from MDA-MB-231 cells cultured on the monolayer and treated with 1 (black circles) and from lysate treated with 1 then applied to the monolayer (white squares). (C) SAMDI analysis of lysate from cells cultured in 96-well plates and treated with 1.....84

CHAPTER 5

Figure 5.1. This work reports the use of surfaces that are nanopatterned with extracellular matrix proteins that support cell adhesion, and where the intervening regions present a peptide substrate for an enzyme, to enable cell-based assays using SAMDI mass spectrometry. Note that the nanoarrays have 100 fibronectin features. Cells that are adherent to the nanoarrays are cultured and treated with small molecules. The media is then removed, and a lysis buffer is applied to each region of cells, where enzymes in the lysate can modify the peptide in the intervening regions. The surface is then rinsed and analyzed with SAMDI mass spectrometry to determine the extent of conversion of the peptide substrate and, therefore, the amount of enzyme activity in the lysate....92

Figure 5.2. (A) Nanoarrays were prepared by using PPL to pattern mercaptohexadecanoic acid (MHA) a gold-coated surface in many 10 × 10 arrays where each spot was 750 nm in diameter and where neighboring spots had a center-to-center spacing of 4.4 μm. (B) The remaining areas of gold were then modified with a monolayer presenting maleimide groups against a background of tri(ethylene glycol) groups and used to immobilize a cysteine terminated phosphopeptide. (C) The surface was then treated with a solution of fibronectin to allow the adsorption of the extracellular matrix protein to the MHA nanoarray. (C) A SAMDI spectrum of the monolayer confirms immobilization of the peptide. (D) The fluorescence micrograph shows fibronectin patterned nanoarrays stained with mouse antibody and AlexaFluor 568-conjugated goat anti-mouse IgG. The scale bar is 40 μm..... 97

Figure 5.3. (A) Cell culture and lysis on mixed monolayers. (B) Cells were cultured on patterned monolayers. Individual cells attached to each 10 × 10 fibronectin nanoarray and remained confined to these regions of the substrate. The media was then removed from the entire plate and a lysis buffer was added to each spot of the 384-spot array to allow phosphatase enzymes in the lysate to act on peptides immobilized on the monolayer. The scale bar is 500 μm. (C) SAMDI spectra of the surface after removal of the lysate showed a peak corresponding to generation of the dephosphorylated product (top spectrum). Addition of the phosphatase inhibitor PTP-1 to the lysis buffer resulted in a loss of phosphatase activity (middle) as did proteolytic removal of the cells without lysis (bottom). Separately, populations of HeLa cells were treated with PTP-I in concentrations ranging from 0 to 200 μM and then lysed and analyzed with SAMDI-MS. A dose-response curve shows half-maximum inhibition at concentration of approximately 22 μM.

Standard errors were determined from three independent experiments with at least five spots per condition..... 99

APPENDIX A

Figure A.1 Calibration curve relating the dephosphorylated peptide peak fraction measured by SAMDI to the ratio of the dephosphorylated peptide to the phosphorylated peptide used during immobilization onto the monolayer..... 10

Figure A.2 Control experiments of compound 1. (a) The cell counts of live cells (cells stained with calcein-AM) and dead cells (cells stained with ethidium homodimer) relative to the total cell count observed in cells treated with DMSO only. (b) Viability, measured by the PrestoBlue assay, of cells treated with **1**, relative to cells treated with DMSO only. (c) Protein concentrations of lysates prepared from cells cultured in 96-well tissue culture plates and treated with **1** for 2 hr, measured by the BCA assay..... 10

APPENDIX B

Figure B.1 Pattern arrangement across multiple length scales. Nanoarrays were prepared on 384-well format gold islands, where each island was patterned using PPL to yield ~ 428 arrays of MHA features. Each array was patterned over a 40 x 40 μm^2 area having a total of 100 MHA features arranged in a 10 x 10 square matrix. The size of each individual MHA feature corresponds to ~ 750 nm..... 10

Figure B.2 MHA features arranged in a square array patterned by polymer pen lithography (PPL). Optical micrograph of raised gold features ~1 μm in diameter made by chemical etching (with an aqueous solution of 13.3 mM $\text{Fe}(\text{NO}_3)_3$ and 20 mM thiourea) a portion of a glass slide having PPL-patterned mercaptohexadecanoic acid (MHA) features. The scale bar is 60 μm 10

Figure B.3 XPS spectra collected after peptide immobilization on Au regions that present a maleimide-terminated monolayer along with MHA nanoarrays. The presence of sulfur (a) and nitrogen (b) peaks indicate the availability of amide bonds and thiols on the surface (black trace), while a control surface consisting of a uniform MHA monolayer (blue trace) only shows presence of thiols. Dashed lines denote the N (1s) and S (2p) peak positions..... 10

CHAPTER ONE

Introduction

Portions of this chapter have been adapted from:

Cabezas, M. D., Eichelsdoerfer, D. J., Brown, K. A., Mrksich, M., and Mirkin, C. A. Polymer Pen Lithography. Book Chapter, (Ed. M. They & Piel) *Methods in Cell Biology*. Elsevier, p. 261-276 (2014).

1.1 Understanding the complexity of the extracellular matrix (ECM) environment

The extracellular matrix (ECM) is a heterogeneous environment present within all tissues and organs, and provides essential ligands, proteins, and polysaccharides that provide essential scaffolding to maintain cellular function (Figure 1.1).¹⁻² During cell adhesion, ECM receptors such as integrins recognize and engage with ECM ligands; recruitment of integrins at sites of cell adhesion assemble protein complexes, termed focal adhesions, which link the cytoskeleton to the ECM.³ The interaction between cell surface receptors and the ECM sets off a cascade of events that get transduced into biochemical signals through a process termed mechanotransduction. The ECM plays a fundamental role in providing structural support, mediating cellular behavior, and maintaining homeostasis. Researchers have been primarily interested in engineering surface that can recapitulate conditions that mimic the ECM to answer fundamental questions about cell behavior, including motility, differentiation, division, and migration. These biological systems can be probed and simulated with engineered surfaces, but doing so demands careful control over the arrangement of ligands. Importantly, studying the properties of the ECM can provide valuable insight into understanding the how changes in physiological states (normal versus cancerous) give rise to the onset of diseases.

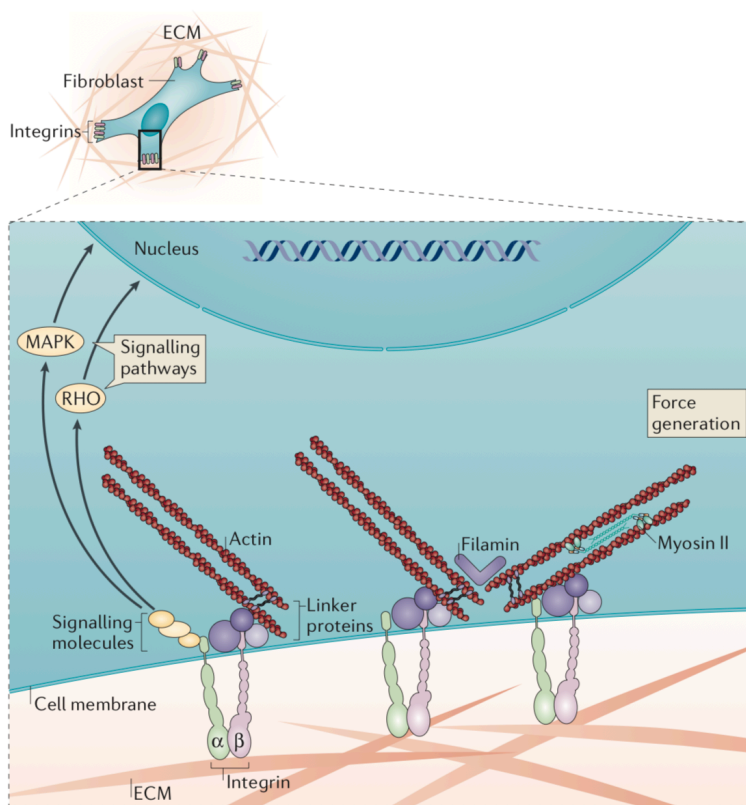


Figure 1.1 Schematic depicting a cell embedded in the extracellular matrix. Main components of the ECM (collagen, fibronectin and glycosaminoglycans) interact with cell membrane receptors associated to intracellular structures to maintain shape and homeostasis.²

1.2 Generating nanopatterned arrays using scanning probe techniques for studying biological systems

Probing the extracellular microenvironment to obtain information about how cell–receptor interactions occur and trigger downstream signaling cascades is a rapidly growing field of multidisciplinary research. However, understanding the effect of cell–receptor events requires careful control at the molecular level over a variety of parameters, such as the arrangement, density, and position of extracellular factors. These parameters can be controlled by molecular patterning techniques, such as dip-pen nanolithography (DPN) or polymer pen lithography (PPL), thus allowing one to answer fundamental questions pertaining to cellular function and the response

of cells to external stimuli. Cantilever-free scanning probe techniques are ideally suited for creating models of the extracellular matrix (ECM) at the length scales of focal adhesions in a deliberate, programmable, and systematic fashion; therefore, they are well suited for studying the fundamental underpinnings of cell adhesion, motility, stem cell differentiation, and many other biological processes. This is in contrast with a technique like microcontact printing that uses a stamp generated by photolithography to transfer a single predefined pattern to an underlying substrate.

1.2.1 Fabrication of nanopatterned arrays using dip-pen nanolithography

In 1999, Mirkin and co-workers invented DPN, a scanning probe technique that allows one to deliver molecules onto a surface in a direct-write manner with sub-50 nm resolution.⁴ In this technique, an atomic force microscope (AFM) probe, which consists of a cantilever with a sharp tip at its end, is coated with a solution containing a molecule onto a substrate, much as a pen deposits ink onto paper. The DPN process is mediated by the formation of a water meniscus between the tip and the substrate which allows the ink material to diffuse from the tip to the surface, as was initially demonstrated by the deposition and formation of self-assembled monolayers (SAMs) composed of alkanethiols on Au-coated substrates. Since then this technique has been used to deposit many other biologically relevant materials such as proteins,⁵ DNA,⁶ polymers,⁷ and a variety of small organic and inorganic molecules on many different substrates.⁸⁻¹¹ Once patterned, nanoscale arrangements of biomolecules can then be used as arrays for combinatorial screening and to address fundamental questions in cell biology.¹² The functionality of such arrays demonstrates the relevance of DPN as a method of choice for conducting studies in the biological sciences. For example, Niemeyer and co-workers showed that DPN can be used to generate protein

arrays and probe protein-receptor interactions inside living cells and that this method can be coupled with traditional biological techniques for the study of biological processes.¹³

1.2.2 Addressing the throughput challenge with PPL

Following extensive research into methods of patterning diverse materials by DPN, it was recognized that throughput was the main limiting factor for many studies, as it will take prohibitively long to pattern cm^2 areas with a single probe. To address this, 1D and 2D arrays of cantilevers were developed to transition this technique from a serial writing process to a parallel one⁹; however, reliance on these fragile and expensive cantilever arrays limited wide-spread adoption of these approaches. To circumvent these limitations, a new architecture that did not rely on cantilevers for mechanical compliance of the probes was developed to generate arbitrary patterns in a high throughput fashion.¹⁴ This cantilever-free method, termed PPL, utilizes a 2D array of elastomeric pyramidal probes that rest on an elastomeric film on a rigid planar substrate to deliver molecules to a surface with nanoscale control over large areas (Figure 1.2A-D). In contrast to microcontact printing, which relies on a lithographically defined master,¹⁵ PPL is a mask-free technique, allowing a user to pattern arbitrary arrangements of materials on a surface. Using this approach, pen arrays with as many as 11 million tips can be easily and cheaply fabricated, thus significantly increasing the patterning throughput without compromising robustness and cost. Furthermore, this platform is commercially available as a designated PPL patterning instrument (Figure 1.2 D).

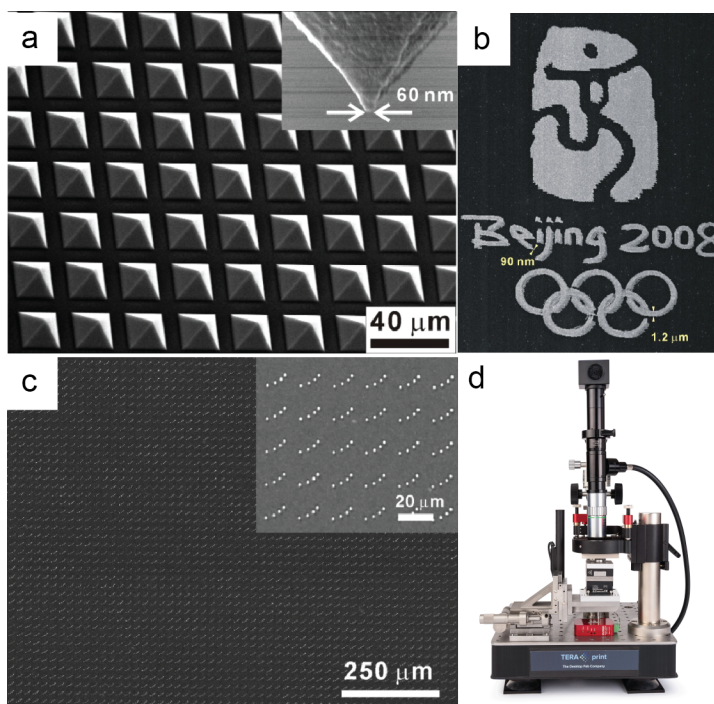


Figure 1.2 (a) Polymer pen arrays composed of elastomeric tips. (b) Micrograph of MHA features patterned on an Au-coated substrate with the Olympic logo show high-resolution nanoscale features. (c) Large area patterning using PPL. (d) Custom-built PPL instrument for nanofabrication.

1.2.3 Nanopatterned arrays enable systematic studies on cell behavior

With the advent of PPL, fundamental questions in cell biology can be answered by recapitulating cell–ECM interactions to explore how these interactions lead to changes in cell behavior. Here, I describe an approach for the combinatorial screening of cell adhesion behavior to gain understanding of how ECM protein feature size dictates osteogenic differentiation of mesenchymal stem cells. The approaches presented in this thesis are generalizable to other biological systems and can be paired with quantitative analytical methods to probe important processes such as cell polarization, proliferation, signaling, and differentiation.

The extracellular matrix (ECM) is a complex, spatially inhomogeneous environment that is host to myriad cell–receptor interactions that promote downstream changes to cell behavior.

These biological systems can be probed and simulated with engineered surfaces, but doing so demands careful control over the arrangement of ligands. In this chapter, I describe how such surfaces can be fabricated by utilizing polymer pen lithography (PPL), which is a cantilever-free scanning probe lithographic method that utilizes polymeric pen arrays to generate patterns over large areas. More importantly, a methodology that combines the synthesis of nanoscale structures with surface analytical techniques, such as mass spectroscopy, is developed in later chapters to enable cell-based assays capable of quantitatively recording enzymatic activity.

1.3 Surface characterization and analysis using SAMDI-MS

Analytical techniques provide necessary information to characterize the molecular composition of complex organic and inorganic structures and assemblies. Characterizing these products and their reaction yields when bound to a surface remains a formidable challenge. Self-assembled monolayer laser desorption/ionization mass spectrometry (SAMDI-MS) provides a label-free and high throughput platform that enables the detection and quantification of a broad range of chemical reactions of molecules – including peptides, proteins, polymers, small organic molecules, etc – attached to self-assembled monolayers of alkanethiolates on gold.¹⁶ Using this platform, molecules and chemical modifications can be identified by a distinct m/z ratio. In a typical SAMDI-MS analysis routine, desorption of the alkanethiolates (and their corresponding disulfides) from the monolayer occurs upon laser irradiation in presence of common adsorbing matrices used in matrix-assisted laser desorption/ionization mass spectrometry (MALDI-MS) (Figure 1.3). More importantly, the sensitivity of this in this way, small molecules and chemical modifications can be identified by a peak with a unique m/z ratio. This convenient platform presents a significant advantage over fluorescence-based approaches since characterization of complex products is not limited to the extensive synthetic efforts to dye-modified substrates. More

importantly, this mass spectrometric-based technique is well-suited for the development of a wide range of high-throughput screening assays and discovery of novel chemical reactions.

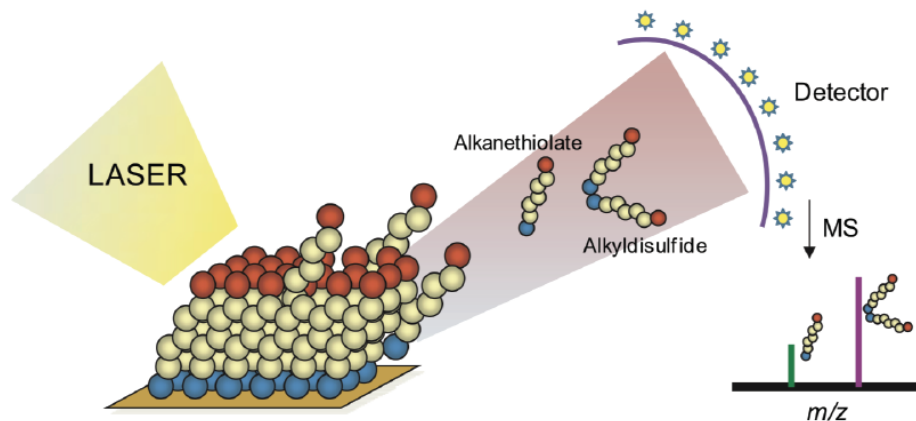


Figure 1.3 Scheme depicting analysis of a monolayer using SAMDI-MS. Laser induced energy desorbs alkanethiolates (and their corresponding disulfides) which can be detected by their unique m/z peaks.¹⁶

1.3.1 Defining the chemistry of self-assembled monolayers

Self-assembled monolayers (SAMs) refer to molecular assemblies of organic molecules formed by adsorption and organized into ordered domains.¹⁷ Throughout this thesis, SAMs of alkanethiolates on gold provide well-defined surface chemistries to prepare bioactive surfaces.¹⁸ Common functional groups – including maleimide, activated esters, epoxides and other nucleophilic groups – provide flexible immobilization chemistries that facilitate covalent capture of analytes. In addition, having a conductive gold-coated substrates enables investigating electrochemical reactions on monolayers such as the redox conversion of a hydroquinone unit to its aldehyde-derived product.¹⁹⁻²⁰ Monolayers presenting maleimide-terminated alkanethiolates selectively react with thiol-terminated ligands via a Michael addition reaction and thus provide an attractive method to immobilize cysteine-terminated ligands and synthesize peptide and carbohydrate arrays (Figure 1.4).²¹ More importantly, these monolayers also display oligo

ethylene glycol-terminated alkanethiolates which act as an inert background to block the non-specific adsorption of proteins and other moieties. Throughout this thesis, maleimide-terminated and ethylene glycol-terminated SAMs will be used extensively to demonstrate the applicability of SAMDI-MS as a workhorse for the development of high-throughput assays.

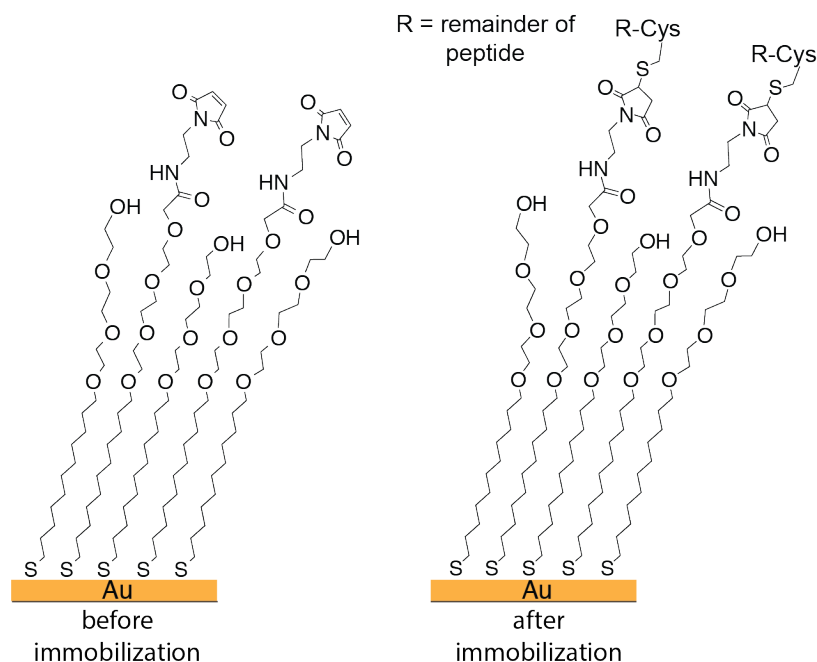


Figure 1.4 A self-assembled monolayer formed with alkyl-disulfides terminated with tri-ethylene glycol or maleimide groups, before and after peptide immobilization.

1.3.2 Developing high-throughput cell and lysate-based assays using SAMDI-MS

Capturing reaction products and quantifying their yield becomes a difficult challenge in lysates and other complex mixtures. Current assays that rely on traditional biochemical methods for analysis and detection require extensive sample purification, direct labeling using synthetic probes, and large sample volumes to ensure assay performance. In contrast, SAMDI-MS offers a platform with the mass-resolving ability to monitor both reaction products and substrates on the same surface in a label-free and high-throughput manner. In a SAMDI assay, the substrate is covalently immobilized on the monolayer against an inert background providing a stable chemical

environment where the interacting species (often an enzyme or small molecule) selectively modifies the substrate. Any by-product or nonreactive species is then rinsed away after the reaction has terminated. An important feature of the SAMDI-MS technique is the capability of multi-analyte detection.²² For example, multiple peptide substrates can be co-immobilized on the same monolayer and independently resolved from their unique mass spectrometric fingerprint.

Previous works have demonstrated that the SAMDI assay is capable of monitoring reactions in complex mixtures, such as lysates. These examples demonstrate that the background monolayer provides an inert background and that any interacting species or cross-reactivity that is captured can be identified and characterized in the resulting spectrum. As such, the SAMDI assay has been successful in capturing post-translational modifications – including phosphorylation,²³⁻²⁶ dephosphorylation,²⁷ deacetylation,²⁸⁻²⁹ among others – in well-controlled reactions where the identity of each species is known as well as complex lysates.

The advantages of SAMDI allow its application for developing high-throughput assays and reaction discovery programs. This feature is paramount for the development of efficient drug screening methodologies to identify novel compounds and design new chemical reactivities. Mrksich and coworkers have illustrated unprecedented ability to enable researchers with adequate tools to obtain molecular readouts in high-throughput.

1.4 Thesis overview

Molecular printing technologies and analytical characterization techniques have enabled studies to answer fundamental questions and develop applications in a wide range of disciplines, from addressing fundamental questions about fluid transport onto surfaces and synthesizing of multi-elemental nanoparticles, to screening nanoparticle properties to find novel catalysts for pharmaceutical discovery and energy storage. Combining these nanoscale tools and making them

accessible to the biological community has the potential to expand our current understanding of how the ECM interact with cells.

CHAPTER TWO

Nanoscale Patterning for Cell-Based Assays Using PPL

Portions of this chapter have been adapted from:

Cabezas, M. D., Eichelsdoerfer, D. J., Brown, K. A., Mrksich, M., and Mirkin, C. A. Book Chapter, (Ed. M. Thery & Piel) *Methods in Cell Biology*. Elsevier, p. 261-276 (2014).

2.1 Designing systematic biological studies of cell behavior using PPL

This chapter will detail a canonical PPL-based cellular biology experiment that involves the patterning of the ECM protein fibronectin. In addition to outlining the procedure for generating patterns and observing cell differentiation, we elaborate on a unique feature of PPL that enables patterning of combinatorial libraries. This ability arises from the deformable nature of the elastomeric pens, which gives rise to a force-dependent feature size. Because of this, PPL can be used to generate patterns with a gradient of feature sizes by intentionally tilting the pen array with respect to the sample. Of course, uniform features on a sample can also be generated if the pen array is leveled with respect to surface. This powerful technique ultimately allows for the screening of conditions that dictate cell behavior (i.e. adhesion, motility, migration) in a combinatorial fashion and was recently shown to be useful for the study of osteogenic induction of mesenchymal stem cells (MSCs) by culturing MSCs on fibronectin patterned substrates with a range of feature sizes from the nano- to microscale.¹² The questions addressed in this chapter, that is, the role of nanoscale variations of ECM proteins on MSC differentiation, are subtle given that many mechanical and chemical factors are known to play a role in differentiation. For example, Discher and co-workers initially observed that MSCs cultured on substrates with different stiffnesses underwent either neurogenesis, myogenesis, or osteogenesis, showing that material properties directed the expression of lineage-specific markers and promoted downstream differentiation.³⁰ Additionally, a recent paper by Trappmann et al., showed that the porosity of the substrate also contributes to cell differentiation.³¹ These studies are representative of the growing trend of exploring the role of physical cues on stem cell differentiation.³² Despite the growing body of work on these topics, there are still many questions to be answered about how the interactions between the cell membrane and the surface trigger signaling pathways that promote downstream changes

in the cellular machinery.³³⁻³⁴ Interestingly, the observations that physical and chemical features of the surface direct differentiation hint at the opportunity for developing tunable substrates with ligand gradients that can be used to rapidly study cell adhesion, polarization, differentiation of cells, or other relevant biological processes.

Herein, I outline the steps required for performing studies to address the questions in this field. The general process of fabricating nano- to micrometer scale protein patterns with PPL is (Figure 2.A):

- i. Fabrication of a polymer pen array master
- ii. Fabrication of PDMS pen arrays
- iii. Patterning of alkanethiol SAMs
- iv. Protein immobilization
- v. Cell seeding and staining

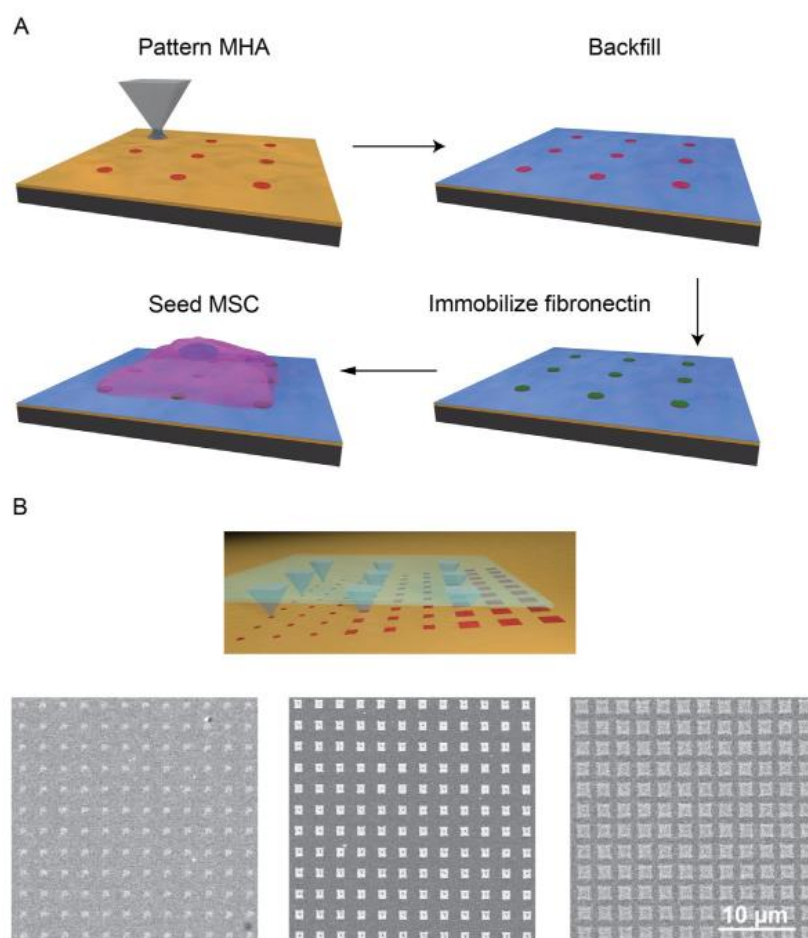


Figure 2.1 Polymer pen lithography (PPL) process used to generate extracellular matrix (ECM) protein patterns. (A) Schematic shows the major steps of this cantilever-free scanning probe technique which include: deposition of a template SAM followed by addition of a passivation layer, protein attachment to the patterned areas, and seeding cells on the molecular patterns. (B) Scheme for generating combinatorial libraries by tilting the polymer pen array. A range of feature sizes (475 nm to 1.2 μm) were obtained by controlling the tilt angle across one substrate. The resulting patterns were arranged in a 60 μm × 60 μm area, where each pen wrote a 15 × 15 array with 4 μm pitch distance. The resulting patterns were imaged by scanning electron microscopy after etching.

2.2 Materials and instrumentation

- (1) Reverse osmosis purified >18 MΩ H₂O (e.g. NANOpure) for rinsing and cleaning steps.
- (2) Ethanol (≥99.5%, Sigma-Aldrich, cat. no. 459844) for cleaning glass slides and preparation of solution.
- (3) Acetone (≥99.9%, Sigma-Aldrich, cat. no. 270725) for cleaning and photoresist lift-off.

- (4) 2-propanol alcohol (99.9%, Sigma-Aldrich, cat. no. 650447) for cleaning and silicon etching.
- (5) Shipley S1805 (MicroChem, cat. no. 10018321) photoresist.
- (6) Developer MF-319 (MicroChem, cat. no. 10018042) for developing the photoresist after the exposure.
- (7) 4" <100> Si wafer (Nova Electronic Materials, cat. no. STK8414) with 5000 Å thermal or wet oxide for photolithography.
- (8) Buffered HF improved (Transene Etchants, pH = 5.0) for SiO₂.
- (9) Si etchant was prepared by mixing 750 g of potassium hydroxide (≥99.995% (metals basis) Sigma-Aldrich, cat. no. 306568) and 500 mL of 2-propanol in 2 L NANOpure H₂O.
- (10) Heptadecafluoro-1,1,2,2-tetra(hydrodecyl)trichlorosilane (Gelest, cat. no. SIH5841.0) for SiF coating.
- (11) Toluene (≥99.5% Sigma-Aldrich, cat. no. 155004) for SiF coating.
- (12) Hard polydimethylsiloxane (h-PDMS) prepolymer was prepared by mixing 500 g vinyl dimethyl siloxane (Gelest, product code VDT-731) with 20 μL Pt divinyl tetramethyl disiloxane (Gelest, product code SIP 6831.2) and 344 μL 1,3,5,7-tetramethyl-1,3,5,7-tetravinylcyclotetrasiloxane (Gelest, product code SIT7900.0). The h-PDMS prepolymer was stirred for 5 days before use.
- (13) 25-35% (methylhydrosiloxane) 65-70% (dimethylsiloxane) copolymer (Gelest, product code HMS-301) for making h-PDMS.
- (14) 16-Mercaptohexadecanoic acid, (90%, Sigma-Aldrich) for forming a SAM on Au coated surface.

- (15) (1-Mercapto-11-undecyl)hexa(ethylene glycol) 1 mM in ethanol (99%, Asemblon, cat. no. 231043-011) for backfilling the surface after patterning to prevent nonspecific adsorption of proteins and cells.
- (16) Au etching solution was prepared by mixing an aqueous 20 mM solution of thiourea ($\geq 99.0\%$ Sigma-Aldrich, cat. no. T8656), with a 13.3 mM solution of iron(III) nitrate nonahydrate (99.99%, Sigma-Aldrich, cat. no. 254223) and hydrochloric acid solution (pH = 1) (37% Sigma-Aldrich, cat. no. 320331) in a 1:1:1 ratio. We recommend that this solution is freshly prepared prior to use. The etchant can be used for ~ 1 day, and then should be disposed of and re-made fresh.
- (17) Human plasma fibronectin (1 mg/mL, Millipore, cat. no. FC010) for protein immobilization.
- (18) Anti-human fibronectin produced in rabbit (Sigma-Aldrich, cat. no. F3648-5 ML) for immunofluorescence.
- (19) Goat ant-rabbit IgG (Invitrogen, cat. no. A11036) for immunofluorescence.
- (20) Au substrate, prepared by physical vapor deposition (i.e. e-beam or thermal evaporation) of 30 nm Au thin film onto a Si wafer or glass slide. Use of a Cr or Ti 5 nm adhesion layer is highly recommended. When possible, substrate should be used within one week of deposition.
- (21) Human alkaline phosphatase antibody (H-300) (Santa Cruz Biotechnology, cat. No. SC30203) for immunofluorescence
- (22) Phosphate buffered saline (PBS) 1 x, pH 7.4 (GIBCO, cat. No. 10010-023) for rinsing steps after protein immobilization and cell adhesion.
- (23) Confocal microscope (Nikon C-Si inverted laser confocal microscope)

- (24) Optical microscope (Zeiss Axiovert)
- (25) Plasma cleaner (PDC-001, Harrick Plasma)
- (26) Scanning probe lithography platform (Park XE-150, Park Systems)
- (27) E-beam evaporator (PVD 75, Lesker)
- (28) Human mesenchymal stem cells (Lonza, cat. no. PT-2501)
- (29) Mesenchymal stem cell growth medium (MSGCM, Lonza, PT-3001)

2.3 Methods

2.3.1 Fabrication of master arrays as molds for polymer pen arrays

Masters for molding polymer pen arrays are fabricated using conventional microfabrication techniques. The photolithography mask used for defining arrays consists of an array of circular holes arranged in a square lattice, where the hole diameter corresponds to the tip base width and the hole-to-hole pitch determines the pen-to-pen distance. The square arrays of holes are grouped into 2 cm × 2 cm arrays, this size was chosen because it easily fits onto standard glass slides.

To begin, spin-coat a 500 nm oxide-coated 4" Si (1 0 0) wafer with S1805 by spinning for 5 s at 500 rpm, followed immediately by 40 s at 4000 rpm, both with 500 rpm/s ramping rates. Soft bake the resist-coated wafer at 115 °C for 60 s, allow it to cool to room temperature, and then expose it in a mask aligner with a dose of ~75 mJ/cm². Note that overexposure is not typically problematic as it will translate to slightly taller pyramids while underexposure will cause the pattern transfer process to fail. Therefore, it is best to err on the side of overexposure. After exposure, develop the patterns in MF-319 for 60 s, rinse with DI H₂O for 10 s, and then blow dry with flowing N₂. It is important to note that the photolithography protocol outlined here with S8015 is just an example; the patterns can be defined using any photoresist and developer. If a

different resist is to be used, consult with the manufacture's data sheets and follow their recommended procedure with regard to exposure and development.

Once photolithography is complete, plasma clean the resist-coated wafer in an air plasma for 2 min at 10 W to remove residual photoresist from the hole regions. After plasma cleaning, submerge the wafer in a buffered oxide etch (BOE) for 6 min to transfer the resist patterns into the underlying oxide. Remove the wafer from the BOE solution, rinse with DI submerge the wafer in acetone for 5 min to remove the resist. After resist removal, sequentially rinse the wafer with isopropanol (IPA), and then blow dry with N₂.

Upon resist removal, place the wafer in an anisotropic KOH etchant solution. This solution consists of 30% w/w KOH in DI H₂O, stirring at 75 °C, with IPA added once the KOH reaches temperature in a 1:4 ratio of IPA:H₂O. Once the temperature of the etchant has stabilized, suspend the wafer in the etchant solution, below the IPA layer and facing the bottom of the container. Etching will take 50–70 min; the extent of etching can be checked by removing the wafer, rinsing with DI H₂O, blowing dry with N₂, and then imaging the tips in an optical microscope. By changing the focal plane, it should be possible to see individual pens converge to a point; if they converge to a square, the wafer should be returned to the etchant until this is no longer the case. Note that the orientation and level of the wafer in the etchant is important and care must be taken to keep the wafer consistently placed within the etchant solution.

Once the pyramidal pits have been etched into the Si, place the master in BOE for 5 min to strip the remaining oxide, and then rinse with DI H₂O and blow dry with N₂. Subject the masters to an air plasma for 2 min at 30 W to regrow a uniform oxide layer, and then place the masters in a desiccator with a solution consisting of 8 – 12 drops of heptadecafluoro-1,1,2,2-tetra(hydrodecyl)trichlorosilane in 2 mL of toluene and immediately pull vacuum on the

desiccator, taking care to mix the fluorosilane and start the vacuum as quickly as possible. Once the toluene begins to boil, turn off the vacuum and leave the masters exposed to the fluorosilane solution for 12 – 24 h. After silanization, immerse the masters in toluene for 5 min to remove any multilayers, and then blow dry with N₂. This step should render the masters hydrophobic, thus facilitating the removal of PDMS in later steps.

2.3.2 Fabrication of polymer pen arrays

Masters of a defined pen-to-pen pitch and array dimension will be used to generate their complementary polymer pen arrays. After thoroughly mixing 3.4 g of h-PDMS prepolymer with 1.0 g copolymer, place the h-PDMS mixture in a desiccator under vacuum for ~15 min to remove trapped air bubbles. During degassing, clean a glass slide by rinsing with IPA and then plasma clean in air for 5 min. Once the PDMS precursor is degassed and a glass slide is prepared, pour a few drops of the PDMS mixture on the master pen array and carefully place the glass slide on the PDMS drop. Let the PDMS cure in an oven at 80 °C for 24 – 48 h. After this baking step, the PDMS pen array should be cured and no longer flow in response to pressure. Peel off the glass slide from the surface of the master by carefully wedging a razor blade between the glass slide and the master and slowly lifting the glass slide to separate it from the master array. Using a razor blade, remove residual PDMS on the periphery of the PDMS tips and clean the surface with a N₂ stream.

2.3.3 Patterning of MHA SAMs

Prior to inking the tip array, place the array in an air plasma for 2 min at 10 W to render the surface hydrophilic. Next, drop cast 100 mL of a solution of 5 mM MHA in ethanol and let the solution evaporate for at least 10 min. Next, for integration into the scanning probe lithography system, mount the tip array on a magnetic holder using double-sided carbon tape and load it onto

the AFM head. Place an Au-coated no. 2 glass slide on the stage and move the x–y control stage so that the pen array is directly below the area of the substrate that will be patterned.

Bring the z-stage slowly into approach with the substrate, being careful not to crush the tips against the substrate. Once the pen array is about 100 mm away from the substrate, move the z-stage in small increments (i.e., ~10 mm). Contact between the pen array and the substrate can be visually identified by the extent of deformation of the polymeric tips upon contact with the surface; this is easily seen by a transition in color at the center of the tip from light (not in contact) to dark (just in contact) and then back to light (hard contact). For small features, gentle contact and small tip deformation is desired. Conversely, if large features are desired, greater tip deformation and harder contact with the substrate is required.

To level the polymer pen array optically, check the four corners of the tip array for contact with the substrate and make sure that all four corners experience the same amount of deformation. If the corners are in different degrees of contact, tilt the sample stage until the sample is level. In order to not damage the probes and ensure rapid leveling, it is ideal to only move one direction at a time (i.e., level the stage in the x-direction first), and make sure to raise the probes from the surface before tilting the stage up in either direction. To create uniform patterns, all four corners of the pen array should be equidistant from the substrate, that is, the amount of tip deformation should be uniform across all corners. A gradient of different feature size patterns can be generated by tilting the stage across the x- or y-axis as desired. The tilting angle will define the size of the features that can be generated, with areas that are in closer proximity to the substrate giving rise to larger features (Figure 2.1B).

After leveling, the desired pattern should be designed and executed by the patterning software. After printing, the sample will be patterned with SAMs of the alkanethiol, however,

these patterns are only directly visible through AFM measurements. In order to rapidly visualize the patterns and ensure successful pattern transfer, the sample can be broken in half and a portion of the patterned substrate can be etched to visualize the patterned features. This procedure works because SAMs form an etch mask where the unpatterned regions will be rapidly removed. The residual Au features can be easily seen in an optical microscope or scanning electron microscope (SEM). To etch the Au on the sacrificial section of the sample, incubate the sacrificial area in a solution of gold etchant for ~7 min. The incubation time in the etching solution will vary according to the thickness of the Au film, with thicker films requiring longer etching times. In general, the rate of etching corresponds to approximately 4 nm/min. To stop the etching, rinse copiously with DI H₂O and blow dry with a N₂ stream. Following etching, the patterns will appear light against a dark background under optical microscopy or SEM. If the patterns are satisfactory, take the portion of the substrate that was not etched and proceed with the protein immobilization steps.

2.3.4 ECM protein immobilization on MHA patterns

Following MHA deposition, backfill the unpatterned Au areas by submersing the substrate in a 1 mM ethanolic solution of (1-mercapto-11-undecyl)hexa(ethylene glycol) for 1 h to prevent nonspecific attachment of biomolecules or cells. Next, remove the substrate and rinse copiously with ethanol and dry with a N₂ stream. Place the substrate in an aqueous solution of 10 mM Co(NO₃)₂ for 5 min. During this step, the cobalt ions chelate to the carboxylic acid groups on MHA, thus directing the attachment of fibronectin without compromising binding site availability and protein functionality. Rinse the substrate with ethanol followed by water to remove any residual Co(NO₃)₂ solution, and then dry with N₂, place the substrate in an aqueous solution of 50 mg/mL fibronectin in 1X PBS and incubate the sample overnight on a shaker at 100 rpm and 4 °C.

After fibronectin immobilization, rinse with copious amounts of 1X PBS and dry with a N₂ stream. At this point, the substrate should present fibronectin patterns and can be subsequently used for cell adhesion studies. To verify protein immobilization, proceed to immunostaining by incubating the substrate in a 1:100 solution of human anti-fibronectin antibody (produced in rabbit) in 1 PBS on a shaker stirring (100 rpm) overnight at 4 °C. Remove the substrate from the primary antibody solution, rinse with 1X PBS, and add a 1:250 solution of fluorophore-labeled secondary antibody (goat anti-rabbit AF 568) diluted in 1X PBS for 1 h. Rinse with 1X PBS, NANOpure H₂O dry under flowing N₂ and then image with fluorescence microscopy. The fluorescence micrograph shows fluorescently labeled fibronectin patterns arranged in a 15 × 15 array over a 60 μm × 60 μm area. These patterns were generated using an array with a pen-to-pen spacing of 80 μm (Figure 2.2A).

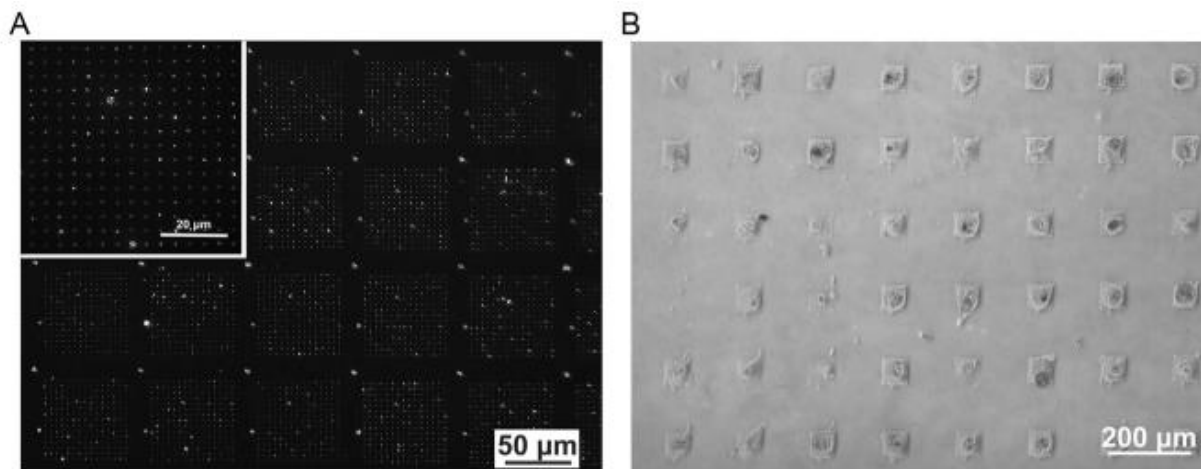


Figure 2.2 (A) The resulting fibronectin patterns can be visualized by immunofluorescence staining with AlexaFluor568-conjugated antibody against fibronectin. The pitch of the master array used to generate these features corresponded to 80 μm. (B) Optical micrograph of mesenchymal stem cells (MSCs) seeded on fibronectin adhesion sites displays cells attached to the patterned square regions. A master array having a pitch distance of 180 μm was used to generate these patterns.

2.3.5 Combinatorial screening of cell attachment

Combinatorial screening of MSC adhesion is necessary to first understand how fibronectin adhesive sites affect cell spreading, adhesion, and subsequent differentiation. Prior to the start of experiments, culture human MSCs under standard growth conditions in normal growth medium at 37 °C with 5% CO₂. We recommend the use of MSCs between passages 2 and 5. Proceed to seed MSCs on patterned substrates presenting a gradient of fibronectin feature sizes at a density of 3000 cells/cm²; this cell density is recommended to ensure that a single cell can be attached to each patterned area (Figure 2.2B). At this point, we recommend handling the substrate with care to prevent cell detachment.

The total area of fibronectin presented to the cell within a patterned region can be modified by defining the dimensions of the array prior to patterning the MHA template. In the case of MSCs, we have previously shown that a total projected area of 3600 μm (60 μm × 60 μm) is sufficient to induce MSC attachment without compromising cell viability. Within this patterned region, one can easily probe how MSC spreading changes as a function of total amount of fibronectin immobilized. At this point, it is evident that combinatorial screening is an efficient approach to determine the total area of fibronectin necessary to obtain fully spread MSCs over a patterned region, because it allows a wide variety of parameters to be explored in a single experiment. After 1 week of cell growth on the patterns, the extent of cell attachment and spreading can be monitored by immunofluorescence using standard protocols for cytoskeleton staining, such as actin staining with phalloidin-AF568, and immunofluorescence using primary and fluorescently labeled secondary antibodies. As shown in below, cells cultured on patterns presenting 225 μm² of total fibronectin lead to complete attachment of MSCs (Figure 2.3A, B).

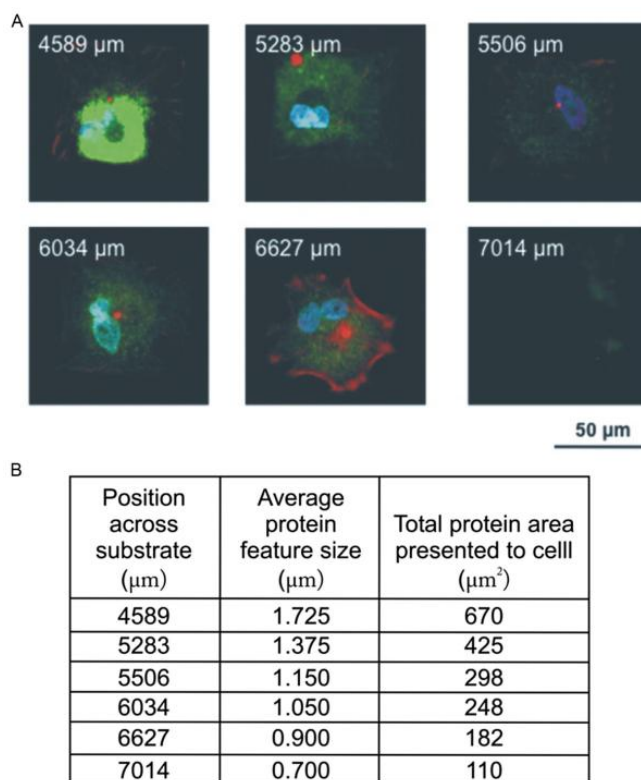


Figure 2.3 Stem cell adhesion study using combinatorial fibronectin patterns to evaluate cell attachment and spreading. (A) A tilted polymer pen array (180 μm pen spacing) was used to generate 15 \times 15 array of fibronectin features spaced by 4 μm . MSCs were cultured on these patterns for 1 week and subsequently stained for alkaline phosphatase (ALP) (green), actin (red), and the nucleus (blue). The labels on the resulting patterns shown in (B) indicate the x-position of patterns of a certain feature size across a substrate. The total area presented to the cell can be obtained by squaring the average protein feature size and multiplying by 225 for a 15 \times 15 array of dot features.

2.3.6 MSC differentiation and analysis

To investigate the effect of fibronectin feature size on MSC differentiation, generate 1 μm and 300 nm fibronectin homogeneous size patterns by leveling the polymer pen array. Proceed to seed MSCs as described earlier and culture the MSCs in the absence of osteogenic differentiation factors for 1 week. Harvest the cells and collect mRNA to quantify expression levels of osteogenic biomarkers, such as alkaline phosphatase (ALP), osteocalcin (OCN), and osteopontin (OPN), using RT-PCR and Western Blotting. In general, the primer sequences for these targets can be

found in the literature or obtained commercially. Qualitative expression of osteogenic markers can be monitored by immunofluorescence (Figure 2.4A). Depending on the application, certain cytoskeletal components, such as actin, can be easily labeled by commercially available kits, without the need for specific antibodies. Specifically, 300 nm diameter fibronectin features were found to be more effective at inducing osteogenesis and expression of related biomarkers, such as ALP, than 1 μm diameter fibronectin patterns, as measured by RT-PCR (Figure 2.4B) and Western Blotting. It is important to point out that elevated expression of osteogenic markers occurred in the absence of differentiation medium, solely as a response to nanoscale structures, even when the total amount of fibronectin presented to MSCs was held constant. These results further demonstrate the importance of designing substrates that present micro- and nanoscale cues to program-specific cell processes.

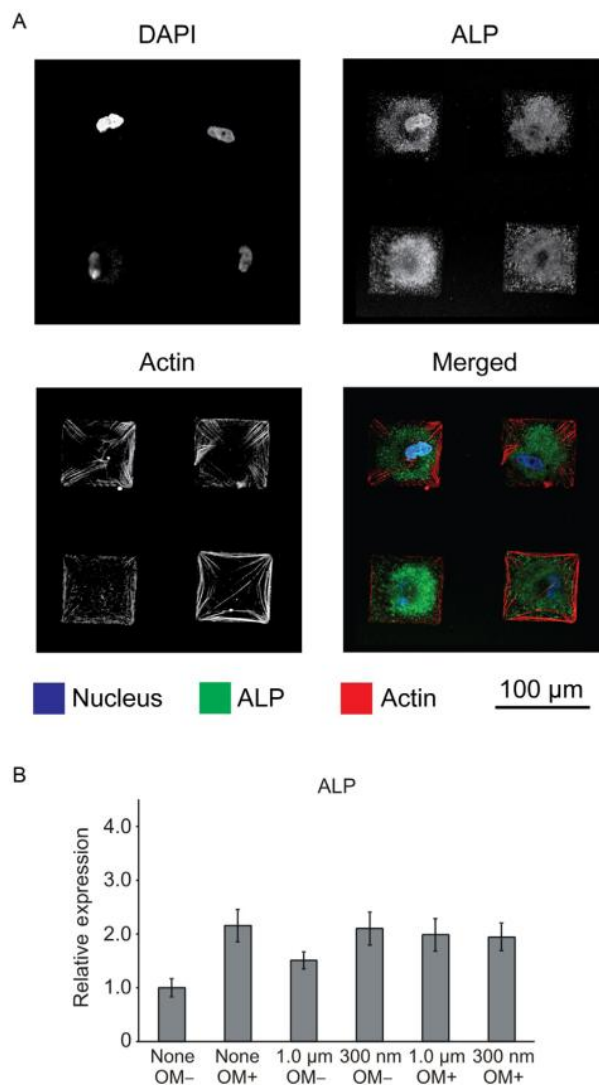


Figure 2.4 Immunofluorescence micrographs show the expression of osteogenic marker alkaline phosphatase (ALP) in MSCs cultured on homogeneous (300 nm diameter) fibronectin patterns. (A) The confocal microscopy images in the merged channel display samples stained for actin in red, ALP in green, and the nucleus in blue. (B) Quantitative RT-PCR results for ALP were normalized to GAPDH levels. The bar graph also displays results that were normalized to the negative control in the absence of osteogenic media (OM-).

2.4 Discussion

The work by Giam et al. provides a compelling example of what can be learned in a biological context by using PPL. Key to the success of this study was the ability to first generate combinatorial libraries of features for high-throughput screening and then select experimental

conditions and generate statistically significant homogenous patterns.¹² By using these methods, the authors addressed the question of how fibronectin feature size and the formation of focal adhesions mediate osteogenic differentiation. Specifically, 300 nm diameter fibronectin features were found to be more effective at inducing osteogenesis and expression of related biomarkers than 1 μm diameter fibronectin patterns, as measured by RT-PCR and Western Blotting. It follows then that the cell–substrate binding signaling events that occur in the ECM are transduced to biochemical cues that trigger intracellular differentiation events. To better understand this phenomenon, focal adhesion kinase (FAK) phosphorylation was studied, an event known to precede expression of osteogenic markers, which led the authors to discover that levels of phosphorylated FAK indeed increased when MSCs were cultured on 300 nm fibronectin patterns, even when the total amount of fibronectin beneath a given cell was conserved. These results further demonstrate the importance of designing substrates that present micro and nanoscale cues to program specific cell processes.

More generally, the outlined protocol presents PPL as a highly versatile and practical approach for generating a range of protein patterns in a high-throughput fashion. This cantilever-free scanning probe technique, which relies on elastomeric pen arrays to deposit molecules, offers an attractive method for generating bioactive surfaces that present gradients of ligand density in addition to protein patterns of uniform size by simply tilting the pen array or holding it level, respectively. An important advantage of this technique over other microcontact printing approaches is the ability to generate thousands of arbitrary patterns rapidly over large-scale areas without the need for fabricating multiple masks, thus enabling rapid prototyping. Patterning over large areas is particularly important for experiments in cell biology, where a statistically significant sample size is necessary for both mRNA and protein quantification. More importantly, tilting the

polymer pen array allows one to generate combinatorial libraries where both size and density of the patterns are controlled with high precision and registration on the substrate. For the life sciences, this feature is of particular interest as the spatial profiling of several cell–substrate interactions opens an attractive avenue to elucidate changes in the biochemical signaling pathways of the cellular machinery. In addition, PPL provides a highly robust method that, in principle, can be coupled with microscopy techniques and surface analytical techniques to obtain spatiotemporal profiles of cell–receptor interactions and enzyme activity profiles that would yield quantitative information for understanding the kinetics of events at the single cell level.

While this chapter describes the methodology to template features of MHA on Au-coated substrates, this approach can be extended to deliver different inks to generate substrates presenting multiple functionalities. Multiplexed printing can be achieved with the assistance of an inkjet-printing platform to first deliver the inks to microfabricated reservoirs.³⁵ By choosing the periodicity of the reservoirs to match the pen-to-pen spacing of the pen, it was possible to achieve perfect registration and eliminate cross-contamination. Inking different pens in the array with different inks allows one to print features of varying composition, adding another experimental handle to the capabilities of PPL. In particular, having combinatorial libraries of multiple ligands would allow scientists to design systematic studies ranging from fundamental questions, such as how ECM factors affect cell polarization, to application-driven questions related to high-throughput drug screening or tissue engineering.

2.5 Conclusions

PPL allows one to construct molecularly patterned surfaces of sizes large enough to be applicable in biologically relevant studies that contain features defined in high resolution. This chapter presents an approach to pattern small molecules that form SAMs as templates for an ECM

protein (here, fibronectin) in order to define adhesion sites for cellular attachment. After protein immobilization, the surfaces were incubated with cells, and their behavior was studied using standard cell biology techniques, such as immunofluorescence, RT-PCR, and Western Blotting. Critical to the success of this work was the ability to first create a gradient of feature sizes that allowed for the screening of reaction conditions of interest. This powerful paradigm of utilizing combinatorial screening in conjunction with uniform samples composed of region of interest conditions can potentially be applied to many cell systems beyond MSCs.

CHAPTER THREE

Nanoscale Patterning Directly Controls Actin Fiber Formation and Cell Behavior

Material in this chapter is based upon on-going work:
Cabezas, M. D.,* Meckes, B. R.,* Mirkin, C. A. and Mirksich, M. (*Manuscript in preparation*)
*Denotes equal contribution

3.1 Introduction

Extracellular matrix (ECM) ligand density and arrangement influence cellular behavior and function by modulating cell shape and cytoskeletal arrangement, recruiting signaling proteins, and altering the distribution and interactions between cell receptors and extracellular matrix proteins, which ultimately impact cell survival, migration, and differentiation.³⁶⁻³⁷ In order to understand how changes in cell geometry and ECM ligand density affect cell behavior, micro- and nano-patterning approaches – i.e. micro-contact printing,³⁸⁻³⁹ laser ablation lithography,⁴⁰ and micelle nanolithography⁴¹⁻⁴³ – have been used to template the arrangement and density of adhesion ligands to define cell shape,⁴⁴ focal adhesion size,⁴⁵ and cell contractility⁴⁶⁻⁴⁷ and ultimately understand how these parameters drive cell adhesion, polarization, division, and differentiation.⁴⁸⁻⁴⁹ However, controlling actin cytoskeletal arrangement and contractility within cells remains challenging as actin fiber assembly is intrinsically coupled to maintaining cell shape within a single patterned geometry. Therefore, achieving higher order control over the arrangement of the actin cytoskeleton by decoupling cell shape and actin fiber architecture in a user-defined fashion would lead to new avenues for modulating and systematically studying cell behavior.

Directing fibers that have a specific arrangement remains challenging as focal adhesion formation is a dynamic process where adhesion complex reassembly occurs because the ECM is continuous within a defined geometry. Therefore, we reasoned that both the geometry and ligand arrangement must be defined through the printing of discrete focal adhesion-sized features within a single pattern geometry; this would lead to the assembly of focal adhesion complexes that direct actin fiber formation. Exploring how these two factors, geometry and ligand arrangement, affect cell behavior presents a significant challenge because screening an extensive parameter space to identify which distinct variations can alter cytoskeletal architecture and shape is prohibitively time

consuming. High-throughput and rapid prototyping tools have enabled the discovery of novel materials with desired properties for a broad range of fields including drug discovery and energy storage. A high-throughput approach to rapidly prototype libraries of pattern geometries and ligand arrangements remains necessary to discover pattern combinations that have desired effects in cellular behavior by controlling the homogeneity of cells in cultures by defining cell shape and direct the sub-cellular organization of complex structures and ultimately influence cell behavior. Generating such libraries remains challenging with conventional approaches where unique geometries and ligand arrangements can only be patterned serially or are mask-dependent and have limited resolution.

To impart organization and directionality to the actin cytoskeleton, we used a cantilever-free scanning probe lithographic technique, termed polymer pen lithography (PPL), to template sites for cell adhesion where both the geometry and the subcellular arrangement of the adhesion features of the pattern was addressed. This massively parallel technique allows to rapidly generate unique and controlled patterns that can be used as combinatorial libraries for cell adhesion studies and cell-based assays with molecular readouts.^{14, 50-53} Here, we use this technique to prototype nanopatterns of fibronectin that alter the arrangement of actin fibers within cells. Significantly, we demonstrate that arbitrary ECM pattern arrangements can be easily explored and small modifications in the pattern arrangement can be used to modulate cytoskeletal organization. Using our patterning approach, we demonstrate that we can modulate fibers along the long axis for square geometries and generate highly periodic radial fibers in cells on circular substrates. Our enhanced control over actin cytoskeleton allows us to direct mesenchymal stem differentiation down osteogenic cell fates.

3.2 Methods

3.2.1 Substrate Preparation

Glass slides (1.9 cm x 1.9 cm, 0.5 mm thick, Ted Pella) were sonicated for 30 min, rinsed in ethanol and dried under a stream of N₂. They were mounted in an electron-beam evaporator (Lesker) and when vacuum reached 2×10^{-7} mTorr, 5 nm of Ti and 35 nm of Au were evaporated. Polymer pen arrays were prepared using conventional photolithography techniques according to published methods. Arrays were coated with an ethanolic solution of 10 mM MHA (16-mercaptohexadecanoic) (Sigma) solution for 2 min and dried under N₂. After mounting the Au substrate and pen array on the PPL system (Tera Fab M Series, Tera Print), the chamber humidity was held at 45% for patterning. Patterns were programmed in the software with tip-substrate dwell times of 2s. Feature size and quality was confirmed by sacrificing a portion of the substrate, etching Au in the unpatterned areas with a mixed aqueous solution of 13.3 mM Fe(NO₃)₃ and 10 mM thiourea, and observing the results under an optical microscope. The patterned substrates were then immersed in an ethanolic solution of 10 mM 1-mercapto-11-undecyl hexa(ethylene glycol) (Sigma) solution for 1 h to reduce nonspecific protein adsorption. After rinsing with ethanol and drying with N₂, the substrates were exposed to 50 µg/mL of human plasma fibronectin (Millipore) in phosphate buffered saline (PBS) and shaken overnight at 4 °C.

3.2.2 Cell Culture

Human MSCs (Lonza) were cultured at 37 °C with 5% CO₂ in MSC growth medium supplemented with MSC growth supplements (Lonza), L-glutamine (Lonza), and gentamycin sulfate amphotericin-1 (Lonza). The cells were used before passage 2. For chemical induction of differentiation, cells were cultured in osteogenic media (Lonza) composed of MSC growth

medium supplement, L-glutamine, penicillin/streptomycin, and β -glycerophosphate (Lonza). Approximately 15,000 cells were seeded per substrate, which corresponds to about 7,500 cells/cm²

3.2.3 Immunofluorescence and Confocal Microscopy

Cells cultured on substrates were fixed in 3.7% paraformaldehyde in PBS for 12 min and then gently washed three times with PBS. Cells were permeabilized using 0.3% triton X-100 in PBS for 1 min and blocked with a 0.1% Triton X-100 in PBS solution with 3% of bovine serum albumin for 1 h. Next, samples were labeled for actin using Alexa Fluor 568-labeled phalloidin (ThermoFisher) according to manufacturer's instruction. Samples were gently washed three times in PBS and mounted onto glass coverslips using Prolong Gold Antifade reagent with DAPI (ThermoFisher). Cells were imaged using a Zeiss inverted laser confocal microscope.

3.2.4 Image Analysis

To generate heatmaps, images of fluorescence images of fixed/stained cells were aligned, stacked, averaged and pseudo-colored to represent regions of high and low density using ImageJ. The orientation of actin fibers in cell micrographs was analyzed using a custom Matlab script that determines orientation using previous reported gradient analysis methods. Briefly, a 5×5 Sobel Filter was used to detect fluorescence gradients; the X and Y components of the gradient were then utilized to determine the orientation and magnitude of the gradient.⁵⁴ A grayscale threshold, as determined using Otsu's method,⁵⁵ was applied the magnitude gradient image to eliminate noise. For square and anisotropic square shaped patterns, fibers were detected within the entire cell as well as those within a region of interest (ROI) that was drawn to exclude fibers around the edge of the cell. Histograms of pixel orientation were generated for each cell after grouping fiber orientations along folding mirrored axes (e.g. -45° and 45°).

For detection of fibers orientation in circular patterns (radial vs circumferential) , the center of the cell was detected by fitting a circle around the cells (details for this procedure are included within the supporting information) to identify the centroid. The pixel alignment was determined by comparing the detected pixel orientation in comparison to the radial coordinates of the pixel around the centroid. The fibers were classified as either radial ($\pm 15^\circ$ from the radial coordinate), circumferential ($90 \pm 15^\circ$ from the radial coordinate), or indeterminate (fiber not fitting within the first 2 groupings). Histograms of the distribution of the fibers were then generated. Fast Fourier transform (FFT) analysis was used to determine the angular periodicity of the fibers within a cell.

3.3 Results and Discussion

3.3.1 Library Pattern Generation

We used polymer pen lithography to rapidly generate patterns with varying geometries and arrangements. Pen arrays consisting of $\sim 10,000$ polymeric tips were inked with 16-mercaptohexadecanoic acid (MHA) and loaded to a PPL instrument. After specifying the printing parameters (i.e. dwell time and extension length), patterns presenting MHA features were generated on Au coated substrates (Figure 3.1A). This iteration of steps was repeated for all designs. Patterns were validated by etching a portion of the Au-coated glass substrates to reveal the printed features that resulted after MHA patterning (Figure 3.1B). Next, the MHA patterned slides were treated with an ethanolic solution containing mercapto uncedyl(hexaethylene) glycol to backfill any exposed Au with a chemically inert monolayer to prevent non-specific protein interactions. Fibronectin was then introduced to the surface where it adsorbed to the MHA features due to non-specific interactions (Figure 3.1A). In this way, cell-adherent features that promote the attachment of cells were defined on the Au coated slides. Fluorescence micrographs show the

discrete localization of antibody-labelled fibronectin on the surface in a pattern resembling the MHA features (Figure 3.1C).

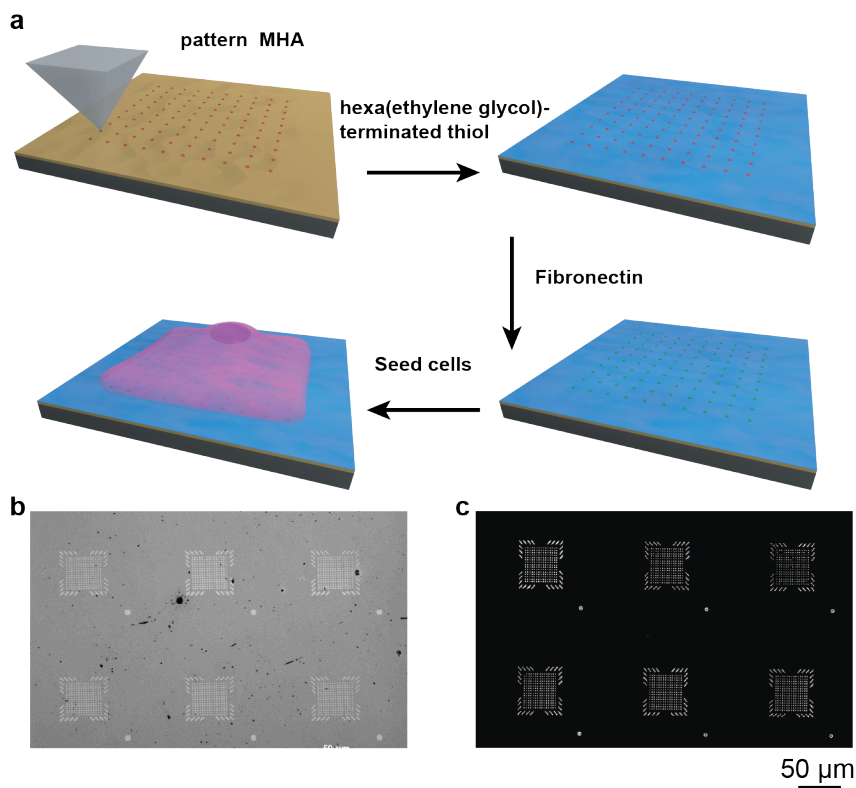


Figure 3.1 (A) Scheme for generating patterns of fibronectin features using PPL. (B) An etched Au-coated substrate reveals printed MHA features printed according to a user-defined pattern. (C) Fluorescence micrograph of antibody stained fibronectin that has selectively adsorbed to the MHA.

3.3.2 Patterning cells in square-shaped geometries

Human mesenchymal stem cells (hMSCs) were seeded and cultured overnight on square patterns ($54\ \mu\text{m} \times 54\ \mu\text{m}$) having features arranged in a dot matrix configuration, where the center-to-center distance between each feature corresponds to $3\ \mu\text{m}$ (Figure 3.2A), to observe the geometric-dependent architecture of cytoskeleton. The pattern dimensions, feature size and adhesion protein density were chosen based on previous work that show that these features support hMSC attachment and spreading. After fixing the hMSCs, we proceeded to stain the actin cytoskeleton with a fluorophore-labeled phalloidin and image using confocal microscopy.

Heatmaps generated from the fluorescence micrographs of the actin cytoskeleton demonstrate that the square dot matrix pattern does not induce any directional assembly of actin filaments (Figure 3.2B, C). Nevertheless, we observed the formation of stress fibers along the periphery of the patterned square shape in most of the hMSCs. This preliminary observation led us to design a unique set of patterns that: 1) had a center region presenting features arranged in a uniform square dot matrix to provide sufficient ligand density to induce and maintain cell attachment and 2) a region along the periphery of the pattern where the orientation and density of features was arbitrarily modified. For these patterns, we only generated shapes that had a 1:1 aspect ratio in order to avoid induced directionality due to aspect ratio effects.

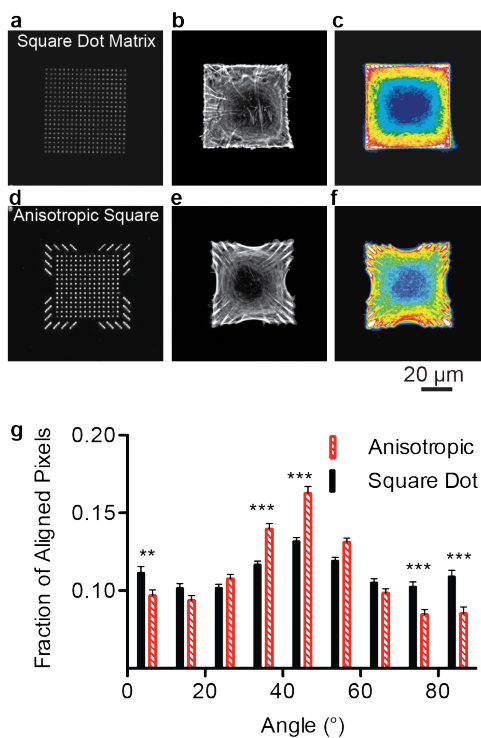


Figure 3.2 Actin fiber orientation within cells on square substrates. (A) Micrograph of an etched gold substrate with an MHA square dot matrix pattern. (B) Representative image of the actin cytoskeleton of a cell on a square dot matrix pattern. (C) Heatmap of the actin fibers in cells on a square dot matrix substrate (n=50). (D) Micrograph of an etched gold substrate with an MHA anisotropic square pattern. (E) Representative image of the actin cytoskeleton of a cell on an anisotropic square pattern. (F) Heatmap of the actin fibers in cells on a anisotropic square substrate (n=50). (G) The actin fiber orientation within cells on anisotropic and square dot matrix patterns.

We reasoned that the assembly of stress fibers within the cell interior can be controlled by changing the directionality and density of fibronectin along the periphery of the pattern. Fluorescence micrographs show that patterns with denser fibronectin features located at the corners of the squared-shaped geometries induce higher alignment of actin fibers along both diagonal axes (Figure 3.3). When we varied the feature directionality such that it was either aligned or perpendicular to the diagonal axis, both sets of features resulted in fibers along the long axis. However, by orienting fibers along the diagonal axis, the number of fibers originating from the corners was better controlled. For other shape variants, fibers originate arbitrarily from the periphery of the cell (Figure 3.3).

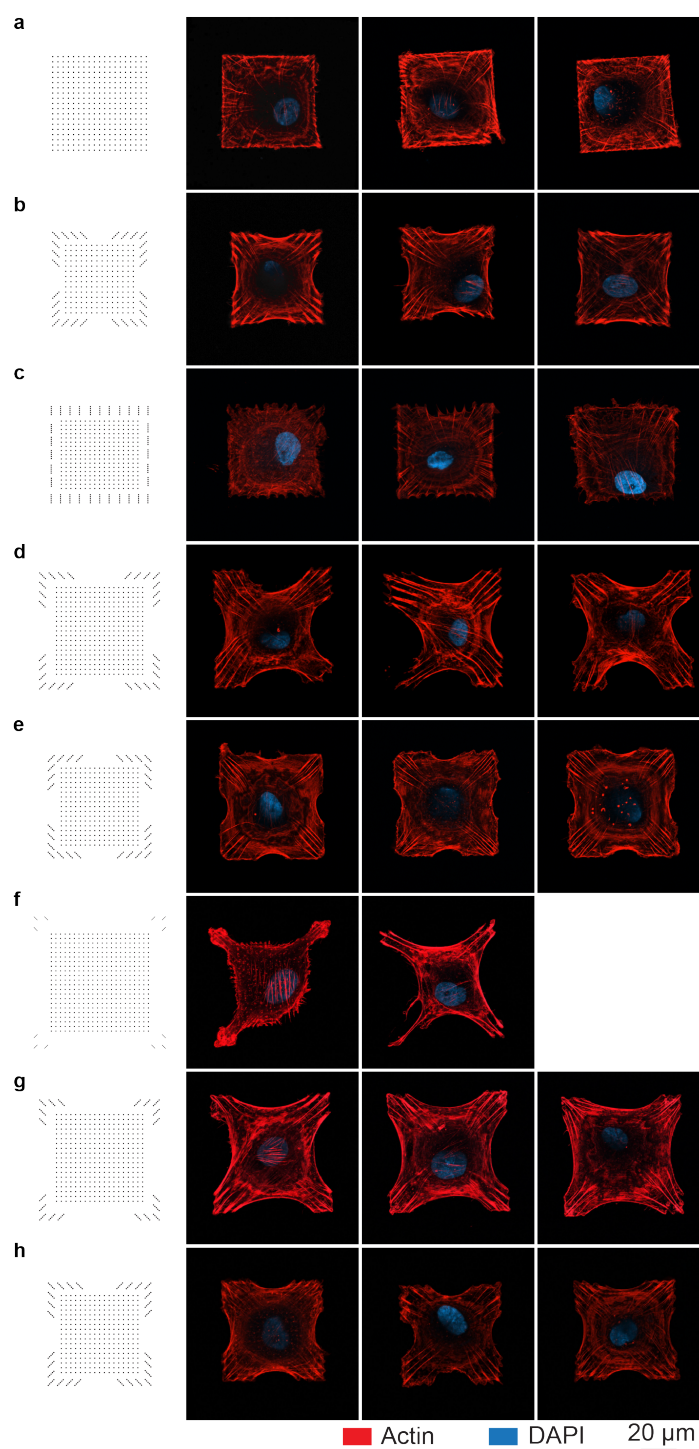


Figure 3.3 Set of patterns used to identify cytoskeletal controlling features in a square geometry. (A)-(G), Computer generated images of the programmed fibronectin features patterned on gold substrates (Panel 1). Representative images of the actin cytoskeleton (red) for cells on these patterns are shown along with the nucleus (blue) (Panel 2-4).

From this preliminary screen, we identified an anisotropic pattern design that directs fibers along the long axes (Figure 3.2D). Patterns with a similar arrangement but different areas had no effect on the fiber arrangement suggesting that actin alignment stems from the arrangement of features at the corners and is invariant of the size of the pattern (Figure 3.3). To quantitatively assess actin fiber directionality, we compared cells on the anisotropic shape (Figure 3.2E) to cells on a control substrate consisting of a square dot matrix (Figure 3.2B). Again, the fluorophore-labeled actin cytoskeleton was evaluated by imaging cells on the patterns with confocal microscopy. Heat maps of the average intensity of actin show preferential alignment of fibers toward the interior of the cell for anisotropic patterns (Figure 3.2F). Furthermore, we quantified fiber orientation using a gradient detection method to confirm that fiber alignment indeed increases along the long axes ($+45^\circ$ and -45°) for cells on anisotropic patterns compared to the square dot matrix (Figure 3.2G).

To assess whether this approach could be applied more generally to other cell types, we seeded NIH 3T3 fibroblasts on a unique set of patterned shapes, but with smaller dimensions ($30\ \mu\text{m} \times 30\ \mu\text{m}$) to compensate for the smaller footprint of these cells. The fluorescence micrographs reveal that the architecture of the actin cytoskeleton of these cells was different than the hMSCs with few fibers spanning from the periphery to the interior of the cells. When we measured the orientation of the actin cytoskeleton for the entire the cell, no significant differences in fiber alignment were detected; we hypothesized that this was because fibers at the periphery of the cell that support cell shape overwhelm any signal from the interior fibers at the center of the cell body (Figure 3.4A-D). To determine whether this was indeed true, we excluded the peripheral fibers from the analysis and then measured only fibers within the interior of the cell (Figure 3.4E). Indeed, preferential orientation along the long axis was detected within the anisotropic pattern,

while this bias is not observed for the dot matrix pattern (Figure 3.4F). Though the actin architecture of the 3T3 cells and hMSCs is globally very different, patterning fibronectin features allows for controlling the actin cytoskeleton.

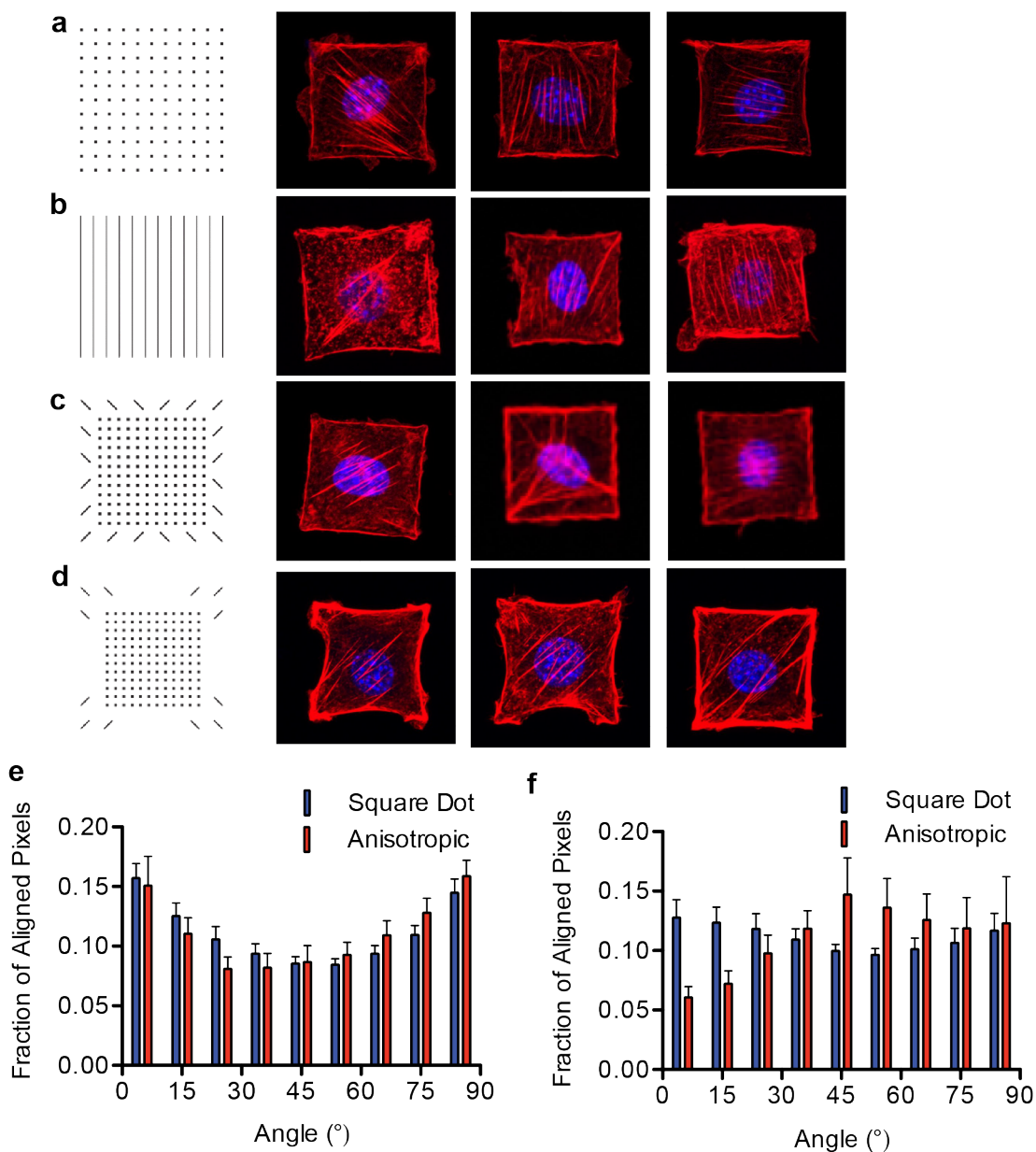


Figure 3.4 3T3 Cells grown on square patterns. (A)-(D) Computer generated images of the programmed fibronectin features patterned on gold substrates (Panel 1). Representative images of the actin cytoskeleton (red) for cells these patterns are shown along with the nucleus (blue) (Panel 2-4). (E) Actin fiber orientation in 3T3 cells on square dot matrix and anisotropic patterns. (F) Fiber orientation in 3T3 cells with the peripheral fibers excluded.

3.3.3 Patterning Cells in Circular Geometries

In addition to examining the arrangement of fibers in square geometries, the ability to modulate cytoskeletal orientation through nanopatterning within circular geometries was also evaluated. To maintain a constant cell spreading area between circular and square geometries, a radius of 31 μm was used for all circular geometries. Again, a set of patterns was generated to examine parameters that might affect actin fiber alignment (Figure 3.5). For this study, our set of structures varied in two-ways: 1) the introduction of concentric rings of features within the circular pattern and 2) the modulation of the arrangement of features along the periphery. We selected these patterning parameters because we were interested achieving control over the formation of transverse fibers and circumferential fibers.

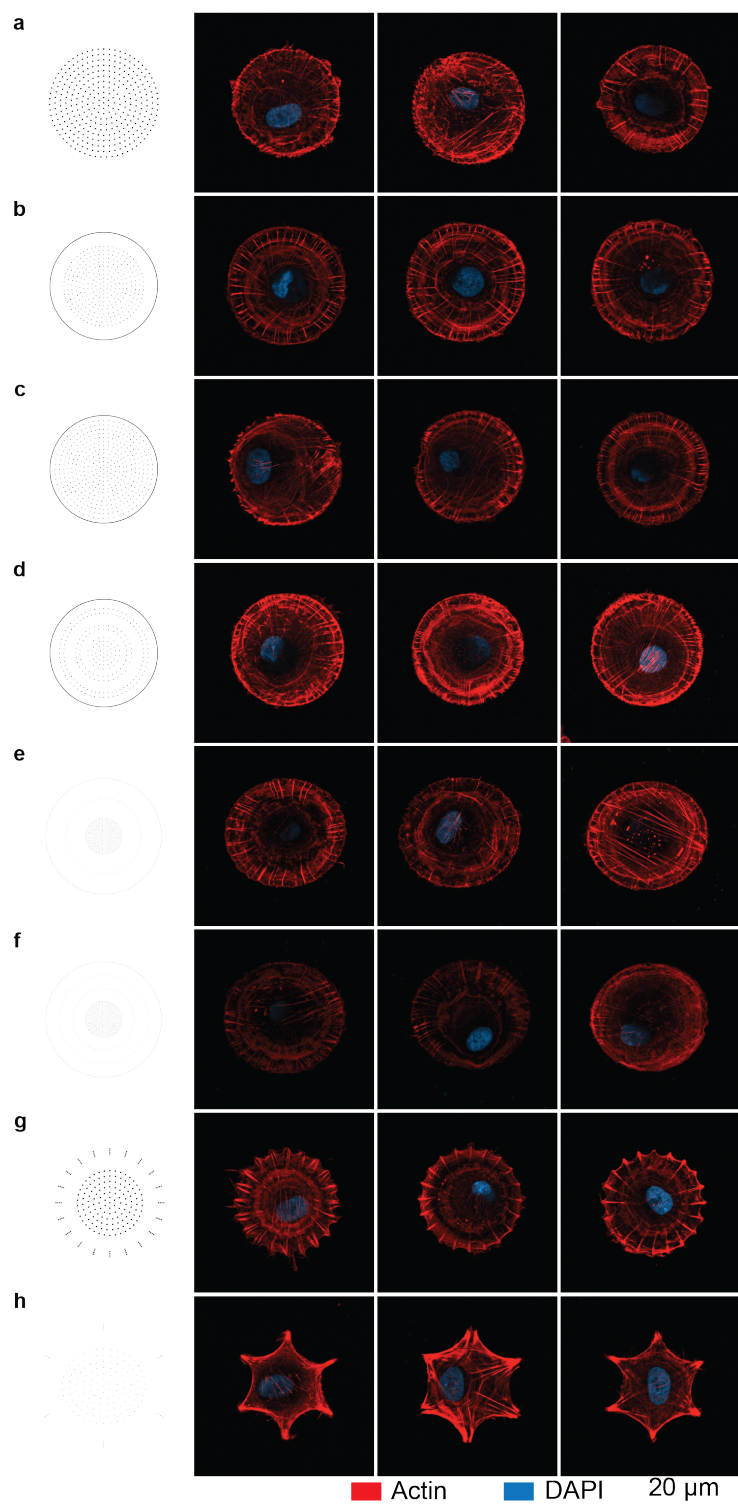


Figure 3.5 Set of patterns used to identify cytoskeletal controlling features in a circular geometry. (A)-(H), Computer generated images of the programmed fibronectin features patterned on gold substrates (Panel 1). Representative images of the actin cytoskeleton (red) for cells on these patterns are shown along with the nucleus (blue) (Panel 2-4).

Fluorescence micrographs confirmed the formation of circumferential and radial actin fibers in all the circular shapes. Circular shapes with concentric rings of different feature densities did not significantly change the circumferential fiber distribution within the cells (Figure 3.5A-F). However, when we oriented features such that they were aligned radially to the center of the circle, actin fibers formed along these features in a predictable fashion (Figure 3.5G).

From these images, we identified a pattern consisting of 20 features arranged around the edge that induced the formation of distinct radial fibers that follow the underlying pattern distribution (Figure 3.6). We quantitatively compared the formation of radial fibers and circumferential fibers between the 20-point circular shape and circular patterns having a uniform distribution of dot features (Figure 3.6A, D). Heatmaps of the actin architecture led us to believe that there is a periodicity in the radial fibers (Figure 3.6B, E). However, it is not possible to discriminate radial and circumferential fibers that overlap within images (Figure 3.6C, F). In order to assess the periodicity of the fibers, the local fiber orientation was determined and the fibers were classified as either radial or circumferential depending on the local orientation of the fiber. Assessment of the angular distribution of the radial fibers reveals a clear periodicity for the 20-point circular pattern, while no obvious periodicity is observed for a dot matrix circle (Figure 3.6G). Fast Fourier transform analysis of the distributions confirms the 18° periodicity for the 20-point circles, which is not present in the dot-matrix circles (Figure 3.6H). This result agrees exactly with the designed periodicity within this structure.

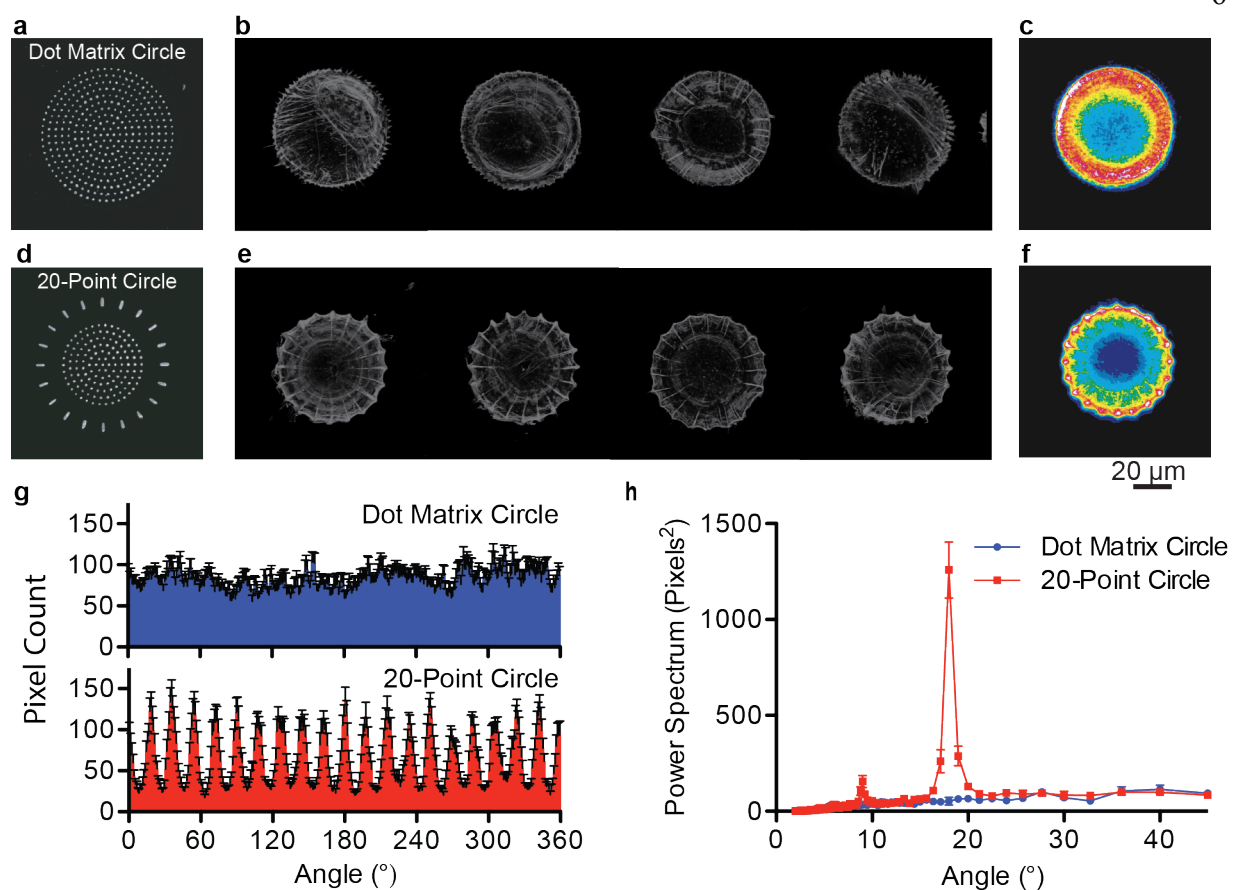


Figure 3.6 Actin fiber orientation within cells on circular substrate. (A) Micrograph of an etched gold substrate with an MHA dot matrix circle pattern. (B) Representative images of the actin cytoskeleton of cells seeded on dot matrix circle patterns. (C) Heatmap of the actin fibers in cells on dot matrix circles ($n=50$). (D) Micrograph of an etched gold substrate with an MHA 20-point circle. (E) Representative images of the actin cytoskeleton of cells seeded on 20-point circles. (F) Heatmap of the actin fibers in cells on the 20-point circle ($n=50$). (G) The distribution of radial fibers within the cells as a function of angle going around the cell for dot matrix and 20-point circle pattern. (H) FFT of the angular distribution of the radially oriented actin fibers within cells on the substrate.

3.3.4 Focal Adhesion Distribution Changes on Patterned Surfaces

Since focal adhesion complexes physically link the actin cytoskeleton with the ECM, we were interested in observing the distribution of focal adhesions in response to the underlying patterns. Immunofluorescence micrographs of vinculin, a focal adhesion protein, show that the focal adhesions selectively form along the periphery of the cell in locations defined by the

underlying pattern (Figure 3.7A-D). Indeed, actin fibers travel along the pathways defined by the focal adhesions towards a defined direction. Together, these results demonstrate that the underlying pattern geometry and distribution of adhesive cues leads to focal adhesion formation at desired locations and drives actin cytoskeletal arrangement.

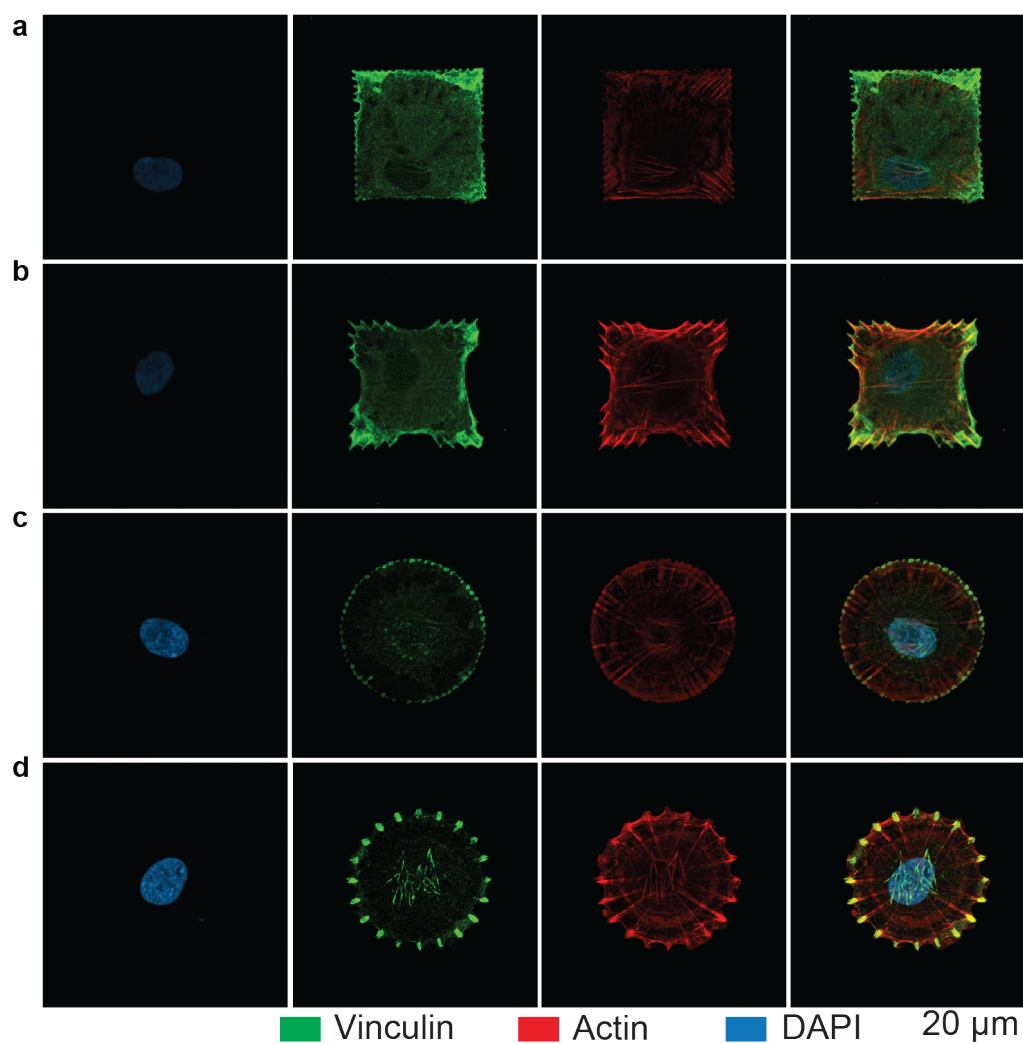


Figure 3.7 Micrographs of the focal adhesions and actin cytoskeleton within cells on patterns. a-d, Representative confocal images of single cells grown on different patterns: square dot matrix (A), Anisotropic (B), dot matrix circles (C), and 20-point circles (C). The nucleus (Panel 1), focal adhesions (vinculin, panel 2), and actin cytoskeleton (panel 3) are labeled within each cell. Panel 4 shows the overlay of the different structures.

3.3.5 Controlling Cell Cytoskeleton Enhances Cell Programmability

We investigated whether patterns that induce actin directionality would enhance differentiation down specific lineages. To evaluate lineage specific differentiation, hMSCs were incubated under mixed adipogenic and osteogenic induction media on the four distinct patterns: square dot matrix, anisotropic square, circle dot matrix, and 20-point circle shapes. Following 7 days, the cells were removed from the patterns and the expression of markers for osteogenesis and adipogenesis was assessed with qPCR. Seeding hMSCs on an anisotropic square shape enhanced expression of osteogenic markers (Figure 3.8A). This likely results from the high cytoskeletal uniformity leading to more uniform differentiation of cells on the anisotropic substrates. Within a circular geometry, which is established to promote adipogenesis, the 20-point circle pattern with oriented radial fibers decreased adipogenesis compared to those on the dot matrix circle (Figure 3.8B). This decrease stems from the increased contractility of the fibers within the cells grown on the 20-point circle, which drives the cells down a more osteogenic lineage compared to cells on an unbiased dot matrix pattern.

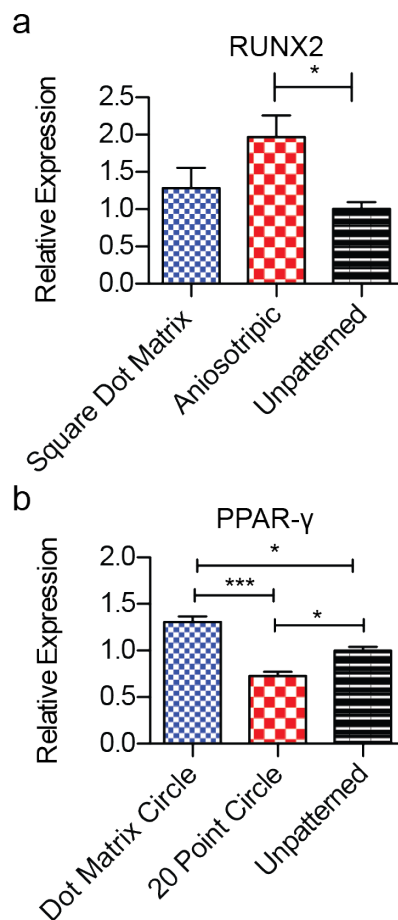


Figure 3.8 qPCR of osteogenic and adipogenic markers by hMSCs on patterned substrates. (A) Relative expression of RUNX2, an osteogenic transcription factor, by hMSCs on square patterns compared to cells grown on unpatterned substrates. (B) Relative expression of PPAR γ , an adipogenic transcription factor, by hMSCs on circular patterns compared to cells grown on unpatterned substrates.

3.4 Conclusion

In this work, we show that nanopatterned fibronectin concentrated in the peripheral areas of cells allow for the controlled reorientation of actin fibers within the interior of cells. Using this patterning approach, the fibers within a cell can be directed across defined axes to alter cell behavior. Significantly, the ability to modulate actin fiber orientation independently of cell shape allows one to confine cells on substrates and program the cytoskeleton in a predefined fashion. The use of PPL to define discrete features enables the ability to tailor focal adhesion formation

over large areas in any arbitrary shape to modulate and study cell behavior. This approach to cellular engineering will have a significant impact on modulating cell behavior in complex biological environments, such as those containing multiple different cell types are present. It opens up the possibility of directing stem cells down different lineages within the same confined space to mimic tissue organization. This ability to control and direct cytoskeletal formation can be extended beyond just stem cell differentiation to study and control other biological systems that including neurite formation and cancer metastasis.

CHAPTER FOUR

Cellular Assays with a Molecular Endpoints Measured

by SAMDI Mass Spectrometry

Portions of this chapter are adapted from
Berns, E. J., Cabezas, M. D., Mrksich, M. *Small* **2016**, 12(28): 3811-18.

4.1 Introduction

Cell-based assays are finding increasing use in modern drug discovery screens because they enable the concomitant evaluation of compound permeability, toxicity, and activity within a more physiologically relevant cellular environment.⁵⁶⁻⁵⁷ However, cell-based assays that measure the activities of specific enzymes can be substantially more difficult to implement than biochemical assays. The common strategies for measuring enzyme activities – including those based on absorbance, fluorescence, and radioactivity – often require reagents that cannot be delivered to the appropriate cellular compartment or are not compatible with the cellular environment.

In this chapter, I describe a method that combines cell lysis with a label-free assay of enzyme activities in the lysate. The assay uses self-assembled monolayers for matrix-assisted laser desorption/ionization mass spectrometry (MALDI-MS) (SAMDI),⁵⁸ where the monolayers are engineered to present enzyme substrates together with a peptide that supports cell adhesion on the assay chip. In this way, lysis of a population of cells occurs in the presence of peptide substrates that record the activity of a defined enzyme. This approach, termed Tandem Culture and Lysis-SAMDI (TCAL-SAMDI) provides a general method for conducting cell-based, chemical screening with quantitative readouts of enzymatic activity, easily adaptable to a wide range of targets. Most cell-based screens use gene expression or phenotypic changes as a readout and require a labeled reporter in addition to compatibility with automated data acquisition and analysis methods. Gene expression reporter systems, such as β -lactamase paired with fluorescence resonance energy transfer (FRET),⁵⁹ fluorogenic,⁶⁰ or chromogenic substrates, have been of significant value in cell-based screening.⁶¹ Protein and other biomolecule labeling methods, including genetic encoding of fusion proteins incorporating fluorescent proteins,⁶² chromophoric, fluorescent, and immuno-labeling,⁶³ have been used to visualize protein expression,⁶⁴

localization,⁶⁵ and translocation between cellular compartments.⁶⁶ High content screens (with automated image acquisition and analysis) using these methods have been used to identify compounds that produce desired molecular and phenotypic changes.⁶⁷⁻⁷⁵

Our previous work has developed SAMDI mass spectrometry as a label-free assay for measuring enzyme activities.⁷⁶⁻⁷⁷ In SAMDI, an enzyme substrate is immobilized to a self-assembled monolayer presenting tri(ethylene glycol) groups. The substrate can be immobilized through a variety of chemical reactions and the glycol groups serve the important role of preventing nonspecific adsorption of proteins to the surface, giving a more quantitative measure of activity. Further, these monolayers are well-suited for analysis by MALDI-MS because irradiation of the monolayer with a laser results in dissociation of the thiolate-gold bond and release of the intact alkanethiolates. In this way, treatment of the immobilized peptide with an enzyme that can modify its structure will result in a change in mass of the peptide alkanethiolate conjugate, which can be directly observed in the SAMDI spectrum.

Here, we demonstrate a strategy for analyzing lysates from small numbers of cells, which relies on culturing cells on a monolayer that presents a peptide for cell adhesion together with a peptide substrate to report on a desired enzyme activity. In this way, cells can be cultured on the monolayer and lysed in place, where enzymes in the lysate can directly and immediately act on the immobilized substrates. The monolayer is then rinsed and analyzed by SAMDI mass spectrometry to quantify the amount of product. We apply this method in a 384-array format for measuring both protein tyrosine phosphatase (PTP) and caspase-3 activities and we also show how this platform was used to perform a cell-based screen to identify modulators of PTP activity.

4.2 Materials and methods

4.2.1 Reagents

PTP Inhibitor I (PTPI-I) was purchased from Santa Cruz Biotechnology. Hexadecyl phosphonic acid and 2,4,6-trihydroxyacetophenone were also purchased from Sigma-Aldrich. The 10,240-chemical library was purchased from Chembridge. Amino acids and peptide synthesis reagents were obtained from Anaspec. The phosphatase substrate (pY peptide; sequence: AIpYENPFARKC), caspase-3 substrate (CGKRKGDEVDSG), and cyclic RGD peptides were synthesized following standard solid phase peptide synthesis protocols as previously described.⁷⁸ The Presto Blue kit, calcein-AM and ethidium homodimer-1 were purchased from Life Technologies and the cell viability assays were performed following manufacturer's instructions.

4.2.2 Preparation of SAMs

Custom fabricated stainless steel plates (8 cm × 12.3 cm) were first cleaned using hexanes, ethanol, and DI water. An electron beam evaporator was used to first deposit 5 Ti (5 nm, 0.02 nm s⁻¹) onto the steel plates. The evaporator was vented to oxidize the Ti layer. Next, an aluminum mask having holes in a 384-well format was placed on top of the plate and an additional Ti (5 nm, 0.02 nm s⁻¹) were deposited followed by Au (35 nm, 0.05 nm s⁻¹). The Au-coated steel plates were soaked overnight at 4 °C in an ethanolic solution containing a 1:4 ratio of an asymmetric disulfide terminated with a maleimide group and a tri(ethylene glycol) group and a symmetric disulfide terminated with tri(ethylene glycol) groups, with a 0.5 × 10⁻³ M total disulfide concentration. The plates were rinsed with ethanol and then immersed in a 10 × 10⁻³ M ethanolic solution of hexadecyl phosphonic acid for 10 min. After rinsing with ethanol and drying under air, an automated reagent dispenser (Multidrop Combi, Thermo Scientific) was used to spot 3 μL of a peptide solution consisting of 32 × 10⁻⁶ M pY peptide and 8 × 10⁻³ M cyclic RGD in 1X PBS at pH 7.5 onto the arrayed plates. The peptide immobilization solution used for duplexed phosphatase and caspase-3

activity measurements consisted of 8×10^{-6} M pY peptide, 8×10^{-6} M cyclic RGD, and 24×10^{-6} M caspase-3 peptides. All peptide immobilization steps were carried out for 1 h at 37 °C in a humidity chamber.

4.2.3 TCAL-SAMDI assay for PTP and caspase-3 activity

HeLa cells and MDA-MB-231 cells were obtained from ATCC and cultured in α MEM (for HeLa cells) or high-glucose DMEM (for MDA-MB-231 cells) medium supplemented with 10% fetal bovine serum, glutamax, penicillin, and streptomycin. All cells were cultured in a humidified incubator at 37 °C and CO₂. Cells were trypsinized and suspended in media, and the average number of cells per μ L was counted using a hemocytometer and Countess automated cell counter (Life Technologies), and cell concentrations were adjusted to seed the desired number of cells per spot in 3 μ L media. Cells were cultured on the monolayers presenting RGD and peptide substrates on steel plates or glass slides for 2 h under standard growth conditions. For PTP activity assays, cells were cultured for 2 h before addition of inhibitors, if any. For caspase-3 activity assays, 1 μ L of 4×10^{-6} M staurosporine (STS) was added to each spot (for a final concentration of 1×10^{-6} M STS), and incubated for 4 h. After culture, media was removed and lysis buffer (1 or 1.5 μ L) was delivered manually or with an automated reagent dispenser to each spot and the lysate was allowed to react with the monolayer for 1 h at 37 °C in a humidity chamber. Lysis buffer was composed of 20×10^{-3} M Tris, 136×10^{-3} M NaCl, 1×10^{-3} M EDTA, 0.5% Triton-X 100, pH 7.4. A protease inhibitor tablet obtained from Roche was added to the lysis buffer. For caspase activity assays, 10×10^{-6} M dithiothreitol was added to the lysis buffer. The surfaces were then rinsed with DI water and ethanol, and dried with air. A 30 mg mL⁻¹ solution of 2,4,6-trihydroxyacetophenone in acetone was delivered to each spot on the array and the surfaces were analyzed using an AB Sciex 5800 MALDI TOF/TOF instrument in positive reflector mode. The area under the curves for the [M +

H]⁺ peaks of disulfides was measured with the Data Explorer software (AB Sciex). Activity was calculated following equation

$$AUC = \frac{P}{P+S}. \quad (1)$$

where the area under the curve (AUC) corresponding to the product peaks (P) were divided by the area under the curve of the summation of the product (P) and substrate peaks (S).

All experiments were repeated at least three times, with at least three spots per condition each time. Presented data represent the means and standard errors of all spots. For lysate experiments (see below for more details), data represent the averages and standard errors from at least three independently prepared lysates. Statistical comparisons between mean activities were made using Student's t-tests.

4.2.4 TCAL-SAMDI assay for chemical screen

A 10,240 chemical library was used to screen for phosphatase inhibitors. For the chemical screen, 100 or 150 MDA-MB-231 cells were seeded on each spot presenting cyclic RGD and pY peptide (phosphatase substrate) and cultured for 2 h. A stock solution of each compound was first prepared in DMSO then diluted in media. Each compound was delivered (1 μ L) to each spot on the array to a final concentration equivalent to 10×10^{-6} M and 1% DMSO. The cells were exposed to the compounds for 2 h under standard cell growth conditions. After media removal, the lysis buffer with protease inhibitor was applied to each spot independently and incubated for 1 h at 37 $^{\circ}$ C in a humidity chamber. The plates were then rinsed with water, ethanol, and dried under air. Matrix was applied prior to mass spectrometry analysis. As described above, the data were analyzed to quantify the levels of phosphatase activity and hits were ranked. The five compounds that produced the greatest inhibition of PTP activity on each plate were chosen for a secondary screen to confirm hits. The secondary screen was carried out following the same conditions stated

above, except that each compound was tested on six spots instead of one. Additionally, some compounds tested in the secondary screen step were tested at 50×10^{-6} M.

4.2.5 Evaluation of dose-dependent inhibition by TCAL-SAMDI

MDAMB-231 cells were seeded at 75 cells per spot on monolayers presenting phosphatase peptide substrates and cyclic RGD as described above. Following cell attachment and culture for 2 h, inhibitors (1 μ L solution in media) were delivered to each spot to achieve a range of final concentrations from 0 to 640×10^{-6} M in media and incubated for 2 h. Following media removal, the lysis buffer with protease inhibitor was applied to each spot independently and incubated for 1 h at 37 °C in a humidified chamber. Plates were then rinsed with water, ethanol and dried. Matrix was applied prior to analysis by mass spectrometry. All experiments were carried out at least twice, with 6 spots per condition each time. Presented data represent the averages and standard errors of all spots. IC₅₀ values and curves were determined using GraphPad prism software.

4.2.6 Evaluation of dose-dependent inhibition in cell lysates using SAMDI

MDA-MB-231 cells were lysed using the lysis buffer containing protease inhibitor described above to achieve the equivalent of 75 cells per 1.5 μ L, after mixing with inhibitor solutions. Inhibitor solutions in lysis buffer at concentrations ranging from 0×10^{-6} to 640×10^{-6} M were added to the lysate and 1.5 μ L of the mixture was spotted on monolayers presenting cyclic RGD and phosphatase substrate. The reaction was carried out for 1 h at 37 °C in a humidified chamber. To evaluate dose-response inhibition under standard culture conditions, MDA-MB-231 cells were plated on a 96-well plate at a density of 6400 cells per well and cultured for 2 h. Culture medium containing inhibitors at final concentrations ranging from 0×10^{-6} to 300×10^{-6} M and 1% DMSO were delivered to each well and culture proceeded for another 2 h. The mixture containing media and inhibitor was removed from each well and centrifuged. Lysis buffer

containing protease inhibitor was applied to each well in the plate and incubated for 10 min at room temperature. The lysate was collected and added to the corresponding cell pellet for each inhibitor concentration sample. The lysate (1.5 μL) was spotted on monolayers presenting RGD and phosphatase substrate. Protein concentrations were measured using a BCA assay (Santa Cruz Biotechnology), following manufacturer instructions. Sample analysis using SAMDI followed as described above. Presented data represent the averages and standard errors from at least three independently prepared lysates. IC50 values and curves were determined using GraphPad prism software.

4.2.7 Cell viability assays

The PrestoBlue assay was performed using MDA-MB-231 cells seeded at 6400 cells per well in a 96 well plate format. After a 2 h culture period, medium containing inhibitors at a range of concentrations from 0×10^{-6} to 300×10^{-6} M was added to each well and incubated for 2 h. PrestoBlue reagent was added to the wells, incubated for 25 min, and fluorescence was measured using a Cytation 3 (BioTek) plate reader. For calcein-AM and ethidium homodimer-1 staining, MDA-MB-231 cells were seeded on glass slides presenting monolayers of RGD and phosphatase peptide substrate at 75 cells per spot. After 2 h of culture, 1 μL of media containing inhibitors for a final concentration of 10×10^{-6} M and 80×10^{-6} M was added to each spot and incubated for an additional 2 h. Media was removed and a solution of calcein-AM and ethidium homodimer-1 in PBS were delivered (3 μL) to each spot and incubated at 37 °C for 20 min. Each spot was imaged using an epifluorescent microscope and cells were counted using ImageJ Cell Counter plug-in.

4.2.8 Z'-factor determination

A gold-coated steel plate with monolayers arrayed in a 384-well format was used to seed 150 MDAMB-231 cells per spot. After 2 h culture, DMSO was added to a final concentration of 1% on 160 spots (negative controls) and PTPI-I was added to a final concentration of 300×10^{-6} M, 1% DMSO, on 160 spots (positive controls). After 2 h, the media was removed and lysis buffer applied for 1 h at 37 °C. Sample analysis using SAMDI followed as described above. Z' -factor was calculated using the following relationship

$$Z' = 1 - \frac{(3\mu_{\sigma^+} + 3\mu_{\sigma^-})}{\mu_{\sigma^+} - \mu_{\sigma^-}} \quad (2)$$

where σ_{c^+} and σ_{c^-} represent the standard deviations of the positive and negative controls, respectively, and μ_{c^+} and μ_{c^-} represent the means of the positive and negative controls, respectively.

4.3 Results

4.3.1 TCAL-SAMDI assay of phosphatase activity

We first prepared an array of monolayers to measure PTP activity in HeLa cell cultures. Each monolayer was composed of alkanethiolates terminated with maleimide groups at a density of 10% relative to total alkanethiolates, against a background of tri(ethylene glycol) groups (Figure 4.1A).

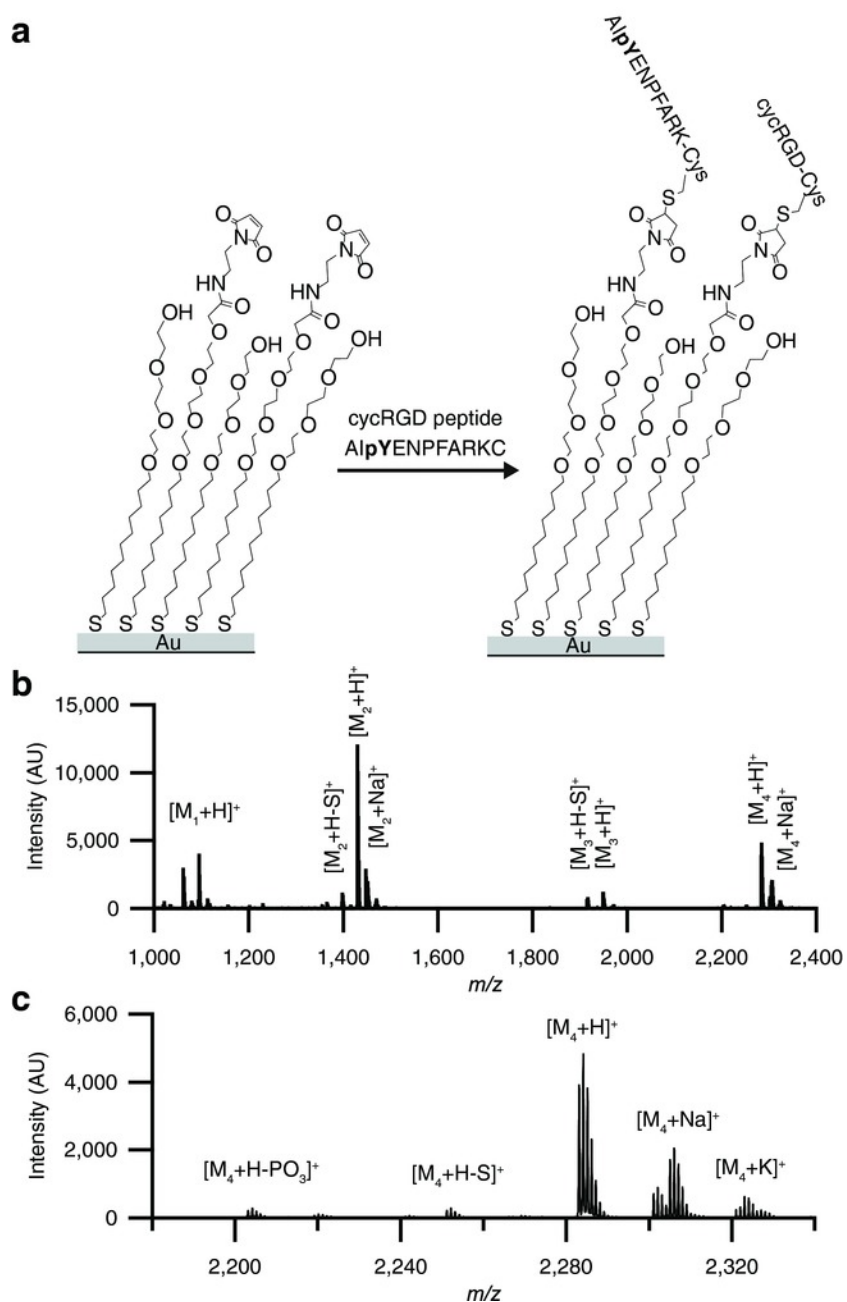


Figure 4.1. SAMDI on monolayers with two peptides. (A) Two peptides with terminal cysteines (a cell adhesion ligand (cyclic RGD peptide – cycRGD) and a phosphatase substrate (AlpYENPFARKC) are immobilized on alkanethiolate monolayers with 10% of the molecules presenting maleimides and 90% terminated with tri(ethylene glycol). (B) SAMDI spectrum of a monolayer with immobilized RGD peptide and phosphatase peptide. M1: alkanethiolate with RGD, M2: alkyldisulfide with RGD, M3: alkanethiolate with phosphatase peptide, M4: alkyldisulfide with phosphatase peptide, M4: alkyldisulfide with phosphatase peptide. (C) The same spectrum, showing the portion of the spectrum used for PTP activity analysis.

We applied a solution containing a cyclic peptide having the cell adhesion RGD (i.e., Arg-Gly-Asp) motif together with a peptide having a phosphorylated tyrosine residue (AIPYENPFARKC)²⁷ to report on phosphatase activity, and the peptides were immobilized onto the monolayer. The RGD motif is found in fibronectin⁷⁹ and mediates cell adhesion and spreading by binding to integrin receptors.⁸⁰⁻⁸¹ The monolayers were formed on a stainless-steel plate having an array of gold spots (2.8 mm diameter) positioned to match a 384-well plate format, as recently described.⁸²⁻⁸³ The area surrounding each spot consisted of a thin layer of evaporated titanium with a monolayer of hexadecylphosphonic acid formed on the titanium dioxide to render the outer area hydrophobic, enabling droplets to be isolated on the monolayer-coated gold spots. HeLa or MDA-MB-231 cells were plated and cultured on the monolayers in individual volumes of media (3 μ L) that were isolated on each spot (Figure 4.2A). After 2 h in culture, the media was rapidly removed from all spots with a robotic liquid-handling instrument and immediately replaced with lysis buffer (1 μ L). After incubating the plates with lysis buffer for 1 h, the plates were rinsed with water and then ethanol and analyzed by mass spectrometry.

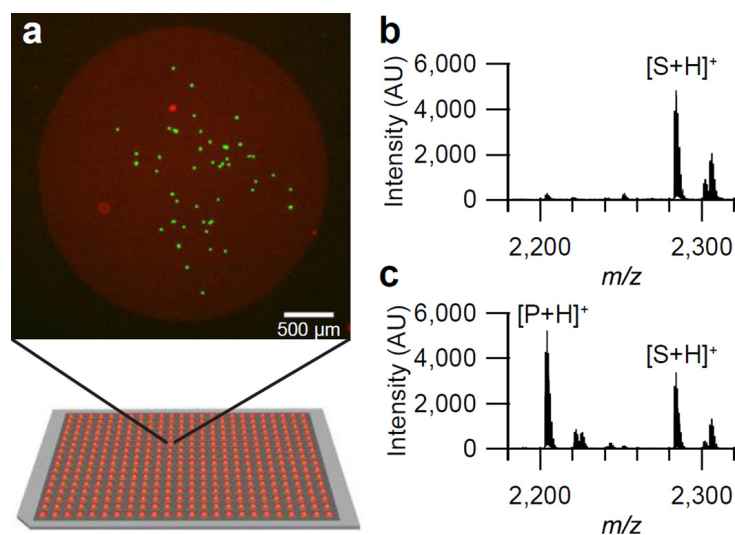


Figure 4.2. Tandem Culture and Lysis SAMDI (TCAL-SAMDI). (A) Cells (MDA-MB-231) are cultured on monolayers presenting both cell adhesion ligands and a phosphatase substrate, on a

384-spot plate. Green: live cells, Red: dead cells and gold spot. (B) A SAMDI spectrum from a spot without cells. (C) A SAMDI spectrum after lysis of cells.

Prior to analysis, the plates were treated with 2,4,6-trihydroxyacetophenone matrix and MALDI spectra were collected for each monolayer island. Performing MALDI on spots without cells produced spectra with peaks at mass-to-charge (m/z) values corresponding to the peptide-alkanethiolate conjugates as well as disulfides formed between a peptide-modified alkanethiolate and a background tri-ethylene glycol-presenting alkanethiolate, along with Na^+ adduct peaks (Figure 4.1 B, C). After lysis of cells on the spots, dephosphorylation of the peptide substrate resulted in the formation of a product peak with a mass shift of -80 Da (Figure 4.2 B). We confirmed that the peak at -80 Da relative to the substrate peak is the product peak by performing the same assay with a substrate of a different mass, in which case no peak appeared at the mass corresponding to the original product peak, but rather, at -80 Da relative to the new substrate.

We observed that as the number of cells cultured on a spot increased, the relative intensity of the product peak grew larger while that for the substrate peak diminished (Figure 4.3A). The extent of phosphatase activity was determined by measuring the area under the curve for the product peak and dividing by the sum of areas for the substrate and product peaks. Because of differences in ionization efficiencies between the phosphorylated and dephosphorylated molecules, to calculate product yield, it would be necessary to scale the observed dephosphorylation peak fractions using a calibration curve as shown in Figure A1 (Appendix A). We observed that the dephosphorylation peak fraction increased with HeLa cell number, before plateauing near 2000 cells per spot. (Figure 4.3B). With this method, we were able to measure phosphatase activity from as few as 25 cells per spot (Figure 4.3B). With MDA-MB-231 cell cultures, we measured PTP activity from only 5 cells per spot (Figure 4.3C).

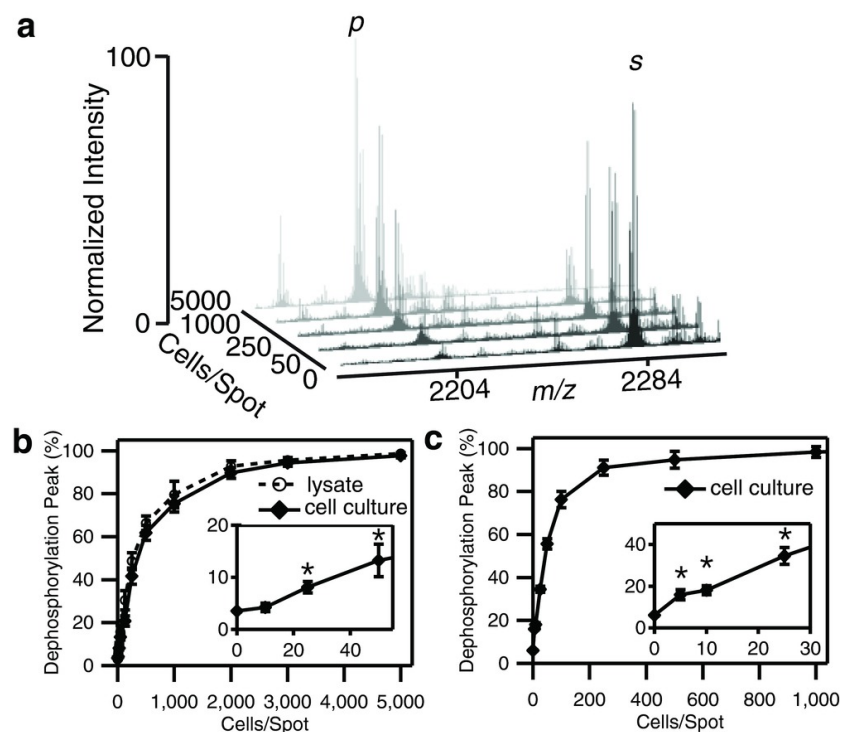


Figure 4.3. Enzyme activity measurement with TCAL-SAMDI. (A) SAMDI-MS spectra showing the conversion of substrate (s) to product (p) as the number of HeLa cells cultured and lysed on monolayer-coated gold spots increases. Quantification of the dephosphorylation peak fraction, defined as the area under the curve of the product peak relative to that of the substrate and the product peaks in the SAMDI spectra, resulting from culturing and lysing. (B) HeLa cells and (C) MDA-MB-231 cells on monolayers presenting adhesion and substrate peptides. Insets in (B) and (C) are magnified regions of the graphs. (* $p < 0.01$).

To determine if culturing cells on the monolayer would interfere with enzyme activity on immobilized substrates, we also measured phosphatase activity from previously prepared HeLa cell lysates. Here, HeLa cells were not cultured on the monolayers but rather lysed and the lysate was applied to the monolayers to measure PTP activity (Figure 4.3B, dashed line). Comparing these two methods revealed that the activity measured with TCAL-SAMDI (Figure 4.3B, black line) was not significantly different at most cell concentrations from the activity measured from cell lysates (Figure 4.3B, dashed line). This result demonstrates that culturing and lysing cells

directly on the surface did not interfere with the ability of enzymes to act on the immobilized substrate or the ability to perform SAMDI on these surfaces.

4.3.2 Duplexing enzyme activity measurements with TCAL-SAMDI

One significant benefit of mass spectrometric assays is that they are well suited to multiplexed formats.⁷³ To illustrate this advantage, we prepared monolayers that presented a mixture of the adhesion peptide, the phosphatase substrate, and a peptide substrate for the protease caspase-3 (CGKRKGDEVDSG).⁷⁵ We cultured HeLa cells on monolayers presenting these three peptides for 1 h and then induced apoptosis by adding staurosporine to the medium.⁸⁴ After 4 h of treatment with staurosporine, the cells were lysed as described above and the monolayers were similarly analyzed by SAMDI mass spectrometry. The mass spectra clearly show the conversion of both peptide substrates to their corresponding products (Figure 4.4A), demonstrating the ability to duplex activity measurements with TCAL-SAMDI. In addition to the peak for the dephosphorylated peptide, we also observed a peak corresponding to the caspase-3 product at 144 Da lower than the initial substrate mass (Figure 4.4A). Monolayers treated with lysis buffer and media, as well as monolayers with cells but without staurosporine show a lack of the caspase-3 product (Figure 4.4B). Interestingly, the conversion of substrate to product was significantly greater when cells were lysed directly on the surface, compared to the conversion observed from applying the cell lysate to the monolayer. This benefit of the TCAL assay may reflect a gradual loss of the enzyme activity in the lysate.

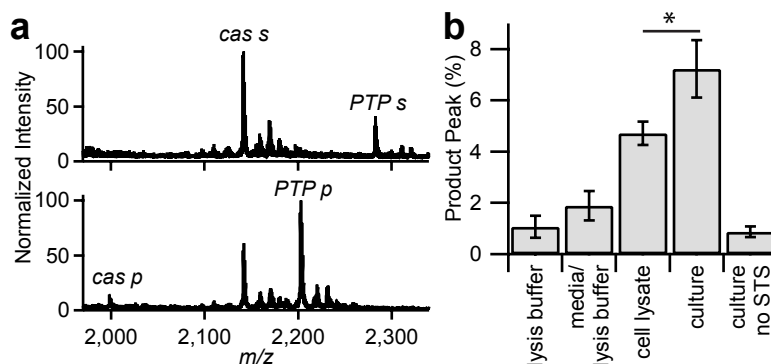


Figure 4.4. Duplexing enzyme activity measurements with TCAL-SAMDI. (A) SAMDI spectra of a spot with no cells (top) and with 10,000 cells (bottom) shows the conversion of two substrates (PTP s: PTP substrate; cas s: caspase-3 substrate) to their products when cells are cultured, treated with STS, and lysed on the surface. (B) Caspase-3 activity measured by SAMDI (* $p < 0.05$).

4.3.3 Screening with TCAL-SAMDI

We next describe a screen where we evaluated 10,240 small molecules in MDA-MB-231 cells to identify those that modulate phosphatase activity. We found that cultures having 100 – 150 cells per spot resulted in approximately equal-sized peaks for the substrate and product peptides in the SAMDI spectra. This small number of cells required in the assay means that the entire screen could be performed with just one million cells. We also measured the Z' -factor, a commonly used statistical measure of assay performance, and found a Z' -factor of 0.66.⁸⁵ A primary screen was carried out by applying one compound per spot, using approximately 30 plates for the entire screen. After culturing cells on the arrays for 2 h, solutions of each compound (1 μ L) were added to the media (3 μ L) on each spot on the array so that the resulting compound concentration was 10×10^{-6} M with 1% dimethyl sulfoxide (DMSO). The cells were incubated for 2 h, media was removed, lysis buffer was incubated on each spot for 1 h, and the plates were analyzed by SAMDI. The five compounds that produced the greatest inhibition of PTP activity on each plate were analyzed in a

secondary screen to verify the activity. This process identified four compounds of interest that were investigated further.

Compound 1 (Figure 4.5A) reduced PTP activity nearly completely with an IC₅₀ of 9×10^{-6} M (Figure 4.5B). However, we found that the compound did not directly inhibit the phosphatase because it was inactive when tested on cell lysates (Figure 5 b). We also verified that the reduced activity was not an artifact stemming from the detachment of cells, by counting the number of cells per spot (Figure A.2A, Appendix A). Addition of compound 1 did decrease cell viability ($\sim 30\%$ at 100×10^{-6} M of 1), but this decrease was small compared to the observed inhibition of PTP activity (Figure A.2A, B, Appendix A). As an additional control to ensure that the reduction in PTP activity was not an artifact resulting from a loss of protein, lysates were prepared from cells treated with the compound while being cultured in standard 96-well tissue culture plates. Treatment of monolayers with these lysates confirmed that 1 reduced PTP activity, with a similar IC₅₀ of 4.2×10^{-6} M (Figure 4.5C), and this was not due to a decrease in protein concentration in the lysates (Figure A.2C, Appendix A).

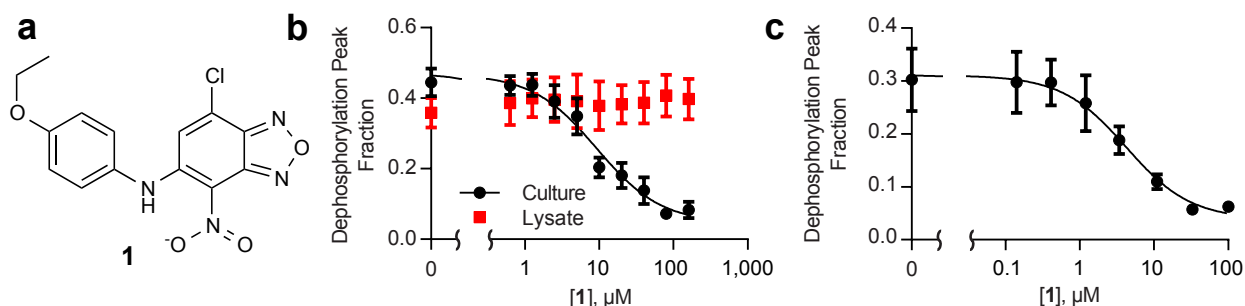


Figure 4.5 Compound 1 identified by chemical screening via TCAL-SAMDI. (A) Chemical structure of 1. (B) SAMDI analysis of PTP activity measured from MDA-MB-231 cells cultured on the monolayer and treated with 1 (black circles) and from lysate treated with 1 then applied to the monolayer (white squares). (C) SAMDI analysis of lysate from cells cultured in 96-well plates and treated with 1.

4.4 Discussion

This work demonstrates an efficient method for isolating lysates from cultured cells and assaying those lysates for enzyme activities. The efficiency of this process – which avoids the need to physically collect and manipulate the lysate – makes the method well-suited to high throughput applications comprising tens of thousands of distinct assay compositions. Here we illustrate the method with assays of phosphatase activity and we demonstrate a cell-based screen to identify molecules that regulate phosphatase activities by acting on upstream targets.

The method is enabled by two properties of the self-assembled monolayers. First, the monolayers give excellent control over the ligand-receptor interactions at the interface, allowing the surface to simultaneously mediate cell adhesion and to present a peptide that serves as a substrate to probe the desired enzyme activity. Were the surface not inert to nonspecific protein adsorption – which is a common challenge with many substrates used in bioanalytical methods – the peptide substrate would be blocked from interacting with the enzymes by way of an adsorbed protein layer. Second, monolayers of alkanethiolates on gold are compatible with analysis by MALDI mass spectrometry and therefore the assays can be performed in a label-free format. This is particularly significant because it allows measurement of virtually any enzyme activity. No other surface chemistry – including common hydrogel polymer layers or alkylsiloxane monolayers has been shown to combine these two benefits and therefore the TCAL-SAMDI method offers a new capability in bioassays.

The measurement of phosphatase activities in this work is also significant because these activities are extremely challenging to measure in cell lysates. The commonly used colorimetric assay based on p-nitrophenylphosphate, which undergoes a shift in absorbance after dephosphorylation, is not able to discriminate between the activities of many phosphatases (acid,

alkaline, protein tyrosine, and serine/threonine). Assays that report on the generation of free phosphate ion that is released from a phosphopeptide of choice, such as the commonly used malachite green assay, can offer greater specificity, but are incompatible with lysate samples because of the difficulty involved in eliminating sources of phosphate present in the cell. The SAMDI assay can be used with any peptide substrate and therefore provide a more specific response on activity. Thus, there are no currently available phosphatase activity assays other than the TCAL assay that can be used to efficiently conduct a cell-based screen of protein tyrosine phosphatase activity. While this alone would be valuable, this method could be applied to a broad range of enzyme activities, including glycosyltransferases, deacetylases, kinases, proteases, and others.⁷¹⁻⁷⁶

An important advantage of the TCAL assay is that it does not require the lysate to be physically manipulated. At the time of the assay, the media is removed from the cell cultures and a lysis buffer is applied to the cells. No further manipulation is required because the lysate that is generated is in contact with the monolayer presenting the substrate for the relevant enzyme activity. For this reason, the TCAL method does not introduce any time delay between generating the lysate and assaying for activities; these time delays often lead to losses of enzyme activities, as does adsorption of proteins from the sample to the walls of pipettes and wells. Because the lysate is not manipulated in TCAL, it is possible to use smaller volumes of lysate and in this work we demonstrated the preparation of lysates from as few as five cells.

An important application of the TCAL method is in screening libraries of small molecules that modulate biochemical activities in cultured cells. Cell-based screens have been particularly important in those cases where a desired downstream biochemical activity is modulated—but where there exist many distinct targets that are relevant – or where a phenotypic response is

desired. Further, cell-based assays have the advantage that they also identify molecules that are cytotoxic or that are unable to cross the membrane. It can also be challenging to develop the reagents required in a cell-based assay. For example, FRET-based reporters of kinase activities⁸⁶ have required a substantial effort to develop, and those assays have a limited quantitative resolution. In other cases, it can be difficult to deliver the reagent to the appropriate cellular compartment. The label-free SAMDI assay can be readily formatted to detect many enzyme activities. Further, the assay is performed after the cell has been lysed and therefore avoids limitations of getting a reagent into the cell. The TCAL method provides a practical method for performing cell-based assays. Gold-coated glass substrates are already commercially available, and metal plates like those used in this work could similarly be made. All components of the monolayer are also commercially available and the required amount of chemicals needed to form the monolayer is minimal. Our 10,000-compound screen required 32 plates for the initial screen, which required ~16 h to analyze by mass spectrometry. The same liquid handling robotic instruments were used for this screen as are used for typical high throughput screens. Standard cell culture was used, though the number of cells required was very small compared to most cell-based assays. The volume of media per assay (4 μ L) and amount of screening compound (0.25 nmol) was very small compared to most assays, minimizing reagent costs. A commercially available MALDI-TOF instrument was used to read the plates. Available software that analyzes the area under the peaks in the mass spectra was used to determine activity, with some post-processing in Microsoft Excel, requiring only a few hours to process the data from 32 plates. Hence, as a screening assay, the TCAL method is reasonably practical, cost-efficient, and rapid.

4.5 Conclusions

The TCAL-SAMDI method enables a broad range of cell-based assays that have as an endpoint a biochemical activity. As such, this method removes the constraints stemming from the incompatibility of many enzyme activity assays with the cellular environment. By integrating the cell culture with the assay on the same spot, the TCAL method requires only tens of cells. Further, because the method uses 384-array plates, it can take advantage of available liquid handling and automation tools. These benefits make the TCAL assay an exciting addition to the current methods for cell-based assays.

CHAPTER FIVE

Nanopatterned Matrices Enable Cell Based Assays with Molecular Readouts

Portions of this chapter are adapted from:
Cabezas, M. D., Mirkin, C. A. and Mrksich, M. *Nano Lett.* **2017**, *17*, 1373-1377.

5.1 Introduction

Cell-based assays are finding wider use in evaluating compounds in primary screens for drug development, yet it is still challenging to measure enzymatic activities as an endpoint in a cell-based assay. This paper reports a strategy that combines state-of-the-art cantilever free polymer pen lithography (PPL) with SAMDI mass spectrometry, to guide cell localization and measure cellular enzymatic activities following treatment with molecules from a drug library. Experiments are conducted with a 384-spot array, where each spot is composed of ~ 400 nanoarrays, and where each array has a 10×10 arrangement of 750 nm features that present extracellular matrix (ECM) proteins surrounded by an immobilized phosphopeptide. Cells attach to the individual nanoarrays, where they can be cultured and treated with small molecules – and where each of the 384 cultures is treated with a unique compound – after which the media is removed and the cells are lysed. Phosphatase enzymes in the proximal lysate can then act on the immobilized phosphopeptide substrate to convert it to the dephosphorylated form. After the lysate is removed, the array is analyzed by SAMDI mass spectrometry to identify the extent of dephosphorylation and therefore the amount of enzyme activity in the cell. This novel approach of using nanopatterning to mediate cell adhesion and SAMDI to record enzyme activities in the proximal lysate will enable a broad range of cellular assays for applications in drug discovery and research not possible with conventional strategies.

Assays that evaluate the biological effects of small molecules in cell cultures are important in many applications including studying the mechanisms of action of natural products, elucidating signal transduction pathways, and screening small molecule libraries in drug discovery programs. Yet, it is still difficult to measure many biochemical activities in cell-based assays, and therefore

these assays cannot be applied to many targets of interest. Indeed, most assays report on a phenotypic behavior, including cell differentiation, cell death, and migration and in those cases, they do not measure the inhibition or activation of specific enzymes. Detection methods based on optical sensors⁶ or fluorescent proteins have allowed the real-time observation of metabolite secretion, and specific protein and enzyme activities as a result of chemical or mechanical stimuli, but it remains challenging to develop these reagents and many biochemical activities have not yet been targeted with these approaches. In this chapter, I describe a strategy wherein adherent cells can be treated with small molecules, cultured, lysed, and then analyzed by mass spectrometry to measure the activities of endogenous enzymes. The implementation of this method relies on the use of surfaces that are nanopatterned with extracellular matrix (ECM) proteins to mediate cell attachment and with a peptide that is a substrate for the desired enzyme activity in the lysate.

Our approach is based on monolayers having two distinct properties; they must present proteins that mediate cell adhesion, and they must also present peptides that are substrates for enzymes whose activities will be measured. Because these two functions are not compatible – since the adhesion proteins would obstruct access of the enzyme to the immobilized peptide – it is necessary to pattern the monolayer into two regions. By using the emerging state-of-the-art cantilever-free polymer pen lithography (PPL) technique to create nanopatterns of the adhesive protein in 750 nm features, cells can still attach and spread but the majority of the monolayer still presents the phosphopeptide substrate that is measured by self-assembled monolayer laser desorption/ionization (SAMDI) mass spectrometry (Figure 5.1 and Figure B.1, Appendix B). In this way, cells adhere to the surface by way of interactions with the matrix proteins, while the other regions of the surface remain available for recording the enzyme activity. A further benefit of this approach is that it can be used to define sites for adsorption of virtually any matrix protein and

therefore it allows the tandem culture and lysis (TCAL-SAMDI) method to be applied to assays using any adherent cell line.

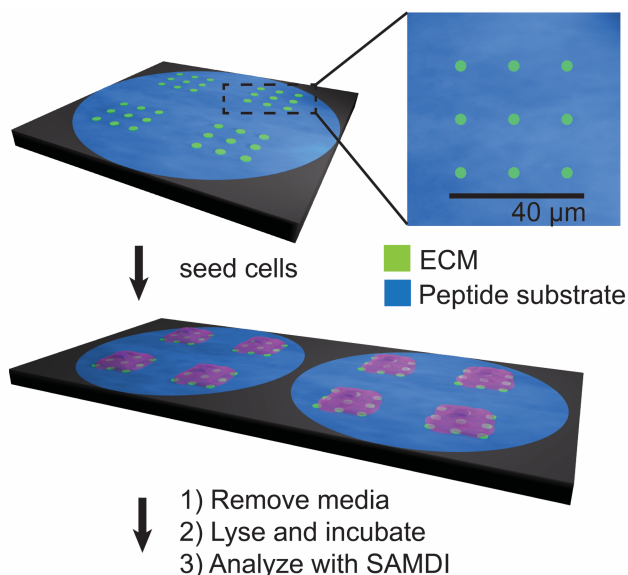


Figure 5.1. This work reports the use of surfaces that are nanopatterned with extracellular matrix proteins that support cell adhesion, and where the intervening regions present a peptide substrate for an enzyme, to enable cell-based assays using SAMDI mass spectrometry. Note that the nanoarrays have 100 fibronectin features. Cells that are adherent to the nanoarrays are cultured and treated with small molecules. The media is then removed, and a lysis buffer is applied to each region of cells, where enzymes in the lysate can modify the peptide in the intervening regions. The surface is then rinsed and analyzed with SAMDI mass spectrometry to determine the extent of conversion of the peptide substrate and, therefore, the amount of enzyme activity in the lysate.

5.2 Materials and methods

5.2.1 Reagents

All reagents were obtained from the supplier and used as received. Phosphatase inhibitor I was purchased from Santa Cruz Biotechnology. Hexadecylphosphonic acid and 2,4,6-trihydroxyacetophenone were purchased from Sigma Aldrich. Amino acids and peptide synthesis reagents were obtained from Anaspec. All peptides were synthesized following standard solid phase peptide synthesis protocols as previously described. A buffer comprising 20 mM Tris at pH

8.0 containing 0.5% triton was used for lysis and a protease inhibitor tablet obtained from Roche (cOmplete, Mini EDTA-free) was added to the lysis buffer prior use.

5.2.2 Preparation of SAMs

Glass slides were first cleaned by sonicating in ethanol for 30 min and dried under a stream of N₂. An electron beam evaporator was used to first deposit 5 nm of Ti onto the glass slides and subsequently vented to oxidize the Ti layer. Next, an aluminum mask having holes in a 384-well format was placed on top of the glass slide and an additional 5 nm of Ti were deposited followed by 35 nm of Au. The pen array was then immersed in a solution of MHA (10 mM in ethanol) for 1 min, dried with N₂, and mounted on Tera-Fab M series cantilever-free scanning probe instrument where the humidity inside the chamber was fixed at 50%. A patterning routine was programmed in the instrument with tip-surface contact times of 1 s for 750 nm features. The Au-coated glass slides were soaked overnight at 4 °C in an ethanolic solution containing a 1:4 ratio of an asymmetric disulfide terminated with a maleimide group and a tri(ethylene glycol) group and a symmetric disulfide terminated with tri(ethylene glycol) groups, with a 0.5 mM total disulfide concentration. The functionalized glass slides were rinsed with ethanol and then immersed in a 10 mM ethanolic solution of hexadecyl phosphonic acid for 10 min. After rinsing with ethanol and drying under air, a solution (3 µL) consisting of 40 µM phosphatase peptide substrate in 1X PBS at pH 7.5 was delivered onto each spot and incubated in a humidity chamber for 1 h at 37 °C. Surfaces were characterized by XPS using an electron spectroscopy for chemical analysis (ESCA) probe (Thermo Scientific EXCALAB 250 xi). Following peptide immobilization, the substrates were exposed to a solution of human plasma fibronectin (30 µg/mL in PBS) overnight at 4 °C.

5.2.3 Cell-based assay for enzyme activity

HeLa cells were obtained from ATCC and cultured in DMEM medium supplemented with fetal bovine serum, glutamine, penicillin and streptomycin. All cells were cultured in a humidified incubator at 37 °C and 5% CO₂. Cells were trypsinized and suspended in media, and the average number of cells per μL was estimated using a hemocytometer to seed the desired number of cells per spot. The volume of media per spot was 3 μL for all experiments. Cells were cultured on the monolayers presenting fibronectin and the phosphatase peptide substrate on glass slides for 2 h under standard growth conditions. Lysis buffer (1 μL) was delivered manually to each spot and the lysate was allowed to react with the monolayer for 1 h at 37 °C in a humidity chamber. The surfaces were then rinsed with DI water and ethanol, and dried with air. A solution of 2,4,6-trihydroxyacetophenone (THAP) in acetone (30 mg/mL) was delivered to each spot on the array and the surfaces were analyzed using an Applied Biosystems 5800 MALDI TOF/TOF instrument with a 20 kV accelerating voltage in positive reflector mode.

5.2.4 Lysis promotes interaction of PTPs with peptide substrate

A mild cell detachment reagent (TrypLE) was introduced to remove cells following culture on the patterned surfaces. This reagent (3 μL) was delivered to each spot and incubated for 5 min. The solution was then removed and the glass slide was rinsed with PBS, followed by DI water and dried with N₂. A matrix solution was applied prior to mass spectrometric analysis as described above.

5.2.5 Evaluation of PTP inhibition with SAMDI

Substrates that were nano-patterned with fibronectin islands surrounded by an immobilized phosphatase peptide substrate were generated using a Tera-Fab M series cantilever-free scanning probe instrument (TERA-print, IL) as described above. HeLa cells were seeded at ~ 500 cells per

spot on the monolayers. Following cell attachment and culture for 2 h, PTPI-I (1 μ L solution in media) was added to each spot to achieve final concentrations ranging from 0 to 300 μ M and incubated for 2 h. Following removal of the media, the lysis buffer with protease inhibitor was applied to each spot and incubated for 1 h at 37 °C in a humidified chamber. The slide was then rinsed with water, ethanol and dried. Matrix was applied prior to analysis by mass spectrometry. All experiments were carried out 3 times, with at least 5 spots per condition each time. The dose-response data shows the averages and standard error of all spots and the IC₅₀ was determined using Origin Pro8.

5.3 Results

5.3.1 Synthesis of mixed monolayers

To prepare the array plates, we first evaporated titanium onto a glass slide and then deposited gold through a mask having an array of holes arranged in the standard 384-well format. The slide was then immersed in a solution of hexadecylphosphonic acid (10 mM in ethanol) for 10 minutes to form a hydrophobic monolayer on the titanium dioxide areas surrounding the gold circular regions. This monolayer serves to confine aqueous solutions to the circular regions of gold and to isolate each reaction. Next, we used PPL to create patterns of a mercaptohexadecanoic acid (MHA) monolayer on the gold-coated regions of the glass plate (Figure 5.2A). This technique has proven useful for patterning proteins, peptides, oligonucleotides, and small molecules for a wide variety of biological applications. In PPL, an elastomeric pen array is coated with a molecular ‘ink’ and subsequently mounted to a scanning probe instrument and pressed onto a gold-coated slide, to create an array of circular MHA monolayer features. This step can be repeated with translational movement of the array to create arbitrary patterns. The feature size can be easily controlled and customized by adjusting the amount of force applied to the pen array and the time the pen array

remains in contact with the surface. Here, we used a SAMDI array that has a portion of a microtiter plate with 384 gold islands, wherein each island is 2.8 mm in diameter. PPL was then used to pattern MHA features within each island. In a typical experiment, a poly(dimethylsiloxane) (PDMS) pen array (1.2 x 1.2 cm²) having 10,000 pens, corresponding to a pen-to-pen distance of 120 μm and each coated with a solution of MHA (10 mM in ethanol), was used to generate 428 regions containing 10 x 10 square arrays of MHA features, each measuring 750 nm in diameter and spaced by a center-to-center distance of 4.4 μm within each gold island (Figure B.1, Appendix B). These MHA features, when later modified with the appropriate ECM protein, mediate the attachment of an individual HeLa cell to each square array. We verified the fidelity of the patterning step by chemically etching a portion of the substrate with a mixed aqueous solution of iron nitrate (13.3 mM) and thiourea (20 mM) to remove the non-patterned gold film (Figure B.2, Appendix B). The non-patterned areas were subsequently functionalized with a mixed monolayer that presents maleimide groups at a density of 10% against a background of tri(ethylene glycol) groups.

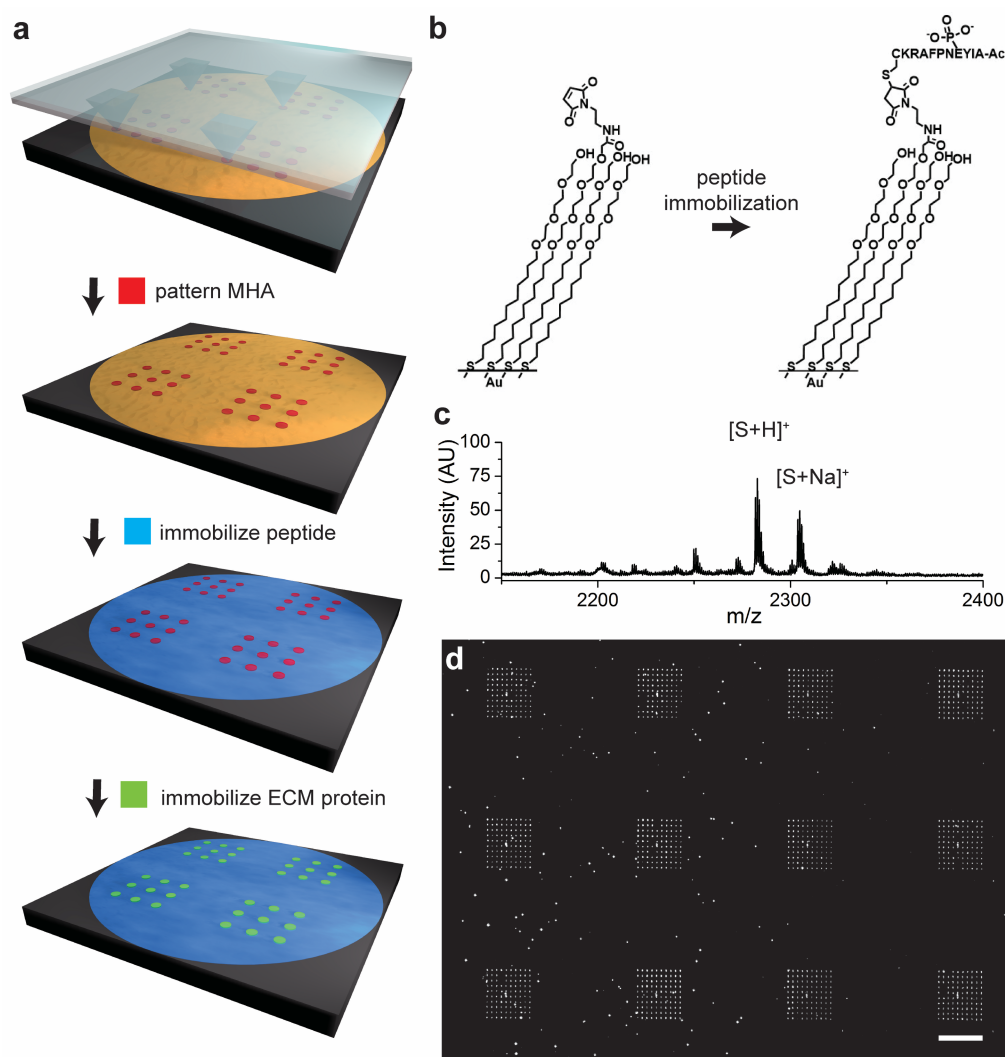


Figure 5.2. (A) Nanoarrays were prepared by using PPL to pattern mercaptohexadecanoic acid (MHA) a gold-coated surface in many 10 x10 arrays where each spot was 750 nm in diameter and where neighboring spots had a center-to-center spacing of 4.4 μm . (B) The remaining areas of gold were then modified with a monolayer presenting maleimide groups against a background of tri(ethylene glycol) groups and used to immobilize a cysteine terminated phosphopeptide. (C) The surface was then treated with a solution of fibronectin to allow the adsorption of the extracellular matrix protein to the MHA nanoarray. (C) A SAMDI spectrum of the monolayer confirms immobilization of the peptide. (D) The fluorescence micrograph shows fibronectin patterned nanoarrays stained with mouse antibody and AlexaFluor 568-conjugated goat anti-mouse IgG. The scale bar is 40 μm .

Finally, a peptide substrate for phosphotyrosine phosphatases (A1pYENPFARKC, where p denotes phosphorylation of the tyrosine residue) was covalently immobilized by a conjugate

addition of the terminal cysteine residue to the maleimide groups present on the monolayer. SAMDI mass spectra confirmed that peptide immobilization was complete, and X-ray photoelectron spectroscopy (XPS) characterization showed the presence of sulfur and nitrogen peaks in the resulting monolayer consistent with the presence of thiols and amide bonds, respectively (Figure 5.2C and Figure B.3, Appendix B). Finally, the patterned substrates were immersed in a solution of fibronectin (30 $\mu\text{g}/\text{mL}$ in PBS) to allow the non-specific adsorption of protein to the patterned MHA features. Immunofluorescent labeling of fibronectin confirmed the adsorption only to the regions of MHA (Figure 5.2D). In general, this approach is applicable to other ECM attachment proteins, such as collagen and laminin, which can also adsorb to self-assembled monolayers by way of non-specific interactions.

5.3.2 Cell seeding and assay development

HeLa cells were seeded on the fibronectin nanopatterned substrates and cultured the cells for two hours under standard media conditions (Figure 5.3A). The cells spread fully within the 10×10 nanoarrays of fibronectin, and they remained adherent during the culture (Figure 5.3B). We only observed cells on the patterned regions presenting the fibronectin, and cells remained confined to those regions of the substrate, showing that the tri(ethylene glycol)-terminated monolayers were effective at preventing cell adhesion and spreading beyond the patterned matrix.

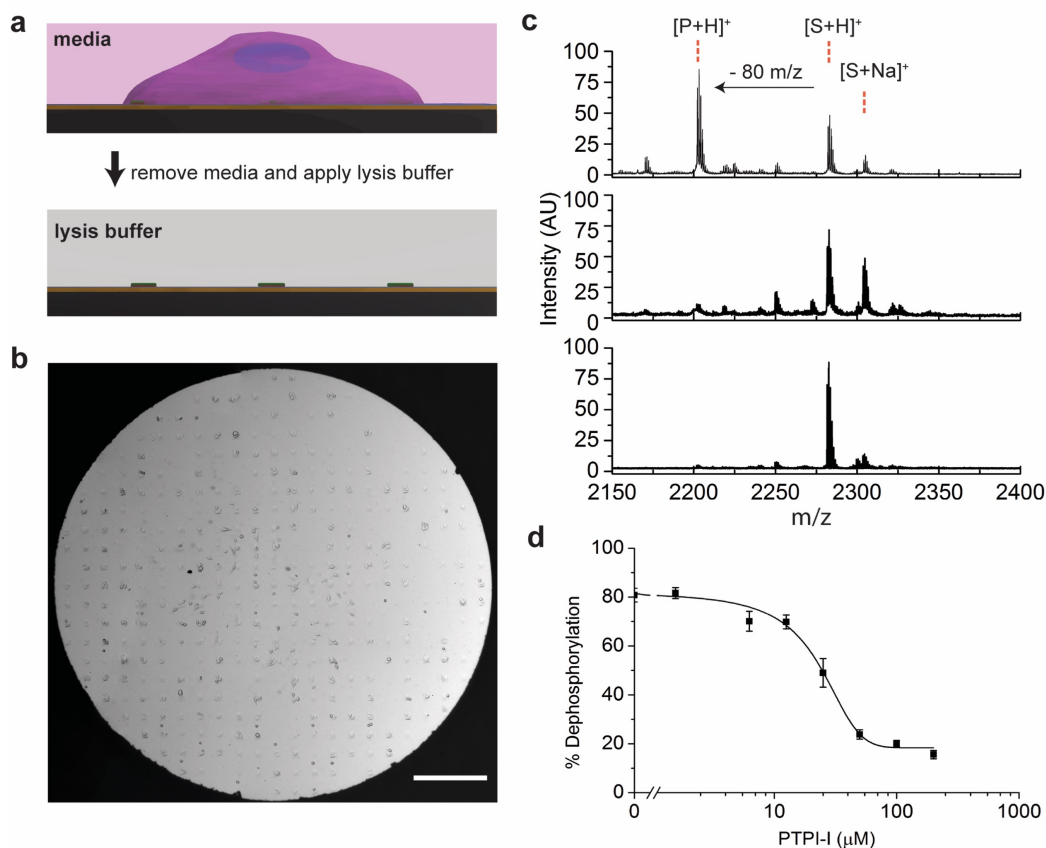


Figure 5.3. (A) Cell culture and lysis on mixed monolayers. (B) Cells were cultured on patterned monolayers. Individual cells attached to each 10×10 fibronectin nanoarray and remained confined to these regions of the substrate. The media was then removed from the entire plate and a lysis buffer was added to each spot of the 384-spot array to allow phosphatase enzymes in the lysate to act on peptides immobilized on the monolayer. The scale bar is $500 \mu\text{m}$. (C) SAMDI spectra of the surface after removal of the lysate showed a peak corresponding to generation of the dephosphorylated product (top spectrum). Addition of the phosphatase inhibitor PTP-1 to the lysis buffer resulted in a loss of phosphatase activity (middle) as did proteolytic removal of the cells without lysis (bottom). Separately, populations of HeLa cells were treated with PTP-I in concentrations ranging from 0 to $200 \mu\text{M}$ and then lysed and analyzed with SAMDI-MS. A dose-response curve shows half-maximum inhibition at concentration of approximately $22 \mu\text{M}$. Standard errors were determined from three independent experiments with at least five spots per condition.

5.3.3 Cell lysis and analysis by SAMDI-MS

After two hours in culture, the monolayers were rinsed with PBS to remove the media and then a lysis buffer containing a protease inhibitor cocktail was applied to each patterned region. The solutions were kept at 37°C for one hour to allow enzymes in the lysate to interact with the

phosphopeptides on the monolayer. The mixed monolayer was rinsed with PBS buffer and then treated with 2,4,6-trihydroxyacetophenone (THAP) matrix (30 mg/mL in acetone) and analyzed with SAMDI-MS.

We first analyzed a control array that was not seeded with cells and we observed peaks in the SAMDI spectrum that corresponded to asymmetric disulfides terminated in one phosphopeptide and one tri(ethylene glycol) group ($m/z = 2282$) as well as the Na^+ ($m/z = 2304$) and K^+ ($m/z = 2320$) adducts of this molecule (Figure 5.2C). For arrays that were treated with cells that had been lysed, the SAMDI spectra revealed corresponding peaks appearing at 80 Da lower mass, which is consistent with dephosphorylation of the peptide (Figure 5.3C, top). The spectra were similar to those acquired from a monolayer that only presented the phosphopeptide against the tri(ethylene glycol) background and that was treated with a lysate isolated in the conventional manner. Hence, the nanopatterned fibronectin features did not interfere with the enzyme action on the peptide or with the SAMDI mass spectrometry of the intervening monolayer. This was expected, since the fibronectin was present on approximately 1% of the patterned surface, leaving most of the monolayer available for analysis by SAMDI, and also because the protein would be observed at a much higher mass range in the spectrum.

We confirmed that the phosphatase activity we observed was due to enzymes present in the cell lysate. For example, when cells were cultured for two hours, and then removed by treatment with the protease TrypLE, a selective protease that reduces the digestion of cell surface proteins, the resulting surfaces had essentially no dephosphorylated peptide, showing that potential secretion of phosphatases by the cell did not significantly contribute to our measurements (Figure 5.3C, middle). Similarly, we assayed conditioned media obtained from cell cultures and did not observe phosphatase activity. We also introduced a known phosphotyrosine phosphatase inhibitor

during cell culture to confirm that the activity was due to cellular phosphatases. PTP Inhibitor (PTPI-I), a covalent inhibitor, was added to cell cultures (300 μM) during the two hour culture period. Following lysis and analysis as described above, we observed a 92 % decrease in phosphatase activity (Figure 5.3C, bottom). To assess the use of the assay to quantitatively characterize the effect an inhibitor has in cultured cells, we cultured several populations of HeLa cells on the nanopatterned monolayers and treated each with a distinct concentration of the PTPI-I inhibitor. We then lysed the cells and used SAMDI mass spectrometry to determine the extent of the reaction by SAMDI mass spectrometry. The degree of inhibition showed the expected sigmoidal-dependence on the concentration of the inhibitor, with an IC_{50} of 22 μM (Figure 5.3D). Further, the experiment was performed three independent times and measurement of the standard error revealed good reproducibility in the measurements. Together, these experiments demonstrate that the TCAL assay quantitatively measures enzyme activities present in the cell lysate.

5.4 Discussion

The nanopatterned substrates reported here are significant because they expand the use of the TCAL assay to a broad range of cell types. Whereas the TCAL assay had previously been limited to the use of cells that could be cultured on monolayers presenting short peptides that mediate cell adhesion (for example, the RGD motif), we now show that monolayers that are patterned with nanoarrays of ECM proteins can support the adhesion and culture of cells and still be analyzed with SAMDI mass spectrometry. Hence, established cultures that use glass or plastic substrates that are uniformly modified with a layer of ECM can be readily translated to the TCAL assay with these nanopatterned substrates. This approach is also significant because it can measure activities in lysates prepared from as few as ten cells and because there is no processing or delay between generation and assay of the lysate, which often leads to loss of protein activity. The use

of SAMDI-MS provides a label-free assay of a broad range of enzyme activities, making ~~103~~ format quite general for applications in different drug development targets. The tri(ethylene glycol)-terminated monolayers have been shown to remain inert for up to one week in culture, making this approach compatible with most cell-based assay protocols. Finally, the TCAL-SAMDI method is not limited to the use of peptides as substrates for the relevant enzyme, but can also use carbohydrates, small molecules and protein substrates, since each of these molecules can be immobilized to a monolayer and characterized with SAMDI mass spectrometry.

5.5 Conclusions

Traditionally, cell-based assays have been employed when the phenotype of interest could not be translated to an enzyme activity – for example, a validated target for blocking metastasis is still lacking. They have not been used when a validated target is available, because molecular assays are faster, less expensive, and far less limited as to the molecular activities that can be assayed. The novel strategy we report here narrows this gap between cell-based and molecular assays and promises to increase the use of cell-based assays in the first phase of drug discovery programs. The ability to assay compounds in cells—which reveals aspects of entry, trafficking and effects owing to interaction with other cellular proteins—but with a molecular readout combines the advantages of molecular and cellular assays and represents a significant advance in both drug discovery and for fundamental studies of signal transduction.

CHAPTER SIX

Conclusions and Outlook

The work on this thesis demonstrates the importance of combining molecular printing and mass spectrometry to a) define the chemistry of SAMs to model bioactive surfaces to systematically probe cell-substrate interactions and b) develop cell-based assays to obtain quantitative readouts of endogenous biochemical events. In Chapter 2, we outline a generalizable protocol for screening conditions that dictate cell behavior using PPL. This powerful technique ultimately enables rapid screening of an extensive parameter space to identify nanoscale variations in ECM composition that lead to desired changes in cell behavior. The protocol presented in this chapter can be easily applied to study a wide range of biological systems. Building upon these concepts, Chapter 3 further examines how cytoskeletal organization can induce osteogenic stem cell differentiation. Here, our approach exploits the advantages of the cantilever-free scanning probe toolbox to rapidly prototype pattern geometries – with a user-defined distribution of subcellular adhesion sites – to selectively control the orientation of subcellular structures, modulate cell contractility and induce expression of lineage specific markers. While it is expected that cell contractility increases with increasing aspect ratio, we were interested in elucidating how to address contractility as a parameter independent of cell shape. Interestingly, our data indicate that the subcellular arrangement and distribution of adhesion cues drive recruitment of mature focal adhesions at specific sites and define the assembly of an organized actomyosin cytoskeleton around highly contractile regions. Furthermore, programming contractility has direct implications in the expression of osteogenic and adipogenic markers.

Beyond addressing fundamental questions about cell-ECM interactions, in Chapters 4 and 5 we introduce a novel method for combining patterned bioactive surface with mass spectrometric techniques for label-free, high-throughput analysis. In Chapter 4, we first develop a cell-based

assay with mass spectrometric readout by designing a mixed monolayer that presents and adheres 105 peptide for cell culture and a reporter peptide for recording endogenous phosphatase activity on the same monolayer. Using this approach, we identify an indirect inhibitor of phosphatase activity from a 10,000 compound library screen. These findings establish the cell-based format of the SAMDI assay (TCAL-SAMDI) as a powerful analytical method for high-throughput drug discovery. In Chapter 5, we expand the scope of the TCAL-SAMDI assay to enable culture of virtually any adherent cell type by presenting a well-defined mixed monolayer patterned with adhesion proteins surrounded by the reporter ligand. The discontinuity does not interfere with acquisition of the readout nor does decrease the sensitivity of the assay, instead, this format provides a homogeneous culture environment effectively normalizing the interaction between cells and the ECM throughout the culture.

6.2 Towards printing orthogonal chemistries and modulating chemical and physical properties of soft materials

The surface chemistry of SAMs can be easily tailored to present orthogonal chemistries that render a multi-functional monolayer, as was discussed in Chapter 5. Moving forward, customizing the chemical composition of the monolayer to present orthogonal functional groups – such as alkynes, activated esters, etc – can enable capturing of cell metabolites and probing interactions between cells and complex structures such as glycans. While the work presented in this thesis is built on the templating SAMs on 2D surfaces, cantilever-free scanning probe techniques (CF-SPL), are uniquely positioned to deposit a wide range of materials and deliver energy, thus expanding the repertoire of 2D and 3D structures that can be synthesized.⁸⁷⁻⁸⁸ Efforts are underway to leverage the capabilities of beam pen lithography (BPL), a CF-SPL technique that delivers light through the apertures of pen arrays, to modulate the chemical and physical properties

of hydrogels. By selectively controlling the cross-linking density via patterning, we can customize the properties of these soft materials to recapitulate the complexity of the ECM and study cell behavior in a physiologically relevant microenvironment.

6.3 Developing assays with single-cell readouts

The work presented in Chapter 3 demonstrates the importance of controlling the registration of ligands on a surface to systematically organize the cytoskeleton in a user-defined fashion and to develop cell-based assays. In these examples, cells act as programmable biological machines that are responsive to changes in the chemical environment thus molecularly textured surfaces can be utilized to control input and output functions that dictate cell behavior. Furthermore, we can leverage the benefits of using bioactive substrates to record cellular input/output functions, however the challenge remains in understanding the heterogeneity of the response of the cell population. Future work will incorporate microfabrication tools (i.e. microfluidic devices) that can enable single-cell readouts. This work will be significant in advancing technologies for developing assays for clinical and diagnostic applications.

REFERENCES

- (1) Frantz, C.; Stewart, K. M.; Weaver, V. M., The extracellular matrix at a glance. *Journal of Cell Science* **2010**, *123* (24), 4195-4200.
- (2) Humphrey, J. D.; Dufresne, E. R.; Schwartz, M. A., Mechanotransduction and extracellular matrix homeostasis. *Nature Reviews in Molecular Cell Biology* **2014**, *15* (12), 802-812.
- (3) Delon, I.; Brown, N. H., Integrins and the actin cytoskeleton. *Current Opinion in Cell Biology* **2007**, *19* (1), 43-50.
- (4) Piner, R. D.; Zhu, J.; Xu, F.; Hong, S.; Mirkin, C. A., "Dip-Pen" nanolithography. *Science* **1999**, *283* (5402), 661-3.
- (5) Lee, K. B.; Park, S. J.; Mirkin, C. A.; Smith, J. C.; Mrksich, M., Protein nanoarrays generated by dip-pen nanolithography. *Science* **2002**, *295* (5560), 1702-5.
- (6) Demers, L. M.; Ginger, D. S.; Park, S. J.; Li, Z.; Chung, S. W.; Mirkin, C. A., Direct patterning of modified oligonucleotides on metals and insulators by dip-pen nanolithography. *Science* **2002**, *296* (5574), 1836-8.
- (7) Su, M.; Aslam, M.; Fu, L.; Wu, N. Q.; Dravid, V. P., Dip-pen nanopatterning of photosensitive conducting polymer using a monomer ink. *Applied Physics Letters* **2004**, *84* (21), 4200-4202.
- (8) Ginger, D. S.; Zhang, H.; Mirkin, C. A., The evolution of dip-pen nanolithography. *Angewandte Chemie International Edition* **2004**, *43* (1), 30-45.
- (9) Salaita, K.; Lee, S. W.; Wang, X.; Huang, L.; Dellinger, T. M.; Liu, C.; Mirkin, C. A., Sub-100 nm, centimeter-scale, parallel dip-pen nanolithography. *Small* **2005**, *1* (10), 940-945.
- (10) Salaita, K.; Wang, Y.; Mirkin, C. A., Applications of dip-pen nanolithography. *Nature Nanotechnology* **2007**, *2* (3), 145-155.
- (11) Su, M.; Liu, X.; Li, S. Y.; Dravid, V. P.; Mirkin, C. A., Moving beyond molecules: patterning solid-state features via dip-pen nanolithography with sol-based inks. *Journal of the American Chemical Society* **2002**, *124* (8), 1560-1561.
- (12) Giam, L. R.; Massich, M. D.; Hao, L.; Shin Wong, L.; Mader, C. C.; Mirkin, C. A., Scanning probe-enabled nanocombinatorics define the relationship between fibronectin feature size and stem cell fate. *Proceedings of the National Academy of Sciences USA* **2012**, *109* (12), 4377-4382.

- (13) Gandor, S.; Reisewitz, S.; Venkatachalapathy, M.; Arrabito, G.; Reibner, M.; Schroder, M.; Ruf, K.; Niemeyer, C. M.; Bastiaens, P. I.; Dehmelt, L., A protein-interaction array inside a living cell. *Angewandte Chemie International Edition* **2013**, *52* (18), 4790-4794.
- (14) Huo, F.; Zheng, Z.; Zheng, G.; Giam, L. R.; Zhang, H.; Mirkin, C. A., Polymer pen lithography. *Science* **2008**, *321* (5896), 1658-1660.
- (15) Qin, D.; Xia, Y.; Whitesides, G. M., Soft lithography for micro- and nanoscale patterning. *Nature Protocols* **2010**, *5* (3), 491-502.
- (16) Mrksich, M., Mass spectrometry of self-assembled monolayers: a new tool for molecular surface science. *ACS Nano* **2008**, *2* (1), 7-18.
- (17) Love, J. C.; Estroff, L. A.; Kriebel, J. K.; Nuzzo, R. G.; Whitesides, G. M., Self-assembled monolayers of thiolates on metals as a form of nanotechnology. *Chemical Reviews* **2005**, *105* (4), 1103-1169.
- (18) Meyers, S. R.; Grinstaff, M. W., Biocompatible and Bioactive Surface Modifications for Prolonged In Vivo Efficacy. *Chemical Reviews* **2012**, *112* (3), 1615-1632.
- (19) Yeo, W. S.; Mrksich, M., Electroactive substrates that reveal aldehyde groups for bio-immobilization. *Advanced Materials* **2004**, *16* (15), 1352-1357.
- (20) Yousaf, M. N.; Houseman, B. T.; Mrksich, M., Using electroactive substrates to pattern the attachment of two different cell populations. *Proceedings of the National Academy of Sciences USA* **2001**, *98* (11), 5992-5996.
- (21) Houseman, B. T.; Gawalt, E. S.; Mrksich, M., Maleimide-functionalized self-assembled monolayers for the preparation of peptide and carbohydrate biochips. *Langmuir* **2003**, *19* (5), 1522-1531.
- (22) Su, J.; Bringer, M. R.; Ismagilov, R. F.; Mrksich, M., Combining microfluidic networks and peptide arrays for multi-enzyme assays. *Journal of the American Chemical Society* **2005**, *127* (20), 7280-7281.
- (23) Houseman, B. T.; Huh, J. H.; Kron, S. J.; Mrksich, M., Peptide chips for the quantitative evaluation of protein kinase activity. *Nature Biotechnology* **2002**, *20* (3), 270-274.
- (24) Liao, X. L.; Su, J.; Mrksich, M., An Adaptor Domain-Mediated Autocatalytic Interfacial Kinase Reaction. *Chemistry a European Journal* **2009**, *15* (45), 12303-12309.
- (25) Min, D. H.; Su, J.; Mrksich, M., Profiling kinase activities by using a peptide chip and mass spectrometry. *Angewandte Chemie International Edition* **2004**, *43* (44), 5973-5977.

- (26) Petty, R. T.; Mrksich, M., De novo motif for kinase mediated signaling across the cell membrane. *Integrative Biology* **2011**, *3* (8), 816-822.
- (27) Li, S.; Liao, X.; Mrksich, M., Steady-state of an enzymatic reaction is dependent on the density of reactant. *Langmuir* **2013**, *29* (1), 294-298.
- (28) Kornacki, J. R.; Stuparu, A. D.; Mrksich, M., Acetyltransferase p300/CBP Associated Factor (PCAF) Regulates Crosstalk-Dependent Acetylation of Histone H3 by Distal Site Recognition. *Acs Chemical Biology* **2015**, *10* (1), 157-164.
- (29) Kuhn, M. L.; Zemaitaitis, B.; Hu, L. I.; Sahu, A.; Sorensen, D.; Minasov, G.; Lima, B. P.; Scholle, M.; Mrksich, M.; Anderson, W. F.; Gibson, B. W.; Schilling, B.; Wolfe, A. J., Structural, Kinetic and Proteomic Characterization of Acetyl Phosphate-Dependent Bacterial Protein Acetylation. *Plos One* **2014**, *9* (4), 2354-2363.
- (30) Engler, A. J.; Sen, S.; Sweeney, H. L.; Discher, D. E., Matrix elasticity directs stem cell lineage specification. *Cell* **2006**, *126* (4), 677-89.
- (31) Trappmann, B.; Gautrot, J. E.; Connelly, J. T.; Strange, D. G.; Li, Y.; Oyen, M. L.; Cohen Stuart, M. A.; Boehm, H.; Li, B.; Vogel, V.; Spatz, J. P.; Watt, F. M.; Huck, W. T., Extracellular-matrix tethering regulates stem-cell fate. *Nature Materials* **2012**, *11* (7), 642-9.
- (32) Lutolf, M. P.; Gilbert, P. M.; Blau, H. M., Designing materials to direct stem-cell fate. *Nature* **2009**, *462* (7272), 433-441.
- (33) Dalby, M. J.; Gadegaard, N.; Tare, R.; Andar, A.; Riehle, M. O.; Herzyk, P.; Wilkinson, C. D.; Oreffo, R. O., The control of human mesenchymal cell differentiation using nanoscale symmetry and disorder. *Nat Mater* **2007**, *6* (12), 997-1003.
- (34) McMurray, R. J.; Gadegaard, N.; Tsimbouri, P. M.; Burgess, K. V.; McNamara, L. E.; Tare, R.; Murawski, K.; Kingham, E.; Oreffo, R. O.; Dalby, M. J., Nanoscale surfaces for the long-term maintenance of mesenchymal stem cell phenotype and multipotency. *Nature Materials* **2011**, *10* (8), 637-44.
- (35) Zheng, Z.; Daniel, W. L.; Giam, L. R.; Huo, F.; Senesi, A. J.; Zheng, G.; Mirkin, C. A., Multiplexed protein arrays enabled by polymer pen lithography: addressing the inking challenge. *Angew Chem Int Ed Engl* **2009**, *48* (41), 7626-9.
- (36) Arnold, M.; Hirschfeld-Warneken, V. C.; Lohmuller, T.; Heil, P.; Blummel, J.; Cavalcanti-Adam, E. A.; Lopez-Garcia, M.; Walther, P.; Kessler, H.; Geiger, B.; Spatz, J. P., Induction of cell polarization and migration by a gradient of nanoscale variations in adhesive ligand spacing. *Nano Letters* **2008**, *8* (7), 2063-2069.
- (37) Letort, G.; Ennomani, H.; Gressin, L.; Theyry, M.; Blanchoin, L., Dynamic reorganization of the actin cytoskeleton. *F1000Res* **2015**, *4*.

- (38) Kilian, K. A.; Bugarija, B.; Lahn, B. T.; Mrksich, M., Geometric cues for directing the differentiation of mesenchymal stem cells. *Proceedings of the National Academy of Science U S A* **2010**, *107* (11), 4872-7.
- (39) Shabbir, S. H.; Cleland, M. M.; Goldman, R. D.; Mrksich, M., Geometric control of vimentin intermediate filaments. *Biomaterials* **2014**, *35* (5), 1359-66.
- (40) Boujemaa-Paterski, R.; Galland, R.; Suarez, C.; Guerin, C.; They, M.; Blanchoin, L., Directed actin assembly and motility. *Methods in Enzymology* **2014**, *540*, 283-300.
- (41) Huang, J.; Grater, S. V.; Corbellini, F.; Rinck, S.; Bock, E.; Kemkemer, R.; Kessler, H.; Ding, J.; Spatz, J. P., Impact of order and disorder in RGD nanopatterns on cell adhesion. *Nano Letters* **2009**, *9* (3), 1111-6.
- (42) Lohmuller, T.; Aydin, D.; Schwieder, M.; Morhard, C.; Louban, I.; Pacholski, C.; Spatz, J. P., Nanopatterning by block copolymer micelle nanolithography and bioinspired applications. *Biointerphases* **2011**, *6* (1), MR1-12.
- (43) Selhuber-Unkel, C.; Erdmann, T.; Lopez-Garcia, M.; Kessler, H.; Schwarz, U. S.; Spatz, J. P., Cell adhesion strength is controlled by intermolecular spacing of adhesion receptors. *Biophysics Journal* **2010**, *98* (4), 543-51.
- (44) Aydin, D.; Schwieder, M.; Louban, I.; Knoppe, S.; Ulmer, J.; Haas, T. L.; Walczak, H.; Spatz, J. P., Micro-nanostructured protein arrays: a tool for geometrically controlled ligand presentation. *Small* **2009**, *5* (9), 1014-8.
- (45) Oakes, P. W.; Banerjee, S.; Marchetti, M. C.; Gardel, M. L., Geometry regulates traction stresses in adherent cells. *Biophysics Journal* **2014**, *107* (4), 825-833.
- (46) Ennomani, H.; Letort, G.; Guerin, C.; Martiel, J. L.; Cao, W.; Nedelec, F.; De La Cruz, E. M.; They, M.; Blanchoin, L., Architecture and Connectivity Govern Actin Network Contractility. *Current Biology* **2016**, *26* (5), 616-626.
- (47) Murrell, M.; Oakes, P. W.; Lenz, M.; Gardel, M. L., Forcing cells into shape: the mechanics of actomyosin contractility. *Nature Reviews in Molecular Cell Biology* **2015**, *16* (8), 486-98.
- (48) They, M.; Racine, V.; Pepin, A.; Piel, M.; Chen, Y.; Sibarita, J. B.; Bornens, M., The extracellular matrix guides the orientation of the cell division axis. *Nature Cell Biology* **2005**, *7* (10), 947-53.
- (49) They, M.; Racine, V.; Piel, M.; Pepin, A.; Dimitrov, A.; Chen, Y.; Sibarita, J. B.; Bornens, M., Anisotropy of cell adhesive microenvironment governs cell internal organization and orientation of polarity. *Proceedings of the National Academy of Science U S A* **2006**, *103* (52), 19771-19776.

- (50) Cabezas, M. D.; Eichelsdoerfer, D. J.; Brown, K. A.; Mrksich, M.; Mirkin, C. A., Combinatorial screening of mesenchymal stem cell adhesion and differentiation using polymer pen lithography. *Methods in Cell Biology* **2014**, *119*, 261-276.
- (51) Cabezas, M. D.; Mirkin, C. A.; Mrksich, M., Nanopatterned Extracellular Matrices Enable Cell-Based Assays with a Mass Spectrometric Readout. *Nano Letters* **2017**, *17* (3), 1373-1377.
- (52) Eichelsdoerfer, D. J.; Liao, X.; Cabezas, M. D.; Morris, W.; Radha, B.; Brown, K. A.; Giam, L. R.; Braunschweig, A. B.; Mirkin, C. A., Large-area molecular patterning with polymer pen lithography. *Nat Protoc* **2013**, *8* (12), 2548-60.
- (53) Giam, L. R.; Mirkin, C. A., Cantilever-free scanning probe molecular printing. *Angewandte Chemie International Edition* **2011**, *50* (33), 7482-7485.
- (54) Quinn, K. P.; Georgakoudi, I., Rapid quantification of pixel-wise fiber orientation data in micrographs. *Journal of Biomedical Optics* **2013**, *18* (4).
- (55) Otsu, N., Threshold Selection Method from Gray-Level Histograms. *IEEE Transactions on Systems, Man and Cybernetics* **1979**, *9* (1), 62-66.
- (56) Fox, S.; Farr-Jones, S.; Sopchak, L.; Boggs, A.; Nicely, H. W.; Khoury, R.; Biros, M., High-throughput screening: update on practices and success. *Journal in Biomolecular Screening* **2006**, *11* (7), 864-869.
- (57) Macarron, R.; Banks, M. N.; Bojanic, D.; Burns, D. J.; Cirovic, D. A.; Garyantes, T.; Green, D. V.; Hertzberg, R. P.; Janzen, W. P.; Paslay, J. W.; Schopfer, U.; Sittampalam, G. S., Impact of high-throughput screening in biomedical research. *Nature Reviews in Drug Discovery* **2011**, *10* (3), 188-195.
- (58) Su, J.; Mrksich, M., Using mass spectrometry to characterize self-assembled monolayers presenting peptides, proteins, and carbohydrates. *Angewandte Chemie International Edition* **2002**, *41* (24), 4715-4718.
- (59) Zlokarnik, G.; Negulescu, P. A.; Knapp, T. E.; Mere, L.; Burren, N.; Feng, L.; Whitney, M.; Roemer, K.; Tsien, R. Y., Quantitation of transcription and clonal selection of single living cells with beta-lactamase as reporter. *Science* **1998**, *279* (5347), 84-88.
- (60) Whitney, M.; Rockenstein, E.; Cantin, G.; Knapp, T.; Zlokarnik, G.; Sanders, P.; Durick, K.; Craig, F. F.; Negulescu, P. A., A genome-wide functional assay of signal transduction in living mammalian cells. *Nature Biotechnology* **1998**, *16* (13), 1329-1333.
- (61) Inglese, J.; Johnson, R. L.; Simeonov, A.; Xia, M.; Zheng, W.; Austin, C. P.; Auld, D. S., High-throughput screening assays for the identification of chemical probes. *Nature Chemical Biology* **2007**, *3* (8), 466-479.

- (62) Tsien, R. Y., The green fluorescent protein. *Annual Review of Biochemistry* **1998**, *67*, 509-544.
- (63) Giepmans, B. N.; Adams, S. R.; Ellisman, M. H.; Tsien, R. Y., The fluorescent toolbox for assessing protein location and function. *Science* **2006**, *312* (5771), 217-224.
- (64) Deshmukh, V. A.; Tardif, V.; Lyssiotis, C. A.; Green, C. C.; Kerman, B.; Kim, H. J.; Padmanabhan, K.; Swoboda, J. G.; Ahmad, I.; Kondo, T.; Gage, F. H.; Theofilopoulos, A. N.; Lawson, B. R.; Schultz, P. G.; Lairson, L. L., A regenerative approach to the treatment of multiple sclerosis. *Nature* **2013**, *502* (7471), 327-332.
- (65) O'Rourke, N. A.; Meyer, T.; Chandy, G., Protein localization studies in the age of 'Omics'. *Current Opinions in Chemical Biology* **2005**, *9* (1), 82-87.
- (66) Wehrman, T. S.; Casipit, C. L.; Gewertz, N. M.; Blau, H. M., Enzymatic detection of protein translocation. *Nature Methods* **2005**, *2* (7), 521-527.
- (67) Ding, S.; Schultz, P. G., A role for chemistry in stem cell biology. *Nature Biotechnology* **2004**, *22* (7), 833-840.
- (68) Johnson, K.; Zhu, S.; Tremblay, M. S.; Payette, J. N.; Wang, J.; Bouchez, L. C.; Meeusen, S.; Althage, A.; Cho, C. Y.; Wu, X.; Schultz, P. G., A stem cell-based approach to cartilage repair. *Science* **2012**, *336* (6082), 717-721.
- (69) Lang, P.; Yeow, K.; Nichols, A.; Scheer, A., Cellular imaging in drug discovery. *Nat Rev Drug Discov* **2006**, *5* (4), 343-356.
- (70) Perlman, Z. E.; Slack, M. D.; Feng, Y.; Mitchison, T. J.; Wu, L. F.; Altschuler, S. J., Multidimensional drug profiling by automated microscopy. *Science* **2004**, *306* (5699), 1194-1198.
- (71) Gurard-Levin, Z. A.; Kilian, K. A.; Kim, J.; Bahr, K.; Mrksich, M., Peptide arrays identify isoform-selective substrates for profiling endogenous lysine deacetylase activity. *ACS Chemical Biology* **2010**, *5* (9), 863-873.
- (72) Kuo, H. Y.; DeLuca, T. A.; Miller, W. M.; Mrksich, M., Profiling deacetylase activities in cell lysates with peptide arrays and SAMDI mass spectrometry. *Analytical Chemistry* **2013**, *85* (22), 10635-10642.
- (73) Min, D. H.; Su, J.; Mrksich, M., Profiling kinase activities by using a peptide chip and mass spectrometry. *Angewandte Chemie International Edition* **2004**, *43* (44), 5973-5977.
- (74) Min, D. H.; Tang, W. J.; Mrksich, M., Chemical screening by mass spectrometry to identify inhibitors of anthrax lethal factor. *Nature Biotechnology* **2004**, *22* (6), 717-23.

- (75) Su, J.; Rajapaksha, T. W.; Peter, M. E.; Mrksich, M., Assays of endogenous caspases activities: a comparison of mass spectrometry and fluorescence formats. *Analytical Chemistry* **2006**, *78* (14), 4945-4951.
- (76) Ban, L.; Pettit, N.; Li, L.; Stuparu, A. D.; Cai, L.; Chen, W.; Guan, W.; Han, W.; Wang, P. G.; Mrksich, M., Discovery of glycosyltransferases using carbohydrate arrays and mass spectrometry. *Nature Chemistry Biology* **2012**, *8* (9), 769-773.
- (77) Min, D. H.; Yeo, W. S.; Mrksich, M., A method for connecting solution-phase enzyme activity assays with immobilized format analysis by mass spectrometry. *Analytical Chemistry* **2004**, *76* (14), 3923-3929.
- (78) Kilian, K. A.; Mrksich, M., Directing stem cell fate by controlling the affinity and density of ligand-receptor interactions at the biomaterials interface. *Angewandte Chemie International Edition* **2012**, *51* (20), 4891-4895.
- (79) Ruoslahti, E., RGD and other recognition sequences for integrins. *Annual Review of Cell and Developmental Biology* **1996**, *12*, 697-715.
- (80) Houseman, B. T.; Mrksich, M., The microenvironment of immobilized Arg-Gly-Asp peptides is an important determinant of cell adhesion. *Biomaterials* **2001**, *22* (9), 943-955.
- (81) Roberts, C.; Chen, C. S.; Mrksich, M.; Martichonok, V.; Ingber, D. E.; Whitesides, G. M., Using mixed self-assembled monolayers presenting RGD and (EG)₃OH groups to characterize long-term attachment of bovine capillary endothelial cells to surfaces. *Journal of the American Chemical Society* **1998**, *120* (26), 6548-6555.
- (82) Gurard-Levin, Z. A.; Scholle, M. D.; Eisenberg, A. H.; Mrksich, M., High-throughput screening of small molecule libraries using SAMDI mass spectrometry. *ACS Combinatorial Science* **2011**, *13* (4), 347-50.
- (83) Patel, K.; Sherrill, J.; Mrksich, M.; Scholle, M. D., Discovery of SIRT3 Inhibitors Using SAMDI Mass Spectrometry. *Journal of Biomolecular Screening* **2015**, *20* (7), 842-848.
- (84) Bernard, B.; Fest, T.; Pretet, J. L.; Mouglin, C., Staurosporine-induced apoptosis of HPV positive and negative human cervical cancer cells from different points in the cell cycle. *Cell Death and Differentiation* **2001**, *8* (3), 234-244.
- (85) Zhang, J. H.; Chung, T. D.; Oldenburg, K. R., A Simple Statistical Parameter for Use in Evaluation and Validation of High Throughput Screening Assays. *Journal of Biomolecular Screening* **1999**, *4* (2), 67-73.
- (86) Ting, A. Y.; Kain, K. H.; Klemke, R. L.; Tsien, R. Y., Genetically encoded fluorescent reporters of protein tyrosine kinase activities in living cells. *Proceedings of the National Academy of Sciences USA* **2001**, *98* (26), 15003-15008.

- (87) Huo, F. W.; Zheng, G. F.; Liao, X.; Giam, L. R.; Chai, J. A.; Chen, X. D.; Shim, W. Y.; Mirkin, C. A., Beam pen lithography. *Nature Nanotechnology* **2010**, 5 (9), 637-640.
- (88) Bian, S. D.; Zieba, S. B.; Morris, W.; Han, X.; Richter, D. C.; Brown, K. A.; Mirkin, C. A.; Braunschweig, A. B., Beam pen lithography as a new tool for spatially controlled photochemistry, and its utilization in the synthesis of multivalent glycan arrays. *Chemical Science* **2014**, 5 (5), 2023-2030.

APPENDICES

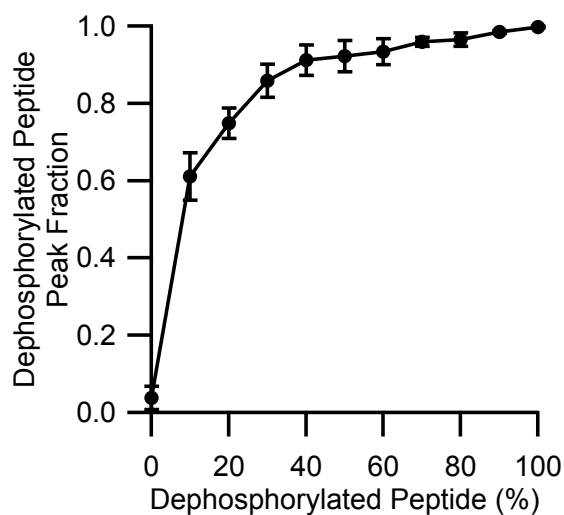


Figure A.1 Calibration curve relating the dephosphorylated peptide peak fraction measured by SAMDI to the ratio of the dephosphorylated peptide to the phosphorylated peptide used during immobilization onto the monolayer.

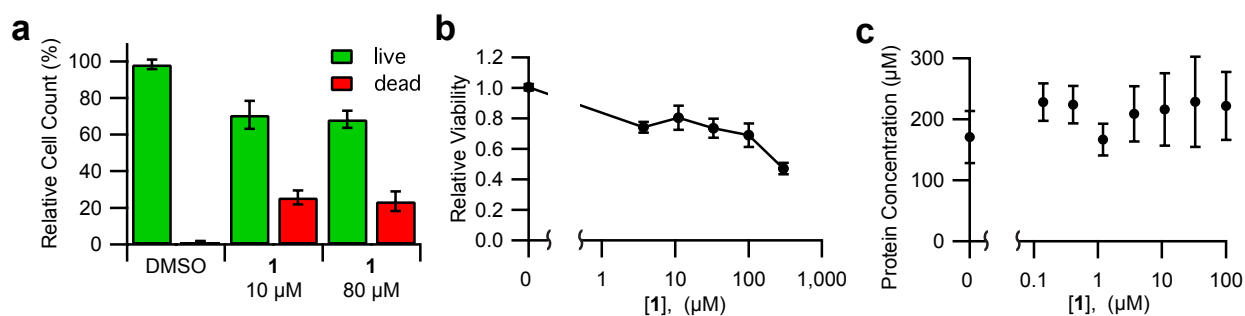


Figure A.2 Control experiments of compound **1**. (a) The cell counts of live cells (cells stained with calcein-AM) and dead cells (cells stained with ethidium homodimer) relative to the total cell count observed in cells treated with DMSO only. (b) Viability, measured by the PrestoBlue assay, of cells treated with **1**, relative to cells treated with DMSO only. (c) Protein concentrations of lysates prepared from cells cultured in 96-well tissue culture plates and treated with **1** for 2 hr, measured by the BCA assay.

APPENDIX B

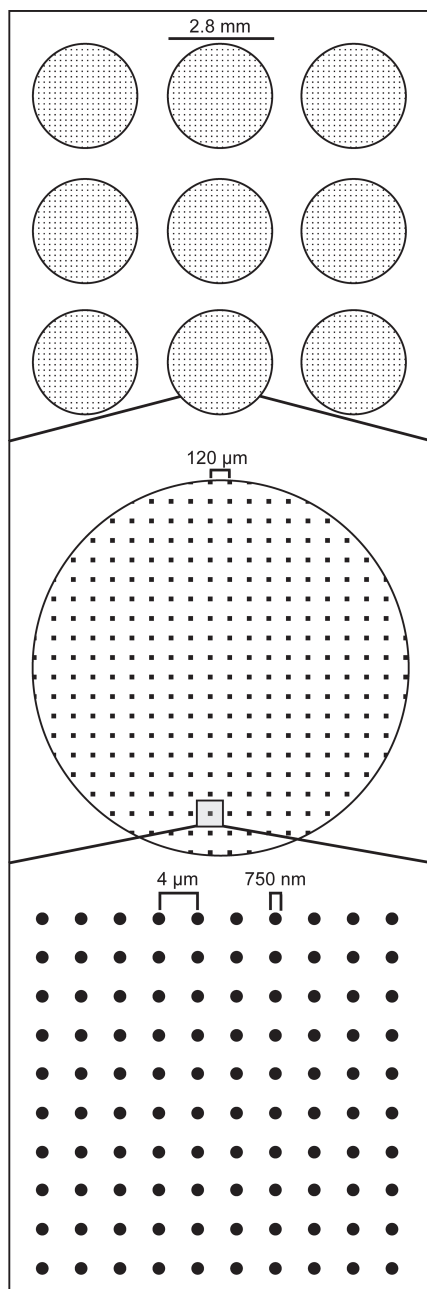


Figure B.1 Pattern arrangement across multiple length scales. Nanoarrays were prepared on 384-well format gold islands, where each island was patterned using PPL to yield ~ 428 arrays of MHA features. Each array was patterned over a $40 \times 40 \mu\text{m}^2$ area having a total of 100 MHA features arranged in a 10×10 square matrix. The size of each individual MHA feature corresponds to ~ 750 nm.

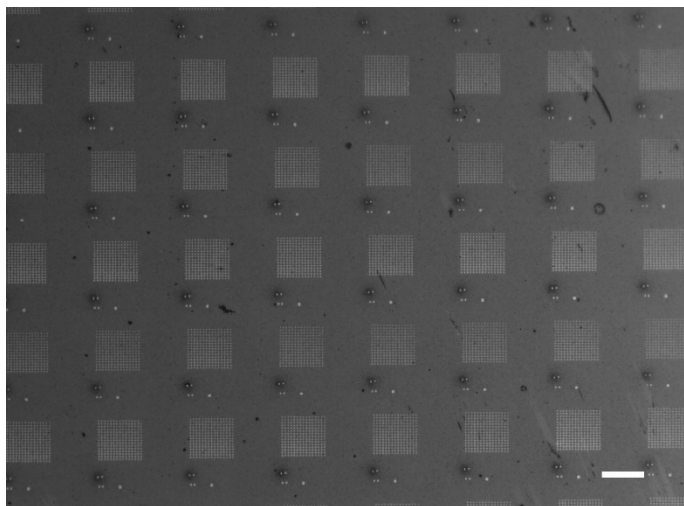


Figure B.2 MHA features arranged in a square array patterned by polymer pen lithography (PPL). Optical micrograph of raised gold features $\sim 1 \mu\text{m}$ in diameter made by chemical etching (with an aqueous solution of $13.3 \text{ mM Fe(NO}_3)_3$ and 20 mM thiourea) a portion of a glass slide having PPL-patterned mercaptohexadecanoic acid (MHA) features. The scale bar is $60 \mu\text{m}$.

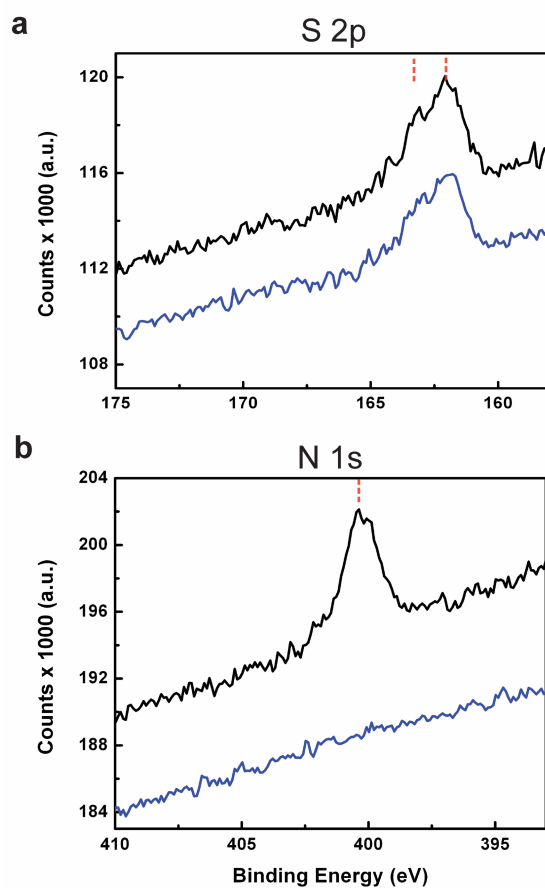


Figure B.3 XPS spectra collected after peptide immobilization on Au regions that present a maleimide-terminated monolayer along with MHA nanoarrays. The presence of sulfur (a) and nitrogen (b) peaks indicate the availability of amide bonds and thiols on the surface (black trace), while a control surface consisting of a uniform MHA monolayer (blue trace) only shows presence of thiols. Dashed lines denote the N (1s) and S (2p) peak positions.

MARIA D. CABEZAS

120

Northwestern University, Department of Chemistry
2145 Sheridan Road, Evanston, IL, 60208-3113

EDUCATION

Northwestern University

Ph.D. in Physical Chemistry (May 2018)

The University of Texas at Austin

B.S. Chemistry (May 2011)

B.S. Biomedical Engineering (May 2010)

RESEARCH EXPERIENCE

2011-2018 “Writing and Reading Chemically Encoded Surfaces for Programming Cell Function and Measuring Enzymatic Activity” Professor Chad A. Mirkin and Professor Milan Mrksich, Northwestern University, Evanston, IL.

2008-2011 “Extraction of Au Nanoparticles from Dendrimer Templates” Professor Richard M. Crooks, The University of Texas at Austin, Austin, TX.

PROFESSIONAL EXPERIENCE

Northwestern University, Evanston, IL (July 2018)

Post-doctoral Research Fellow, Jewett Lab

Northwestern University – Mirkin Lab (November 2011- June 2018)

- Developed cantilever-free scanning probe lithographic (CF-SPL) methods for introducing extracellular matrix proteins and chemical inducing ligands to study cell mechanics and stem cell differentiation
- Combined CF-SPL with mass spectrometry to develop a novel and robust label-free cell-based assay for direct measurement of endogenous enzyme activity from a limited population of cells
- Developed ink delivery methods for the synthesis of highly dense nanoparticle arrays and the combinatorial synthesis of nanoparticle libraries

Northwestern University – Mrksich Lab (November 2011 – June 2018)

- Developed a cell-based assay for the measurement of enzyme activities on monolayers presenting ligands that support cell culture and report on a desired enzyme reaction
- Screened a library of > 10,000 compounds and identified inhibitors of phosphatase activity using high-throughput self-assembled monolayer desorption/ionization (SAMDI) mass spectrometry
- Profiled global phosphatase activity throughout mesenchymal stem cell differentiation (osteogenic and adipogenic lineages) using SAMDI mass spectrometry

AWARDS AND HONORS

121

2017	IIN Excellence in Research Award
2017	Kemin Industries ACS Travel Fellowship
2013	Science in Society Image Contest Honorable Mention
2012-2013	Biotechnology Cluster Training Program
2008-2011	Undergraduate Research Fellowship, The University of Texas at Austin
2008	Diamond UREKA Scholarship, Dublin City University
2008	Norman Hackerman Award in Biochemistry, The University of Texas at Austin

LEADERSHIP AND OUTREACH EXPERIENCE

2015-2018	Mirkin Lab DPN Subgroup Leader
2015-2018	Science Blog Writer, HELIX Science in Society Magazine
2011-2014	Science in the Classroom (SITC) Student Volunteer
2012	Physical Science Weekend Academy (PSWA) Student Volunteer

PUBLICATIONS

1. **Cabezas, M. D.***, Meckes, B. R.*, Mirkin, C. A. and Mrksich, M. Nanoscale Control of Actin Assembly. (*in preparation*)
2. **Cabezas, M. D.**, Mrksich, M and Mirkin, C. A. Nanopatterning Matrices Enable Enzyme Activity Measurements Using SAMDI Mass Spectrometry. *Nano Letters* 2017, 17, 1373-1377
3. Berns, E. J., **Cabezas, M. D.**, and Mrksich, M. A Cell Based Assay Using Self-Assembled Monolayers and MALDI Mass Spectrometry as a Platform for High-Throughput Screening. *Small* 2016, 12, 3811-3818.
4. Hedrick, J. L., Brown, K. A., Kluender, E. J., **Cabezas, M. D.**, Chen, P., and Mirkin, C. A. Hard Transparent Arrays for Polymer Pen Lithography. *ACS Nano* 2016, 10, 3144-3148.
5. Morris, W., Briley, W. E., Auyeung, E., **Cabezas, M. D.** and Mirkin, C. A. Nucleic-Acid Metal Organic Framework (MOF) Nanoparticle Conjugates. *Journal of the American Chemical Society*, 2014, 136, 7261-7265.
6. Eichelsdoerfer, D. J., Liao, X., **Cabezas, M. D.**, Morris, W., Radha, B., Brown, K. A., Giam, L. R., Braunschweig, A. B., and Mirkin, C. A. Large-Area Molecular Patterning with Polymer Pen Lithography. *Nature Protocols* 2013, 8, 2548-2560.
7. **Cabezas, M. D.**, Eichelsdoerfer, D. J., Brown, K. A., Mrksich, M., and Mirkin, C. A. Combinatorial Screening of Mesenchymal Stem Cell Adhesion and Differentiation Using Polymer Pen Lithography. In M. Thery & M. Piel (Vol. Eds.) *Methods in Cell Biology*. Elsevier, 2014, 119, 261-276.

* Denotes equal contribution

PATENT APPLICATIONS

1. Mirkin, C. A., Mrksich, M., Meckes, B. R. and **Cabezas, M. D.** "Nanopatterning for Controlling Cell Cytoskeleton" United States Provisional Patent Application Number: 62/635,928.
2. Mirkin, C. A., Mrksich, M. and **Cabezas, M. D.** "Nanopatterned Extracellular Matrices Enable Cell-Based Assays with a Mass Spectrometric Readout" United States Patent Application Number: 15/10,475.

3. Mrksich, M., Berns, E. J., and **Cabezas, M. D.** “Cellular Assays with a Molecular Endpoint Measured by SAMDI Mass Spectrometry” International Patent Application Number: PCT/US2016/046027.
4. Mirkin, C. A., Mrksich, M. and **Cabezas, M. D.** “Nanopatterned Extracellular Matrices Enable Cell-Based Assays with a Mass Spectrometric Readout” United States Provisional Patent Application Number: 62/396,972.
5. Mrksich, M., Berns, E. J., and **Cabezas, M. D.** “Cellular Assays with a Molecular Endpoint Measured by SAMDI Mass Spectrometry” United States Provisional Patent Application Number: 62/202,417.

CONTRIBUTED PRESENTATIONS AND POSTERS

- 2017 ACS Spring Conference (San Francisco, CA). **Cabezas, M. D.**, Mirkin, C. A., and Mrksich, M. Nanopatterned Matrices Enable Measurements of Enzyme Activity Using SAMDI Mass Spectrometry. (Oral Presentation)
- 2016 PITTCO~~N~~ Conference and Expo (Atlanta, GA). **Cabezas, M. D.**, Mirkin C. A. and Mrksich, M. Nanopatterned Matrices Enable Measurements of Enzyme Activity Using SAMDI Mass Spectrometry. (Oral Presentation)
- 2015 PITTCO~~N~~ Conference and Expo (New Orleans, LA). **Cabezas, M. D.**, Berns, E. J., Mirkin C. A. and Mrksich, M. Bioactive Surfaces for Simultaneous Cell Culture and High-Throughput Lysate Analysis Using SAMDI-Mass Spectrometry. (Poster)
- 2015 BEST Dow Symposium (Midland, MI). Cabezas, M. D., Berns, E. J., Mirkin C. A., and Mrksich, M. Developing Cellular Assays with a Molecular Endpoint Measured by SAMDI Mass Spectrometry. (Oral Presentation)
- 2010 PITTCO~~N~~ Conference and Expo (Orlando, FL). **Cabezas, M. D.**, Guerra, F. J., and Crooks, R. M. Solid Extraction of Au Nanoparticles from Within Dendrimers. (Oral Presentation)

TEACHING AND TRAINING

- 2017 **Case Western Reserve University**, Cleveland, OH
Future Faculty Workshop, Student Participant
- 2016 **Johns Hopkins University**, Baltimore, MD
Teaching Institute, CIRTL Participant
- 2015–2017 **Northwestern University**, Evanston, IL
Teaching Assistant, Biosensors in Biomedical Engineering
- 2011–2013 **Northwestern University**, Evanston, IL
Teaching Assistant, Undergraduate General and Advanced Chemistry
- 2008–2010 **The University of Texas at Austin**, Austin, TX
Teaching Assistant, Undergraduate General Chemistry

PROFESIONAL AFFILIATIONS

- 2015–2018 Biomedical Engineering Society
- 2015–2018 Graduate Women in Science National Member
- 2015–2018 Graduate Women in Science Chicago Chapter
- 2014–2018 American Chemical Society
- 2013–2018 Phi Lambda Upsilon Chemistry Honor Society